PERFORMANCE ENHANCEMENT OF PV/T SYSTEMS USING NANO -ADDITIVES

2022
MASTER THESIS
MECHANICAL ENGINEERING

Bassam Asaad Shallal SHALLAL

Thesis Advisors
Assoc. Prof. Dr. Engin GEDİK
Assist. Prof. Dr. Hasanain A. Abdul WAHHAB

PERFORMANCE ENHANCEMENT OF PV/T SYSTEMS USING NANO - ADDITIVES

Bassam Asaad Shallal SHALLAL

Thesis Advisors

Assoc. Prof. Dr. Engin GEDİK

Assist. Prof. Dr. Hasanain A. Abdul WAHHAB

T.C.

Karabuk University

Institute of Graduate Programs

Department of Mechanical Engineering

Prepared as

Master Thesis

KARABUK

December 2022

I certify that in my opinion the thesis submitted by Basam Asaad Shallal SHALLAL titled "PERFORMANCE ENHANCEMENT OF PV/T SYSTEMS USING NANO - ADDITIVES" is fully adequate in scope and quality as a thesis for the degree of Master of Science.

Assoc. Prof. Dr. Engin GEDİK .....
Thesis Advisor, Department of Mechanical Engineering

Assist. Prof. Dr. Hasanain A. Abdul WAHHAB .....
Thesis Advisor, Department of Mechanical Engineering

This thesis is accepted by the examining committee with a unanimous vote in the Department of Mechanical Engineering as a Master of Science thesis. Dec.22,2022

Examining Committee Members (Institutions)	Signature
Chairman : Prof. Dr. Kamil ARSLAN (KBU)	.....
Member : Assoc. Prof. Dr .Mustafa YILMAZ (MU)	.....
Member : Assoc. Prof. Dr. Engin GEDİK (KBU)	.....
Member : Assist. Prof. Dr. H. A. Abdul WAHHAB (UOTECH)	.....
Member : Assist. Prof. Dr. Mutlu TEKİR (KBU)	.....

The degree of Master of Science by the thesis submitted is approved by the Administrative Board of the Institute of Graduate Programs, Karabuk University.

Prof. Dr. Muslum KUZU .....
Director of the Institute of Graduate Programs

"I declare that all the information within this thesis has been gathered and presented in accordance with academic regulations and ethical principles and I have according to the requirements of these regulations and principles cited all those which do not originate in this work as well."

Basam Asaad Shallal SHALLAL

ABSTRACT

M. Sc. Thesis

PERFORMANCE ENHANCEMENT OF PV/T SYSTEMS USING NANO - ADDITIVES

Basam Asaad Shallal SHALLAL

Karabük University
Institute of Graduate Programs
The Department of Mechanical Engineering

Thesis Advisors:
Assoc. Prof. Dr. Engin GEDİK
Assist. Prof. Dr. Hasanain A. Abdul WAHHAB
December 2022, 124 pages

This thesis presents an experimental and theoretical study on the performance of the Photovoltaic/Thermal (PV/T) system by using nanofluid with a new design of the collector. Experiments were carried out in Iraq/Baghdad/University of Technology. Two photovoltaic cells were used in the experiments, one of which was connected to a collector consisting of 120 spherical protrusions in the form of 8*15 and the other was used for comparison purposes. Water and two kinds of nanofluid (Al_2O_3/water, CuO/water) were used at different volume concentration ratio as 1%, 2%, and 3% with the flow rate 1.5, 2, 2.5, 3.5 l/min for cooling of PV panels. According to the results obtained from the study, the cell surface temperature decreased with increasing flow rate when water was used as the cooling fluid. The highest decrease was obtained at 3.5 l/min with 17.6%, while an increase of 7.5% in electrical efficiency compared to

PV panel without cooling and 27.4% in thermal efficiency than the thermal efficiency when we used (1.5 l/min) was found.

Using CuO/water and Al_2O_3/water at a volumetric concentration of 3% reduces the cell temperature 24% and 22.3% respectively compared to PV panel without cooling. Also increase in electrical and thermal efficiency was found as 10% and 40.7%, 9.1% and 38% when we use CuO and Al_2O_3 respectively at flow rate 3.5 l/min. The percentage of total difference (error) between the experimental and numerical work was 8.7% for ΔT (temperature differences between inlet and outlet) and 3.1% for the surface temperature of the collector at 3.5 l/min.

Key Words **:** PV/T, solar energy, nanofluid, thermal performance.
Science Code : 91408

ÖZET

Yüksek Lisans Tezi

NANO KATKI MALZEMELER KULLANARAK FV/T SİSTEMLERİN PERFORMANSININ İYİLEŞTİRİLMESİ

Basam Asaad Shallal SHALLAL

Karabük Üniversitesi
Lisansüstü Eğitim Enstitüsü
Makina Mühendisliği Anabilim Dalı

Tez Danışmanları:
Doç. Dr. Engin GEDİK
Dr. Öğr. Üyesi Hasanain A. Abdul WAHHAB
Aralık 2022, 124 sayfa

Yapılan bu çalışmada yeni tasarlanan bir kolektörde nanoakışkan kullanımı ile fotovoltaik/termal (FV/T) sistemin performansı deneysel ve teorik olarak incelenmiştir. Deneyler Irak Teknoloji Üniversitesinde gerçekleştirilmiştir. Deneylerde iki fotovaltaik hücre kullanılmış olup bunlardan birisi 8*15 şeklinde 120 adet küresel çıkıntıdan oluşan kollektöre bağlanmış diğeri ise karşılaştırma amacıyla sabit hücre kullanılmıştır. PV panellerin soğutulmasında su ve %1, %2, %3 hacimsel konsantrasyon oranlarına sahip iki farklı nanoakışkan (Al_2O_3/su, CuO/su) 1.5, 2, 2.5, 3.5 L/dk debilerinde kullanılmıştır. Yapılan çalışmada farklı kollektör yapıları için nanoakışkan kullanımın PV panel termal ve elektriksel verim üzerindeki etkileri incelenmiştir. Çalışmadan elde edilen sonuçlara göre, soğutma sıvısı olarak su kullanıldığında artan debi ile hücre yüzey sıcaklığı düşmüştür. En yüksek düşüş 3,5 L/dk'da %17,6 ile elde edilirken elektriksel verimde %7,5 ve ısıl verimde %27,4 artış

olarak bulunmuştur. %3 hacimsel konsantrasyon oranında CuO/su ve Al_2O_3/su kullanılması ile soğutmasız PV panele kıyasla hücre sıcaklığı sırasıyla %24 ve %22,3 oranında azalmıştır. Ayrıca 3,5l/min debide CuO ve Al_2O_3 kullanıldığında elektriksel ve termal verimde sırasıyla %10 ve %40.7, %9.1 ve %38 artış bulunmuştur. Deneysel ve sayısal çalışma arasındaki toplam fark (hata) yüzdesi, 3,5 l/dk'da ΔT (giriş ve çıkış arasındaki sıcaklık farkları) için %8,7 ve toplayıcının yüzey sıcaklığı için %3,1 bulunmuştur.

Anahtar Kelimeler : Düz plakalı güneş kolektörü, güneş enerjisi, nanoakışkan, ısıl verim.

Bilim Kodu : 91408

ACKNOWLEDGMENT

Praise be to Allah and May God's peace and blessings be upon our master Muhammad. I would like to express my deep gratitude to my supervisor Assoc. Prof. Dr. Engin GEDIK and Assist. Prof. Dr. Basam Asaad Shallal SHALLAL for giving me all the important information during this Work. I would like to express my gratitude to the staff of (Nano materials Laboratory) at the University of Technology for help and support through this Research. Finally, I also thank my family for their help Encouragement and different types of help as well as for whom Somehow help me get this work out. God Give health and happiness to all of them.

CONTENTS

Page

Page

Page

Page

LIST OF FIGURES

Page

Page

Page

Page

LIST OF TABLES

Page

SYMBOLS AND ABBREVIATIONS

SYMBOLS

A*c*	:	Area collector channel surface
A	:	Area of the PV module m^2
Ac	:	Area of collector m^2
AL	:	Altitude of location above mean sea level km
AM	:	Air mass kg
Bv	:	Viscous friction coefficient Nms/rad
Cp	:	Specific heat capacity J/kg.oC
Cpf	:	Heat capacity of the base fluid J/kg.oC
Cpnf	:	Heat capacity of the nanofluid J/kg.oC
Cpp	:	Heat capacity of the nano particles J/kg.oC
D	:	Tube diameter m
De-s	:	Distance between the earth and the sun m
Dm	:	The mean sun earth distance m
dn	:	Number of days
Ece	:	Electrical energy produced by photovoltaic cell J
Ect	:	Thermal energy released by photovoltaic cell J
Eloss	:	Energy losses J
ET	:	Equation of time minutes
ET	:	RATE of solar energy absorbed by Tedlar (Back sheet) J
F	:	Friction factor
G (t)	:	Solar irradiation incident on the glass cover W/m^2
hc	:	Convection coefficient of fluid flow in the pipe $W/(m^2.K)$
hg	:	Convective heat transfer coefficient of the glass $W/(m^2.K)$
hs	:	Hour angle degree
Ia	:	Current in phase (*a*) A
Ib	:	Beam radiation W/m^2

Ib	:	Current in phase (*b*) A
Id	:	Diffuse radiation W/m^2
Imp	:	PV current at maximum power point under standard condition
Impp	:	Maximum power point current A
Io	:	Extraterrestrial solar radiation W/m^2
Isc	:	Solar constant
J	:	Moment of inertia kg-m^2
Kf	:	The base fluid thermal conductivity W/m.oC
Km	:	Motor constant Vs/rad
Knf	:	Thermal conductivity of the nanofluid W/m.oC
$K\rho$	:	Thermal conductivity of the nano particle W/m.oC
L	:	Latitude angle degree
La	:	Self-inductance in phase (a) mH
Lb	:	Self-inductance in phase (b) mH
LST	:	Local standard time hr
Lst	:	Standard meridian for local time zone degree
Nr	:	Number of the teeth on the rotor
P	:	Cell packing factor
Pmax	:	Maximum power W
qc	:	Heat flux which transferred to the fluid flow in the cooling pipes
R	:	Resistance in each phase ohm
ST	:	Solar time hours
Ta	:	Ambient temperature oC
Tc	:	Cell temperature oC
Te	:	Electromagnetic torque Nm
Tg	:	Glass temperature oC
Tin	:	Inlet temperature of the cooling fluid oC
Tl	:	Load torque Nm
To	:	The temperature of standard condition oC
Tout	:	Outlet temperature of cooling fluid oC
V	:	Wind speed m/s
Vmp	:	PV voltage at maximum power point under standard condition
Vmpp	:	Maximum power point voltage V

VNP	:	Volume of the nano particles m^3
VT	:	Total volume m^3
αs	:	Solar altitude angle deg
γz	:	Solar azimuth angle deg
ϕ	:	Volume concentration ratio of the nano particles
v	:	Kinematic viscosity m^2/s
va	:	Voltage in phase (a) V
vb	:	Voltage in phase (b) V
λ	:	Wavelengths μm
αc	:	Cell absorptivity to sunlight
αg	:	Absorptivity of glass
αnf	:	Thermal diffusivity of nanofluid m^2/s
αT	:	Absorptivity of the Tedlar
β	:	Temperature coefficient of silicon cell
δs	:	Sun's declination angle deg
εg	:	Emittance of the glass
ηel	:	Electrical efficiency
ηo	:	Nominal electrical efficiency under standard condition
ηth	:	Thermal efficiency
$\eta total$	:	Total efficiency
θ	:	Module inclination to the horizontal deg
θi	:	Incident angle deg
θz	:	Zenith angle deg
μnf	:	Nanofluid dynamic viscosity kg/m.s
μw	:	Water dynamic viscosity kg/m.s
ρf	:	Density of the base fluid kg/m^3
ρnf	:	Density of the nanofluid kg/m^3
ρp	:	Density of the nano particles kg/m^3
τg	:	Transmitted through the front glass
Re	:	Reynolds number
Nu	:	Nusselt number

Pr	:	Prandtl number
Pe	:	Peclet number
el/insul	:	Electrical/insulator
f	:	Fluid
nf	:	Nano fluid
p	:	Particle
e-s	:	Earth to sun
el	:	Elictrical
th	:	Thermal
loss	:	Losses
T	:	Tedlar
C	:	Cell
g	:	Glass
b	:	Beam
np	:	Nano particles
d	:	Diffuse
a	:	Ambient
in	:	Inlet
out	:	Outlet

ABBREVIATIONS

AC	:	Alternating current
AL_2O_3	:	Alumina oxide
CdS	:	Cadmium sulfide
CNT	:	Carbon nano tubes
COP	:	Coefficient of performance
CPC	:	Compound parabolic concentrator
Cu2S	:	Copper sulfide
DC	:	Direct current
ETR	:	Extraterrestrial solar radiation
EVA	:	Ethylene vinyl acetate
FPPV	:	Flat plate photovoltaic

PV/T	:	PV/T
HSM	:	Hybrid stepping motor
IPVTS	:	Integrated photovoltaic and thermal solar system
IR	:	Infrared
LDR	:	Light Dependent Resistors
LFR	:	Linear Fresnel Reflector
MPPT	:	Maximum power point tracking
Mtoe	:	Million tonne of oil equivalent
MWCNT	:	Multi-Walled Carbon Nano tube
PLC	:	Programmable Logic Controller
PV	:	photovoltaic
PV/T	:	photovoltaic/thermal hybrid system
SWH	:	Solar water heater
TiO_2	:	Titanium oxide
TPT	:	Tedlar/Polyester/Tedlar
TW	:	Trillion Watt

PART 1

INTRODUCTION

1.1. STUDY BACKGROUND

The world is in its search for new sources of energy to replace fossil fuel which is causing catastrophic damage to our environment and to also meet the increasing demand for energy to keep pace with the rapid technological development and massive population growth [1]. There are many sources of clean energy that humans can use such as solar energy, wind energy, biomass energy, tidal energy, geothermal energy, etc. [2]. Solar energy is one of the most popular and widespread types of clean energy and that is because it is considered one of the safest sources. The Earth annually receives solar energy that exceeds the amount of the total amount of annual consumed energy by humans. The utilization of this huge amount of solar energy will help in protecting the environment and strengthening the global economy and reducing harmful emissions [3]. To benefit from incoming solar radiation, it is converted into other types of energy to facilitate storage, transportation, and use for different needs. There are two main ways of conversion of solar radiation to other types of useful energy. The first way is the solar thermal system (T) and the second way is the solar photovoltaic cell [4].

Photovoltaic Cells (PV) are devices made of semiconductor materials that is used to convert solar energy to electrical energy in the form of a constant current. It is manufactured in different sizes and can be linked together in the form of arrays in series or parallel circuits according to use. The efficiency of the photovoltaic cell increases with the increase in solar radiation while its generation efficiency decreases with the increase in Photovoltaic Cell temperature above the standard temperature. Electricity is generated when sunlight falls on solar cells. PV cells usually consist of two layers. The first layer (P) has a positive charge while the second layer (N) has a

negative charge. The point of intersection of the P and N layers in PV cells is called the P-N junction. The P-N junction acts as a passageway for electrons which move by solar photon effect [3].

Photovoltaic solar cells can be divided into several types, including [4]:

1. Mono crystalline silicon photovoltaic cells: they are produced from strips that are cut from a single cylindrical crystal and it has high efficiency compared with other types of photovoltaic cells.
2. Polycrystalline silicon photovoltaic cells: These cells consist of very thin strips cut from an alloy of crystalline silicon after melting. It is characterized by its low manufacturing cost and at the same time its low efficiency.
3. Thin film silicon photovoltaic cells: they are made by depositing a thin homogeneous layer of silicon on a solid or flexible substrate according to the user's need. This technology is characterized by ease of manufacture and low cost, while at the same time characterized by low efficiency.

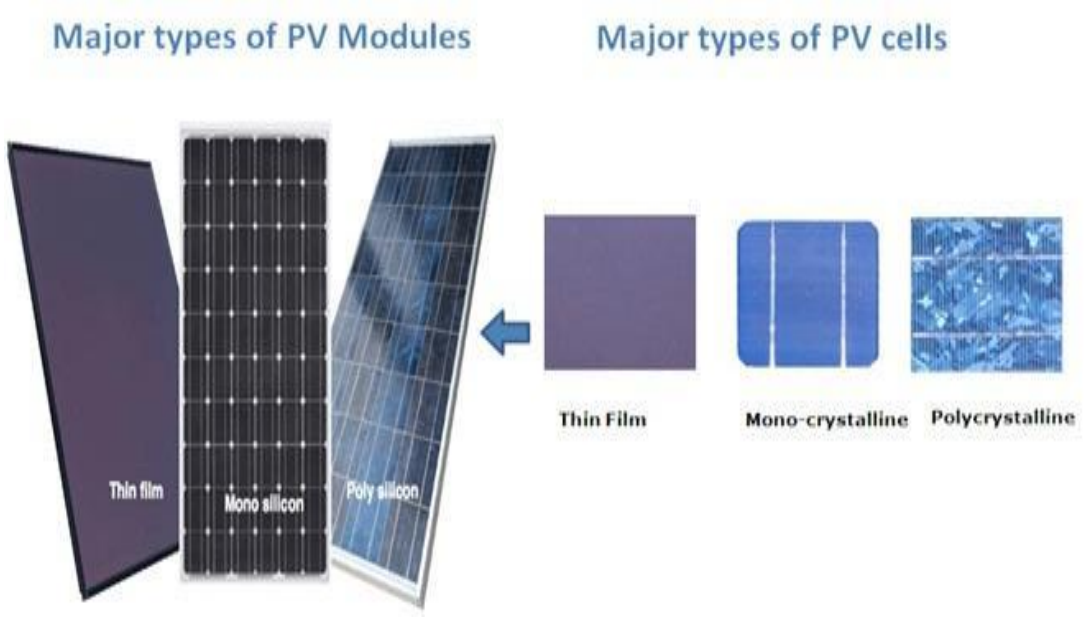

Figure 1.1. Pv panels types [5].

PV panels are highly and directly affected by temperature. Efficiency of PV panels decreases when temperature is increased.

PV panels are designed to work in specific conditions depending on the geographic region they are used in. For example, there are some PV panel which work with the highest efficiency at these conditions: (1000 W/m2 solar radiation and 25° C), and thus the efficiency decreases when the temperature increases over 25° C, therefore, researchers implement methods to decrease overheating. One of these methods is using PV/T system [6].

1.2. FLAT PLATE SOLAR COLLECTOR SYSTEM

It is a device that converts solar energy into thermal energy by heating the fluid passing through it. This energy can be used directly or stored and then used later. The solar thermal system or solar heater, or solar collector is made up of a flat metal plate that receives and absorbs solar radiation. This metal plate is isolated from five sides by a thermal insulating material that prevents heat from leaking out. The plate receives radiation from the sixth exposed side through a glass sheet. Solar collectors are classified into two categories in terms of the type of heat transmitting fluid used in them.

The first type is the air collector: this is a type of a solar heater where air is passed into the system from an entry hole to slide over the relatively hot metal plate to raise its temperature before it exits the system to be used directly in many applications such as heating, drying, and others [7].

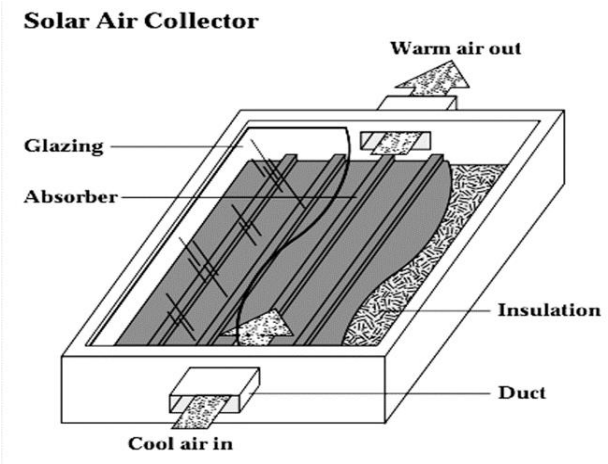

Figure 1.2. Air collector [7].

The second type is water collector: this is a type of solar heater where water passes through metal tubes in contact with the flat metal plate. The water absorbs heat from the plate then exits the system at a higher temperature. The heat either gets directly used, stored, or transferred to another type of energy to be used later [8].

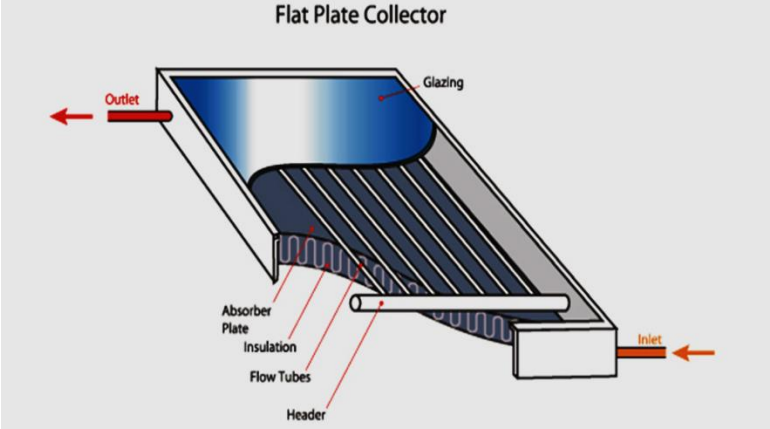

Figure 1.3. Water collector [8].

Solar collectors can also be classified according to the required temperature.

The first type is low temperature solar collector.

It is used in applications that require low temperatures. It works on increasing temperatures 10-20 ℃. It is usually used in heating swimming pools and is of a flat plate type and does not usually contain a glass cover.

The second type is medium temperature solar collector.

It is used in applications that require a temperature increase of up to 70 ℃. It has multiple types such as flat plate solar thermal collectors and evacuated solar thermal collectors. The evacuated solar thermal collectors consist of a closed metal tube with a black copper fin attached to it. The tube is affixed inside an airless glass tube. The metal tube contains a small amount of a liquid with special thermal specifications which evaporates when it absorbs the heat of radiation. The heat of the vapor heats up the heat transfer fluid. After losing its heat, the liquid condenses and the cycle repeats and so on. Additionally, the PV/T is very similar to the low temperature flat plate

collector except that it contains a glass cover which traps in the heat. Medium temperature solar collectors are used to heat water for domestic and industrial uses. The last type of high temperature solar collector One type of this high temperature solar collector is the concentrating solar collector, which contains parabolic shaped reflective plates that focus heat energy on a focal point or on a central axis where the heat transfer fluid flows. It is used for applications that require high temperatures that may reach 300 ℃. For example, it is used in electrical power plants, where the steam produced by this type of collector is used to produce mechanical energy by rotating turbines to generate electrical power. The efficiency of this type of collector can be increased by using fluids with a high boiling point, such as thermal oils [9].

When we connect a flat plate thermal solar collector with a photovoltaic solar panel, we get a hybrid device which is named PV/T. By affixing the photovoltaic panel directly to the absorbent flat plate, we maintain the efficiency of the electrical generation of the photovoltaic solar cell and not allow its temperature to rise as that heat will be repurposed as the thermal solar collector absorbs heat from the cell and thus this hybrid collector will provide us with electrical energy and thermal energy at the same time.

This (PV/T) is divided into several types depending on the type of solar thermal collector used, as well as on the type of fluid used to transfer the heat.

The first type is PV/T air collector: it uses air as a heat transfer fluid and is either one-pass or two-pass, and there are many designs of passages to allow the air to absorb as much heat as possible from the photovoltaic cell. The second type is PV/T water collector. This type of photovoltaic collector uses water as a heat transfer fluid and has been manufactured in a variety of designs to allow the water to absorb as much heat as possible from the photovoltaic cell. The third type is called compound thermoelectric solar collectors which consists of special passages for air and others for water. Those passages surround the cell, with different designs for the purpose of cooling the solar cell and at the same time benefiting from the heat taken in many thermal applications [7].

1.3. NANOPARTICLES ADDITIVES

To improve the heat transfer efficiency of the used conventional fluids (water, thermal oils, etc.), solid materials are added in nanosizes with good thermal specifications and high conductivity, which gives a noticeable increase in the heat transfer efficiency of the base fluid. These fluids are called nano fluids.

Nanofluid are compounds of a base liquid mixed with a solid substance. The solid substance contains nanoscale sizes ranging from 1-100 nano meters. These materials are mixed with the liquid in studied proportions to give the nanofluid additional specifications in thermal conductivity and heat transfer substances [10].

There are many types of nano particles such as metal and metal-oxide based nano particles, carbon based nano particles, and nanocomposites as is shown below [11].

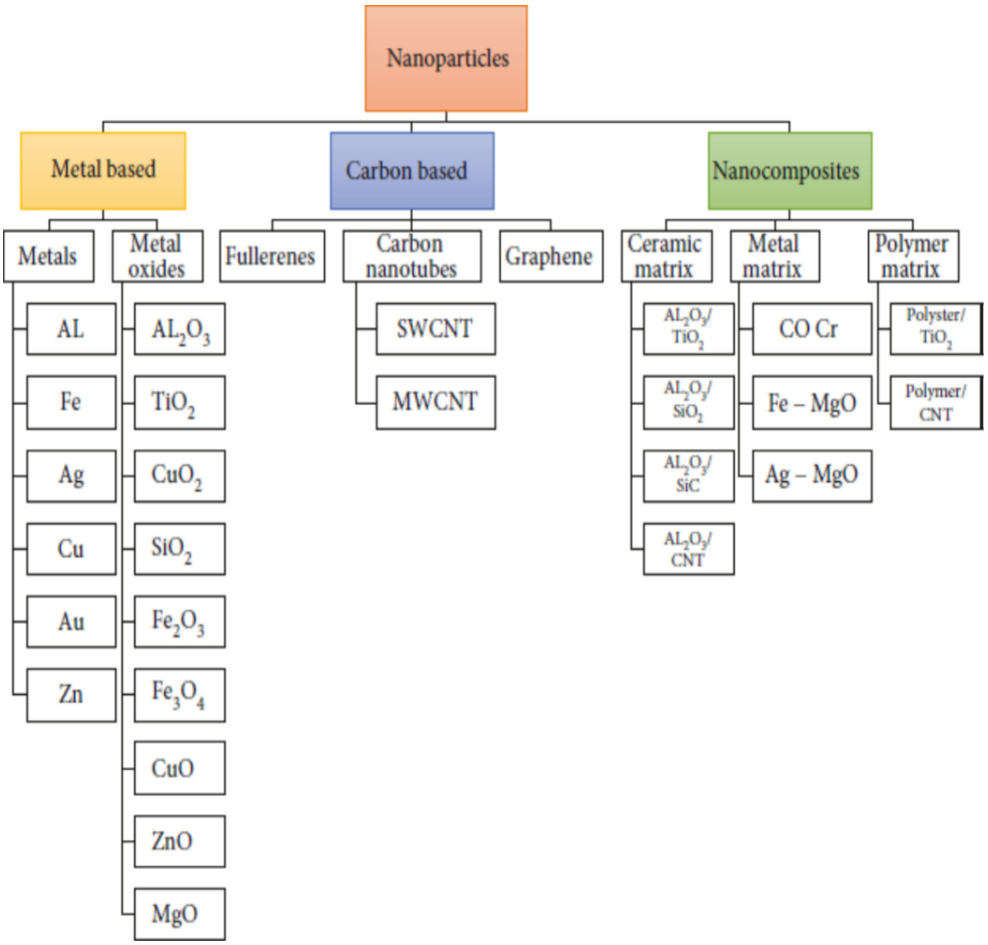

Figure 1.4. Nanoparticles types [9].

For nano particles to be used, they must be mixed with a base fluid. There are many types of base fluids to which nano particles are added to form nano fluids, including: (water, ethylene glycol, water/ethylene glycol mixture, vegetable oil, PAO oil, transformer oil, naphthenic mineral oil, diathermic oil, paraffin oil, and SAE oil [12].

Nanofluid has different properties which depend on the type of base fluid, size and shape of nanomaterials, and concentration of nanofluid. Nanofluid have some important properties such as [13]:

1. Thermal conductivity: nanofluid have a relatively higher thermal conductivity than the base liquid because they contain high conductivity nanoparticles.
2. Density: an important characteristic of nanofluids because it is closely related to the pumping capacity to circulate the liquid within the system, as the required capacity for pumping increases with the increase in density.
3. Specific Heat: is the amount of heat required to raise the temperature of the unit mass of a given substance by a given amount.
4. Heat Transfer by Convection: compared with base fluid, the suspension of nanoparticles notably increases the heat transfer coefficient by convection.

1.4. PROBLEM STATEMENT

Photovoltaic (PV) solar cells convert solar energy from the sun into electricity. Photovoltaic cells are produced by semi-conducting materials to convert the energy into electricity and during this process heat is absorbed by PV cells. This heat causes a loss of electricity generation efficiencies. Many studies are using PV/Ts (PV/T) for PV panel heating reduction in order to increase the power supply in power storages. In industry, cost saving is the most concern by reduced power consumption. The temperature reduction for PV panel by using nanomaterial's additives to water for PV/T increases power generation and improve the cooling process for PV panel therefore, in this current study, the new model of PV/T was applied to cooling the PV panel after enhancing the flat collector performance by add different types of nanoparticles to water for increase heat transfer rates. The investigation of PV/T has been performed and evaluated using experimental and numerical methods.

1.5. RESEARCH OBJECTIVES

The primary goal of this research is to fabricate, characterize and evaluate outdoor conditions on the performance of a nanoadditive to water in PV/T system integrated with thermal loss system. Specific objectives of this work are:

1. To investigate the augmentation of thermal energy loss from PV panel with nano additive materials to water on the solar collector performance**.**
2. To assess the influence of nanomaterial types on the cooling rate and development of the PV/T system **.**
3. To computationally simulate the transient thermal behavior of the integrated solar collector system using ANSYS and compare with experimental data

1.6. SCOPE OF WORK

In this current study, the new model of PV/T was applied to cooling the PV panel after enhancing the flat collector performance by adding different types of, nanoparticles to water for increase heat transfer rates. The investigation of PV/T has been performed and evaluated using experimental and numerical methods

1.7. THESIS DESIGN

The following chapters make up this thesis: introduction, literature review, research methods and theoretical work, experimental work, findings and discussions, conclusions, and suggestions. Each chapter's summary is presented below: Chapter one presents the study's background, highlighting the history of PV cells, PV panel types, the flat solar collector PV/T application in PV/T system, enhancement nanofluid alter the physical and thermal properties of water. Issue statements, research objectives, and area of study are also given.

The second chapter provides an overview of PV/T system, experimental and theoretical background on PV/T models, explanation, and discussion on the collector

design characteristics in different types and a review of using nanomaterials to enhancement thermal properties of water to improve heat transfer in PV/T system.

The third chapter discusses research technique and theoretical simulation, including the determination of the numerical simulation for the PV/T system. Modeling configuration is used to create the model. Assumptions, as well as the governing equations that determine the PV/T model's behavior have been given. The numerical solution of governing equations (mass, energy, momentum) has been done. The ANSYS Fluent 17 commercial program was used to perform numerical simulation.

The fourth chapter describes the experimental setup and measurement methodologies for a PV/T system influenced by nanomaterial additions. To conduct an experimental investigation of this topic, PV/T performance was determined using thermal measuring methods. The CFD simulation findings were validated using experimental data. The fifth chapter reviews the findings and gives the analysis, which is divided into:

1. The findings of the PV/T system experimental models,
2. The findings of the numerical simulation of the sensitivity analysis of PV/T system performance are given.
3. Validation and comparisons of simulation results with experimental data.

Chapter six contains the work's results as well as ideas for further development.

PART 2

LITERATURE REVIEW

2.1. INTRODUCTION

Several research papers have investigated the effect of cooling in a PV/T system on the performance of a photovoltaic cell. Some of them used air as a cooling fluid, others used water as well as nanofluid as cooling fluids to improve the performance of solar collectors. The main field of application of the PV/T system is power generation and thermal application. Different designs of collectors were used, and their performance was studied under different conditions.

2.2. PV/T AIR COLLECTOR

Bashria et al. [14] studied two types of solar air heaters by mathematical simulations which the first type is single-pass and the second type is double-pass. She used A V-shaped cavity absorber with both types. She showed when use the porous media in the double-pass heater has increased the efficiency by 7% and she concluded that the efficiency of the double-pass heater was increased by 4-5%.

Ozgen et al [15] studied double-pass solar collector experimentally for heating air. In the study, some cans from aluminum were added to the lower and upper ducts of the collector at the absorber plate to increase the rate of heat transfer. They tested three types of collectors' thermal efficiency. One of them is aluminum cans arranged in a zigzag shape. The other aluminum cans were arranged systematically, and the third one, there were no aluminum cans. The air flow rates were 0.03 and 0.05 kg/s. They concluded the highest efficiency with a flow rate of 0.05 kg/s.

Bakari et al [16] studied the effect of glass thickness on the performance of the solar air collector experimentally. Glass with thickness 3, 4, 5, and 6 mm used with four solar collectors with an inclination angle of 10 degrees. He showed that the efficiency of the solar collector was 27.8% when using glass 6 mm thickness and the efficiency of the solar collector was 35.4% when using glass with a thickness of 4 mm.

2.3. PV/T WATER COLLECTOR

Several researchers used water as a coolant in solar thermal collectors (PV/T) systems to study the effect of cooling on the performance of the photovoltaic cell. All studies demonstrated a significant increase in the electrical efficiency of the cell compared to the same cell without the use of cooling.

Swapnil Dubey et al [17] used water only as a coolant for the purpose of studying the performance of the PV/T system. For two different types of thermal collectors (A) and (B), as shown in the figures, the electrical and thermal efficiency of Figure (A) was 11.8% and 40.7%, respectively, and for the thermal collector of type (B) was 11.5% and 39.4%, respectively.

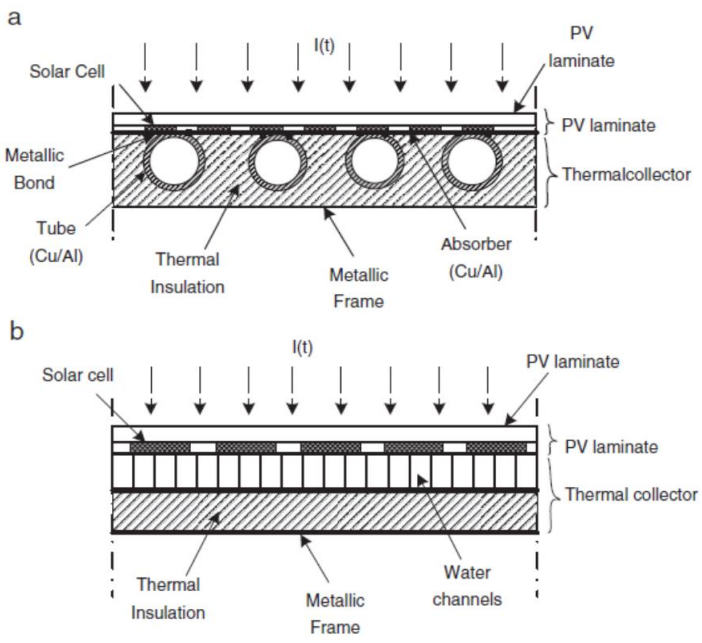

Figure 2.1. The thermal collectors (A) and (B)[17].

Johana et al. [18], used two types of photovoltaic cells, the first type is monocrystalline silicon photovoltaics, and the second type is polycrystalline silicon. Two pieces of each type were used, one of them was connected to a solar thermal collector, while the second cell was left without a solar thermal collector. Water was used as a coolant in the solar thermal collector, and it was concluded through practical experience that the temperature of the photovoltaic cells connected with the solar thermal collector does not exceed 35 ℃compared to the other uncooled cell whose surface temperature reaches 60 ℃.

Kazem [19] used water as a coolant in a solar thermal collector (PV/T) system to study the performance of a photovoltaic cell in Amman, Jordan, and compared it with the performance of a conventional cell. The result was the output power rate of PV/T panel is 6% higher than the average power of traditional PV panels.

Bishal Podder et al. [20] studied the performance of a thermoelectric system (PV/T) using water as a coolant in northeastern India. They used several values for the water flow rate (1 to 4 liters per minute) and obtained thermal efficiency values ranging from (33.14% to 45.55%) and electrical efficiency ranging from 9.99% to 10.2% at a radiation rate of 643.51 Watts per square meter and an ambient temperature of 24.3 ℃. The highest overall efficiency of the system was at a flow rate of 4 liters per minute with a value of (72.12%).

Singh et al. [21] used water only as a coolant for the purpose of studying the performance of the PV/T system and compared to the performance of the same cell without cooling, where the water passed through a 6.35 mm diameter copper pipe network installed on the copper absorption plate. It has been noticed that an increase in electrical efficiency by up to 6.08% at mass flow rate 0.0166 kg/sec compared to the photovoltaic system alone, open circuit voltage and short circuit current increases 3.45% and 2.4%, respectively and 15.23% reduction in temperature.

2.4. COOLING THE COLLECTOR BY NANOFLUID

In recent years, the use of nano fluids has become widespread, especially in the applications of heat transfer and the utilization of solar thermal radiation due to their good physical and chemical properties.

Researchers conducted many different experimental and theoretical studies to examine the effects of nano fluids on the efficiency of solar photovoltaic cells by controlling the type and percentage of nano material added to fluid, the volumetric flow rate of the nanofluid, the concentrations of solar radiation, and other variables. Also recording the difference in the efficiency of cells for each of these variables was essential and comparing it with the performance of the photovoltaic solar cell alone or cooled with water only and without nano - additives. Some of those are as follows:

Sardarabadi et. al [22] used silica (SiO_2) with water as a nano -cooling fluid in a solar thermal collector with mixing ratios by weight (wt. %) 1% and 3%. They concluded that the overall efficiency of the system increases by 3.6% in the case of using nanofluid with 0.01 percent than when using pure water and it increases by 7.9% when using nano fluids with a mixing ratio of 0.03.

Al-Shamani et. al [23] used different nanoparticles (SiO_2, TiO_2 and SiC) with water as a coolant in the (PV/T) system to study its effect on the performance of the cell. They found that the highest thermal efficiency obtained was 81.73% and electrical efficiency was 13.52% when using (SiC) material with a flow rate of 0.170 kg/s and a solar radiation level (1000W/m2).

Gangadevi et. al [24] used Al_2O_3/water as a coolant in the (PV/T) system to study its effect on the cell performance, where (1%wt) and (2%wt) of the nanoparticle were used with a volumetric flow rate (40 l/h) and got the highest efficiency value. 13% electrical and 45% thermal efficiency at a mixing ratio (2%wt).

Al-Waeli et. al [25] the researcher used (SiC) (3% by weight with water) as a coolant for the purpose of studying the performance of the PV/T system. The researcher

noticed an increase in electrical efficiency by up to 24.1% compared to the photovoltaic system alone, while thermal efficiency increased by up to 100.19% compared to using water for cooling.

Hassan et. al [26] used SO_2, SiC, TiO_2//water (1wt%) and as a coolant in the (PV/T) system to study its effect on cell performance, where they concluded that the highest efficiency was achieved when using (SIC) and the highest electrical efficiency was 12.7% and thermal efficiency 85%.

Sardarabadi et.al [27] designed and fabricated two PV/T and PVT/PCM systems and investigated the positive effects of using these collectors as cooling systems for photovoltaic modules. The researcher chose to use a ZnO/water nanofluid with 0.2 wt% as a nanofluid coolant. It was found that the temperature of the PV/T fluid/nanofluid coolant system with a PCM medium reduced by more than 16 degrees, while a PVT system which used deionized water or nano fluids only as coolants which reduced the cell temperature by only about 10 degrees in comparison with the conventional PV module. Additionally, the PCM/nanofluid based collector system's average electrical output increased by about 13% compared with the conventional PV module. Compared with the case of the water-based collector without PCM medium, there was a 42% increase in the average thermal energy output of the PCM/water-based collector.

Al-Waelia et.al. [28] as part of a techno-economic analysis on a Grid-Connected Photovoltaic Thermal system, the researchers discovered that using nano fluids as coolants instead of water reduced PV module temperature by 28.1%, increased thermal energy by 1129%, and increased thermal efficiency by up to 89.75% when compared to water.

Aberoumanda et. al [29] used pure water and Ag/water nano fluids (at concentrations of 2 wt% and 4% wt%) as working fluids in a PV/T system and compared the performance indicators of the system. They discovered that there is a greater positive effect in efficiency when using Ag/water nanofluid rather than pure water. This becomes more evident when the nanofluid concentration and flow rate are increased.

The power output of the plate increased by 35% and 10% when using 4 wt% nanofluid compared to no cooling and water cooling, respectively.

Younis et al [30] In this research, pure water was used as a coolant in a solar thermal collector system and compared with the use of a nanofluid consisting of water and Al2O3-ZnO mixed with ethylene glycol as a surfactant. The particle size used (10-30 nm) recorded an increase of 4.1% in Overall system efficiency as well as a 4.6% increase in usable energy efficiency.

Sharafeldina et.al. [31] studied a nanofluid of CeO_2-water as a working fluid They have tested three different volume fractions of 0.0167%, 0.0333%, and 0.0666% at three mass fluw rates, which were 0.015, 0.018 and 0.019 kg/s m2.The researcher was able to elucidate from the results that using CeO_2-water nanofluid increased the efficiency of the solar collector more than using only water.Findings stated that the maximum efficiency was 10.74%, volume fraction (φ) was 0.066% and mass flux rate was 0.019 kg/s m2.

Rukman et. al [32] conducted an experimental study on the performance of the (PV/T) system using TiO_2 and MWCNT as a heat transfer nano fluid. They used a mass flow rate (0.012 kg / sec to 0.0255 kg / sec) and solar radiation intensity (500 W/m2 to 900 W/m2). The researcher obtained the lowest temperature of the photovoltaic cell and extracted the highest difference in the temperature of the cell at a concentration of 1.0% TiO_2 which is 2.01 °C and 1.80 °C.

Rukman et. al [33] the researcher used TiO2/water (0.5wt% and 1.0wt% TiO2 in water) nano fluids as coolant in (pv/t) system to study its effect on cell performance with solar-radiation levels of 700 and 900 W/m2 and mass-flow rate (0.012 kg/s to 0.0255 kg/s).

Where the researcher obtained the efficiency of the (pv/t) system ranging from 75% to 90% compared to the efficiency of the solar cell alone and without cooling, which ranged between 9.9% to 10.6%. In addition to obtaining a thermal efficiency ranging from 65% to 80%.

Al-Waeli et al [34] the researcher used sic // water (3wt%) and nanoPCM with concentrations (0.1%, 0.5%, 1%, 2%, 3%) as coolant in the (pv/t) system to study its effect on the performance of the cell with, where the researcher obtained an electrical efficiency 13.7% and 72% thermal efficiency.

Wole-Osho et. al [35] the researcher used Al2O3-Zno/water as a hybrid coolant in the (pv/t) system to study its effect on the performance of the cell, where he concluded that the highest efficiency was achieved when using (0.47) a mixing ratio of (Al2O3) as an ideal ratio to obtain the highest efficiency of the system and it was the highest electrical efficiency 13.8% and 55.9% thermal efficiency.

Yuting Jia et. al [36] the researcher performed a numerical analysis of a solar thermal collector system for the purpose of studying the effect of some operational elements on the performance of the collector, where he used nano materials mixed with water as a coolant for the purpose of reducing the temperature of the photovoltaic cell. Where the researcher concluded that Al2O3/water gave better results than TiO2/water nanofluid at the same bump rate. The researcher also concluded that the electrical power produced when using nano fluids at a flow rate of 0.03 kg/s is higher than those values that were obtained using flow rates of 0.0005 kg/s, 0.001 kg/s and 0.01 kg/s.

Samylingam et.al. [37] the researcher investigates thermal and energy performance improvement of hybrid PV/T systems by using olein palm oil with MXene as a new class of heat transfer fluid with concentrations of 0.01, 0.03, 0.05, 0.08, 0.1 and 0.2 wt %. Improvement in thermal conductivity obtained reached a maximum of 68.5% at 0.2 wt % at 25 ◦C, also, this nanofluid provided in increase in heat removal from the PV/T system of 8.5% compared to alumina nano fluid. There was also an increase in electrical efficiency by 13.8% and thermal efficiency by 11.2% compared to alumina Nanofluid.

Fadli1 et al [38] the researcher used (Tio2) with a mixing ratio of 0.5% vol with water as a basis for a cooling fluid in a solar collector and at a radiation density of 1100 watts per square meter in the country of Indonesia, where the coolant reduced the working

temperature of the solar panels by 11.4 ℃, as well as increasing the resulting energy by 10.38W and 2.69% efficiency compared to PV panels without cooling.

Bharathwaj et al [39] in this study, the researcher used CuNP nano particles with mixing ratios of (2.5, 4, 5, 7.5) (V%) by volume% in a flat panel solar water heater. The study included two parts: an experimental and a simulation. Simulation was performed using ANSYS software. The simulation was validated through experimental data, where it was found that the best mixing ratio of 4% of CuNP was to give the best heat transfer improvement. For minimal pumping power.

Adun et al [40] the researcher studied the effect of ternary hybrid nano fluids consisting of CuO-MgO-TiO2 on the performance of a photovoltaic cell using it as a coolant in the pv/t system. By changing the volume fraction, solar irradiation, and mass flow rate, the study showed that at the optimum volume fraction of 0.01, the maximum cell temperature drop was 8.24 °C and at a mass flow rate of 0.1 kg / s. Where electrical efficiency of 13.54% was calculated. thermal efficiency 58.38% and energy efficiency 15.68%.

Sangeetha et.al. [41] the nano fluids were used as coolants to reduce the temperature in the PV panels at a constant volume ratio of 0.3%. After an analysis of the results, it was found that the use of nano fluids showed significant results in thermal efficiency, electrical output, and overall efficiency. The nano fluids MWCNT, Al2O3, and TiO2 reported 47%, 33% and 27% improvement in electrical efficiency respectively and 45%, 36% and 25% increase in electrical power.

From the fluids used, MWCNT proved to have superior thermal conductivity and better physical properties than Al2O3, TiO2, and water. The panel's temperature was reduced by 27%, 26% and 26.5% respectively for MWCNT, Al2O3, and TiO2 when there was an increase in the mass flow rate of the nanofluid from 0.08 kg/s to 0.20 kg/s. The nano fluids MWCNT, Al2O3, and TiO2 reduced the PV cell's temperature by 48%, 37% and 36% respectively.

Saeed Abdul-Ganiyu et.al. [42] the researcher studied the effect of mass flow rate on a water PVT system in the dynamic tropical environment of Ghana an experimental study. The performance of PVT was studied for mass flow rates of 0.025 kg/sec and 0.083 kg/sec. specific solar energy radiation, no significant change in unit temperature occurs when the flow rate is increased above 0.082 kg/sec.

PVT demonstrated a constant power efficiency of about 12.75% at the mass recommended by manufacture. The flow rate is 0.033 kg/sec regardless of radiation. Although the energy-saving efficiency of PVT generally exceeds 50%, its thermal efficiency from 38.8 to 43.1% was below average compared to experimental (non-commercial) PVT systems. This can be attributed to the poor thermal contact between the photovoltaic layer and the thermal absorber in the studied PVT unit.

PART 3

METHODOLOGY OF RESEARCH AND THEORETICAL WORK

3.1. CHAPTER OVERVIEW

This chapter discusses the technique and theoretical analysis used to meet the study objectives, as well as the numerical approach and novel models. The entire numerical research is included in the new PV/T collector model. The simulation was conducted using the ANSYS FLUENT 17.0 software and a new PV/T collector module. The CFD simulation is adopted to predict the collector performance for cooling PV panel under the influence of nanoparticle additives and changing of water flow rate conditions. They were used to two types of nano particle: CuO and Al_2O_3. The last section examines collector thermal performance, which is often expressed as usable heat production is a function of incoming solar radiation and collector operating temperature in respect to its surroundings.

3.2. RESEARCH METHODOLOGY

The flow chart in Figure 3.1. depicts the research topological sequence used in this study. A more detailed discussion of the experimental work will be provided later in Chapter 4. The numerical implementation combined the two methods utilized in this study. The two approaches contain; the first part included firstly, to draw of the collector geometry for new shapes bulges. Secondly, to simulate this model by using nano material additives CuO and Al_2O_3 mixed with water at different collector conditions. The second part included a mathematical approach was adopted and established to test flat plate photovoltaic panel systems with alone PV and with water cooling system PV/T to examine the heating effect on PV systems and tested the performance. The absorbed heat energy behind the photovoltaic cell's surface in

insulated ambient was removed by means of a water/nanofluid cooling system and the study for the system was a different condition.

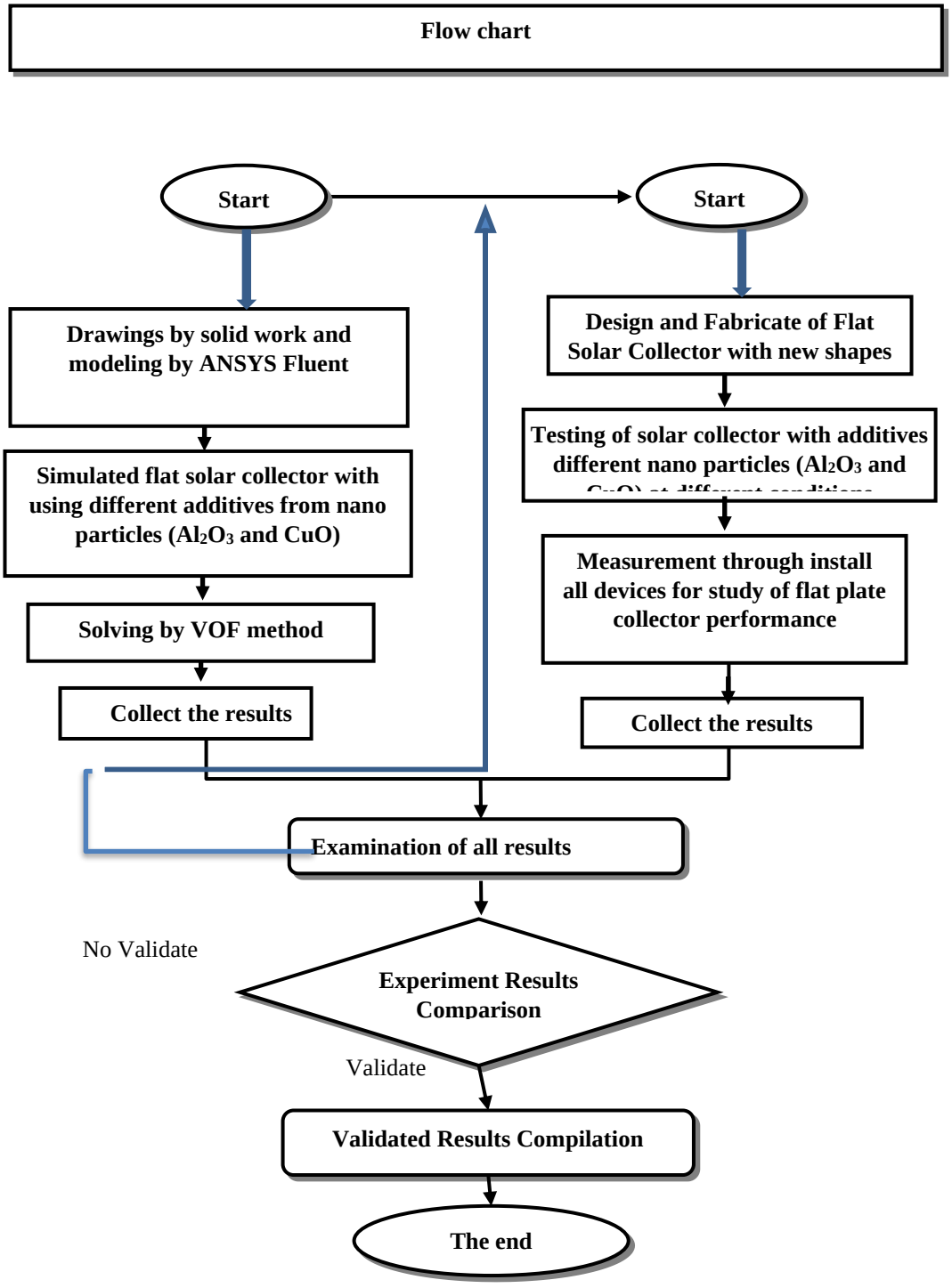

Figure 3.1. Research technique sequence flow chart.

3.3. CFD SIMULATION OF FLAT SOLAR COLLECTOR

For engineering applications, CFD simulation techniques are an effective tool for depicting mechanical problems and understanding associated physical phenomena. The commercial CFD program ANSYS 17.0 FLUENT radiation model pre-processing tool (provides a solar load model with nano material additives mixed with water at different conditions. that may be used to calculate radiation effects) was utilized in the current simulation. sold work ver. 2019, are used to model the solar flat collector, there are various procedures that must be completed to run the simulations; these processes are depicted in Figure 3.2. The modelling is done in Solid work, and the mesh is then imported into the FLUENT Radiation Module for solution and post-processing as a solar collector issue. This simulation is divided into two parts based on the characteristic nanomaterials used to study the research targets, CuO and Al_2O_3. To predict the thermo-hydrodynamic behavior of the system, a full standard numerical model of PV/T simulation was built. The model solving technique was accomplished by computational coding in (ANSYS) software. The results of the model were confirmed by comparison with experimental measurements.

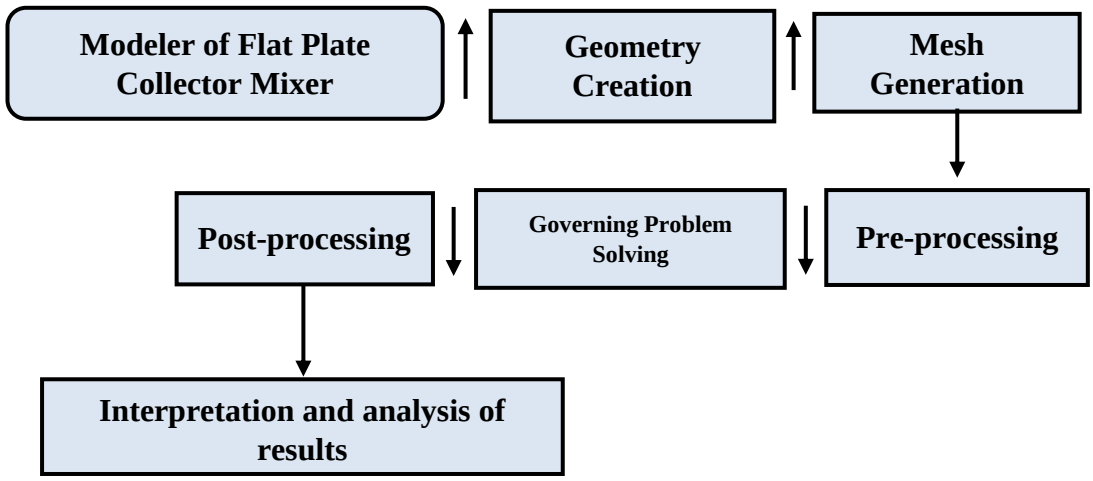

Figure 3.2. Procedures for Simulation in ANSYS 17.

3.3.1. Flat Solar Collector Pre-Processing

A computational fluid dynamics (CFD) model is used to investigate the heat loads for the different nano material additives to water and parameters, such as the inlet and

outlet water temperature, temperature distribution on collector surface. Preparing a computational domain is the first step in CFD simulation. A new 3D-dimensional flat plate collector model created with Solid work program model-SS. Table 3.1 shows the dimensions of the collector geometry collected from the experimental setup. The geometrical model of PV/T is shown in Figure 3.3. This collector is designed with sphere bulges. The dimensions of collector are (600×1100×30 mm). The water inner and outer pipe diameters of the collector are 13 mm. Sphere shapes of aluminum bulges at the total number 120 pieces are used. The sphere shape is 25 mm diameter.

Table 3.1. Dimensions of PV/T model.

Model	**Parameters**
Model-SS	Collector dimensions (600*1100*30 mm)
	Bulge shape (sphere)
	Bulges no. (120 pcs)
	Bulge dia.(25mm)

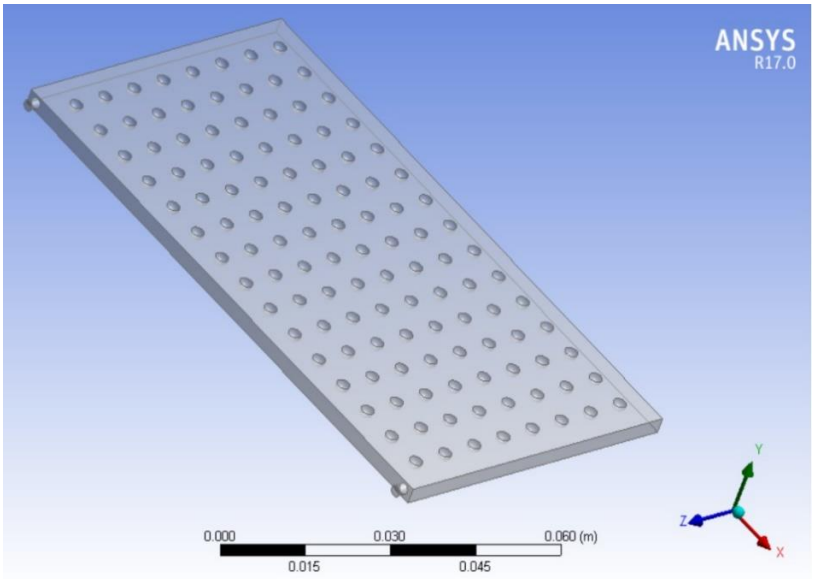

Figure 3.3. Computational domain prepared of flat collector model-SS.

3.3.2. Grid Computation

The development of the computational grid, which is made up of computational cells, is one of the most significant operations in CFD. The governing equations are solved

in computational cells. Unstructured meshing is used to mesh the collector domain with tetrahedral pieces. Because of the difficult geometry, unstructured tetrahedral meshing was used the optimal grid size is chosen in that point when the incresing in the grid size has no big effect on the solution. The highly precise and analogous out comes for the water velocities in the flow region, difference of temperature as well as surface of collector temperature beneath the effect of different values of water flow rates were determined when the fine mesh used. Therefore, this fine mesh was chosen for performing the simulations in addition to the interpretation of result. For all domain, 2.0× 106 number of cells selected in all simulations according to grid dependency as shown in Figure 3.4.

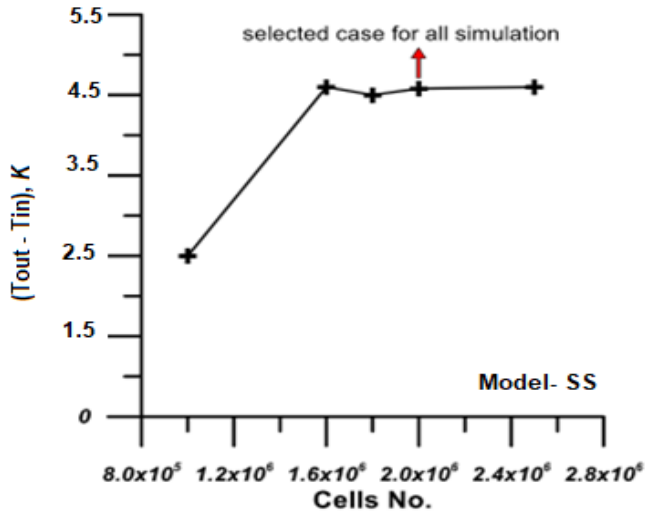

Figure 3.4. Cells selected for all simulation models.

The 3D meshed geometrical model of a flat solar collector is shown in Figure 3.4. It depicts the collector with (a) coarse, (b) medium, and (c) fine mesh. Figure 3.4 shows a closer look at the meshed bulges in the collector (d). The fine meshing system produced the most accurate and similar findings for heat transfer inside the collector, velocity, and temperature distribution behavior under the impact of different nano material additions. As a result, the tiny mesh was chosen for the simulations and result interpretation. Model-nodes SS's and fine mesh elements were 94844 and 523711, respectively.

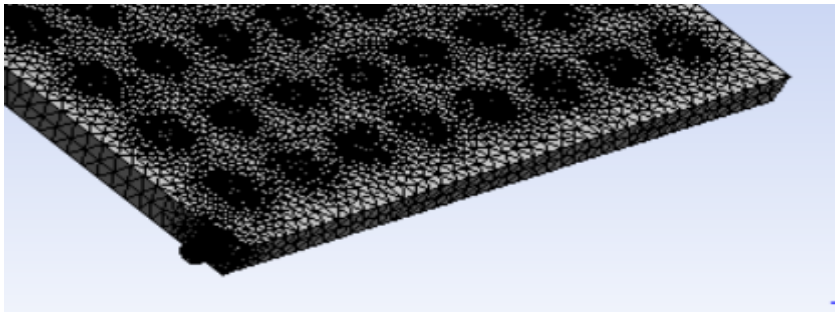

a. Coarse Mesh

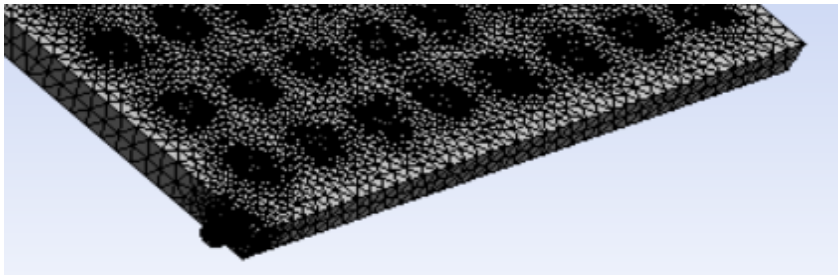

b. Medium Mesh

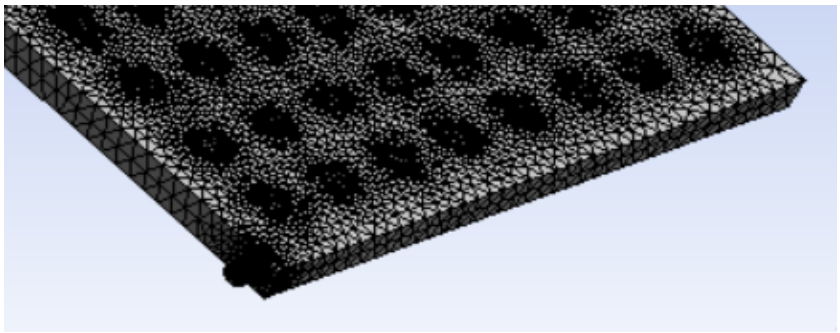

c. Fine Mesh

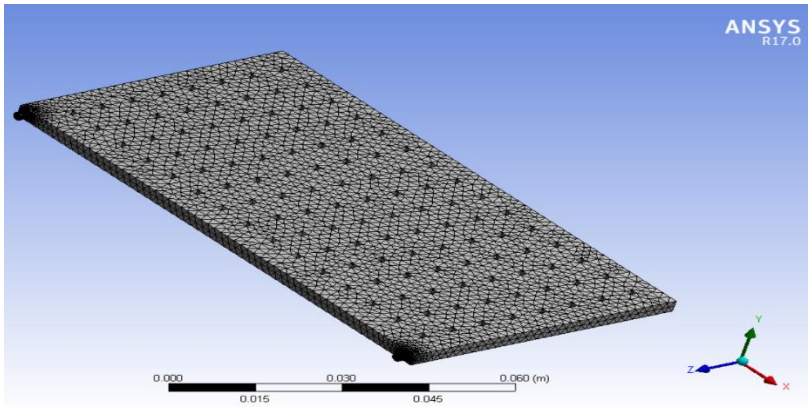

d. A close-up of the bulging form.

Figure 3.5. Geometrical mesh model of flat plate collector. a. Course mesh, b. Medium mesh, c. Fine mesh, d. A close-up of the bulging form.

3.3.3. Governing Equations Solving

Under turbulent and steady conditions, the PV/T model and domain were simulated in three dimensions. The governing equations of continuity, Navier-Stokes, and thermal energy are as represented in equations in 3D Cartesian coordinates [43].

- Using terminology to express each term of velocity components gives (continuity equation).

$$\frac{\partial \rho}{\partial t} + \frac{\partial}{\partial x}(\rho u) + \frac{\partial}{\partial y}(\rho v) + \frac{\partial}{\partial z}(\rho w) = 0 \tag{3.1}$$

- (Momentum equation);

$$\rho \frac{D\vec{V}}{Dt} = \rho \vec{g} - \nabla \vec{\rho} + \frac{1}{3}\mu \nabla\left(\nabla . \vec{V}\right) + \mu \nabla^2 \vec{V} \tag{3.2}$$

- (Energy equation);

$$\rho \, C_p \frac{DT}{Dt} = \nabla . K \nabla T + \beta T \frac{DP}{Dt} + \mu \emptyset \tag{3.3}$$

β is the coefficient of thermal expansion, defined as

$$\beta = -\frac{1}{\rho}\left[\frac{\partial \rho}{\partial T}\right]_p \tag{3.4}$$

Furthermore, the dissipation function is related to energy dissipation owing to friction. It is critical in high-speed flow and for extremely viscous fluids [44] is given in Cartesian coordinates by:

$$\emptyset = 2\left[\left(\frac{\partial u}{\partial x}\right)^2 + \left(\frac{\partial v}{\partial y}\right)^2 + \left(\frac{\partial w}{\partial z}\right)^2\right] + \left[\left(\frac{\partial u}{\partial y} + \frac{\partial v}{\partial x}\right)^2 + \left(\frac{\partial v}{\partial z} + \frac{\partial w}{\partial y}\right)^2 + \left(\frac{\partial w}{\partial x} + \frac{\partial u}{\partial z}\right)^2\right] - \frac{2}{3}\left(\frac{\partial u}{\partial x} + \frac{\partial v}{\partial y} + \frac{\partial w}{\partial z}\right)^2 \quad (3.5)$$

3.3.4. Simulation Analysis Parameters

The flat solar collector (PV/T) measured data from the experimental model is used to calculate the values of the PV/T system's input parameters, which are temperature, nano particles concentration (vol.%), and mixed mass rate. Table 3.2 shows the experimental parameters measured at the FPC's inlet and outflow, as well as on the collecting surface. The numerical simulation was then performed using identical experimental values. The FPC numerical simulation was completed successfully, with results compared to experimental data. Further assessment was accomplished by using significant values of the same parameters to investigate the impacts of increasing temperature, water/nano particles flow rate, and nano particles concentration (vol.%) on PV panel cooling. Table 3.2 contains the configuration of simulation variables. These parameters and variables were used as inputs to the CFD simulation, whereas the output parameters were related to temperature distribution, pressure distribution, velocity gradation of tangential and vertical components, and so on. In chapter four, the parameters (density, viscosity, specific heat, and thermal conductivity) of the two types of nano particles utilized are shown.

Table 3.2. Simulation parameters.

Model-SS		
Temperature (K)	Water flow rate (l/min.)	Initial-reference values
Tc_o = 303 to 357 Tw_{in}= 303 to 314 Tw_o = 325 to 345	1.5 2.0 2.5 3.5	Dencity =1000km/m^3 T_{amb}=303 k Viscosity=1.0016 kg/m.s Solar intensity 23 to 1112 Watt/m2 Gravitational acceleration for (z-axis) = -9.81 m/s^2
Nano particles concentration (vol. %)		
1% vol.	CuO diameter 40 nm	Al_2O_3 diameter 20nm
2% vol.		
3% vol.		

3.3.5. Setup of Numerical Solutions

The high degree of coupling between momentums equations created when rotational components have a significant influence causes the issues associated with solving swirling and rotating flows. A high degree of rotation generates a significant radial pressure gradient, which forces flow in both the axial and radial directions [45]. The following setup is one solution strategy that may be useful in whirling flow calculations:

1. "Pressure-Based" scheme and absolute velocity formulation were employed as the solver type.
2. Selecting a viscous model for turbulent flow: k-epsilon model using RNG approach; Near-wall treatment employs typical wall functions.
3. Zone materials include fluid water/nano particle for the PV/T interior and computational domain, solid aluminum for the top collector cover, and cubic and spherical bulges under the collector cover.
4. Table 3.2 describes the boundary conditions.
5. The solution approach employs "Pressure - Velocity Coupling" in conjunction with:
   - Simple scheme with zero skewness correction
   - Spatial discretization employs a "Green - Gauss Cell Based" gradient for linearization, a PRESTO scheme for pressure gradient, and second order upwind for the discretization of the non-linear equations of momentum, energy, turbulent kinetic energy, and turbulent dissipation rate.
6. Under - relaxation factors = 0.2 for pressure, and 0.5 for the rest (density, body forces, momentum, turbulent kinetic energy, turbulent dissipation rate, turbulent viscosity, and energy).
7. The solution starts with the initialization of pressure, X, Y, and Z velocities, k, epsilon, and temperature and continues until convergence is achieved. Finally, the results were graphically represented as contours, vectors, path lines, and XY plots.

8. The convergence criteria are fulfilled when the maximum mass imbalance ratio for each control volume is less than 0.01, the velocities and k-viscous are less than 0.001, and the energy is less than 10^{-6}.

3.4. PERFORMANCE OF PV/T COLLECTOR

3.4.1. Principle of Flat Plate Collector

The steady state thermal efficiency (η_{th}) of a conventional PV/T is calculated by [43]:

$$\eta_{th} = \frac{Q_u}{G} \tag{3.6}$$

And the useful collected heat (Qu) is given by;

$$Q_u = \dot{m}Cp(T_o - T_i) \tag{3.7}$$

or it is simply the difference between the absorbed solar radiation and the heat losses:

$$Q_u = A_c F_r\left[S - U_L(T_{p,m} - T_a)\right] \tag{3.8}$$

Where,

$$F_r = \frac{\dot{m}cp}{A_c U_L}\left[1 - e^{\frac{A_c U_L F'}{\dot{m}Cp}}\right] \tag{3.9}$$

In Equation (3.9) F ‘is the collector efficiency factor given by:

$$F' = \frac{\frac{1}{U_L}}{W\left[\frac{1}{U_L[d_o + (W - d_o)F']} + \frac{1}{C_b} + \frac{1}{\pi d_i h_{fi}}\right]} \tag{3.10}$$

The collector overall heat loss coefficient is the sum of the top, edge and bottom loss coefficients:

$$U_L = U_t + U_b + U_E \tag{3.11}$$

For a well-designed collector having a very small collector perimeter to area ratio, the edge losses are almost negligible [46]. The bottom loss coefficient, U_b derives from the thermal conductivity, k_s and the thickness, L_s of the bottom insulator as:

$$U_b = \frac{k_s}{L_s} \tag{3.12}$$

Thus,

$$U_L = U_t + U_b \tag{3.13}$$

Equation for the top loss coefficient, U_t as (Yeh et al., 2003):

$$U_T = \left[\frac{N}{\frac{C}{T_{p,m}}\left[\frac{T_{p,m}-T_a}{N+f}\right]^e} - \frac{1}{h_w}\right]^{-1} + \frac{\sigma\left(T_{p,m}+T_a\right)\left(T_{p,m}^2+T_a^2\right)}{\left[\left(\varepsilon_p + 0.00591Nh_w\right)^{-1} + \frac{\left[2N+f-1+0.133\varepsilon_p\right]}{\varepsilon_g} - N\right]} \tag{3.14}$$

$$f = (1 + 0.089hw\ -0.1166hw\ \varepsilon_p)(1\ +\ 0.07866N) \tag{3.15}$$

$$C_{air}\ =\ 520\ (1 - 0.00005\beta^2) \tag{3.16}$$

$$e\ =\ 0.43\ (1 - \frac{100}{T_p}) \tag{3.17}$$

$\boldsymbol{\beta}$, is the collector tilt and $\boldsymbol{\sigma}$, is the Stephan Boltzmann constant. The convective heat-transfer coefficient h_w, for air flowing over the outside surface of the glass cover depends primarily on the wind velocity, V and can be determined from [47]:

$$h_w = 5.7 + 3.8\,V \tag{318}$$

3.4.2. Theory of Photovoltaic Modules

The electrical efficiency (η_{el}) of a PV module is given by:

$$\eta_{el} = \frac{I_m V_m}{G A_c} \tag{3.19}$$

As mentioned earlier, the performance of a photovoltaic module deteriorates with increase in its temperature and this dependence of PV module electrical efficiency on PV module temperature is typically given by Equation (3.20), from Zondag et al [48].

$$\eta_{el} = \eta_o(1 - \beta[T - 25^oC]) \tag{3.20}$$

The constants and the calculated variables for use in the above expressions are found in Table 3.3.

Table 3.3. Constants and variables for use in efficiency expressions.

G	1112 W/m2
η_0	0.1711
U_L	14.8
$\eta_{el.ref}$	16%
β_{eref}	0.005
T	313K-

3.4.3. Energy Into the Collector

The useful heat generation as a function of incoming radiation and collector operating temperature relative to its surroundings is commonly referred to as collector thermal performance. When the equation for a particular solar collector's performance curve is known, the system designer has the knowledge required to use any of many established computational methodologies to forecast the collector's daily, seasonal, or yearly energy production under the system's anticipated usage conditions. The analytical derivation of this efficiency is addressed briefly in the next section expression [48, 49]. The net rate of solar radiation absorbed by a collector, q_{solar}, is governed by the amount of radiation on the cover plate as well as the optical and radiative characteristics of the materials used to make the cover plate and absorber. Because no true glazing material is completely transparent, one-half of the radiation that reaches the cover is absorbed, while the other half is reflected by the glazing material; only a small amount penetrates through the cover. The reflected radiation is partially transmitted through the cover, partially absorbed, and partially reflected to the absorber. A part of it is due to repeated absorption, reflection, and transmission [49].

$(\tau\alpha)$ e defines the collector's capacity to absorb solar energy. While the energy absorbed is primarily dictated by the transmittance of the glazing (s) and the absorption of the absorber plate surface, the multiple interactions mentioned above have a complicated influence on the result $(\tau\alpha)$ e, particularly in collectors with two or more glazing layers. $(\tau\alpha)$ e is the net rate of incoming solar energy absorbed by a collector [49]:

$$q_{solar} = GA_a[(\tau\alpha)_e] \tag{3.21}$$

Where G denotes the total incoming radiation per unit area measured in the collector's aperture plane, and Aa denotes the collector absorber area. The relationship between collector performance and physical parameters of the cover and absorbers is more complicated than the preceding description suggests because these material properties also impact radiative heat losses from the absorber plate.

3.4.4. The Collector's Heat Losses

Solar collector thermal losses occur in three ways: conduction, convection, and radiation. Heat losses due to conduction are normally insignificant unless the collector case or mounting structure comes into direct thermal contact with the absorber or input and outlet pipes owing to poor collector design or construction. Convective losses are proportional to the temperature differential between the collector glazing and the surrounding air. The impact of wind on the exterior glass can cause significant losses. Convection also transports heat from the absorber to the glazing(s) within the collector. Radiative losses are minimal at standard home water or space heating temperatures. However, because radiative losses are a function of the difference between the fourth power of the absorber absolute temperature and the sky absolute temperature, which is typically several degrees lower than the ambient air temperature, they may become considerable at higher working temperatures. Although convective and radiative losses occur from all exposed collector surfaces, it is usual practice to represent the overall heat loss as a function of the absorber area, Aa. This is since many radiative and convective losses in a well-insulated collector occur predominantly via the glass.

For both experimental and analytical purposes, it is common practice to combine the convection and radiation heat transfer terms to obtain a single heat loss coefficient based on the temperature differential between the average collector absorber plate temperature and the ambient temperature. The radiation heat transfer term must then be linearized. Thus.

$$U_L = F'(U_{conv.} + U_{rad.}) \tag{3.22}$$

and

$$Q_{loss} = U_L A_a (T_p - T_a) \tag{3.23}$$

Where U_{conv} and U_{rad} are the overall convection and linearized overall radiation heat transfer coefficients, respectively T_p is the average temperature of the absorber.

3.4.5. The Collector's Useful Energy

The equation characterizing the quasi-steady performance of a solar collector is obtained by inserting the previously published formulas for (q) solar and (q) loss [50]:

$$q_{useful} = A_n F'[(\tau\alpha)_e G - U_L(T_n - T_a)] - q_{el} \quad (3.24)$$

Electrical energy extracted from collector may be approximated by a linear function of irradiance and temperature difference $T_n - T_a$

$$q_{el} = A_n E_0[(\tau\alpha)_e G - E_t(T_n - T_a)] \quad (3.25)$$

Where E_0 the efficiency of PV is cells, and E_t is their temperature coefficient. So, we can write:

$$q_{useful} = A_n[(F'(\tau\alpha)_e - E_0)G - (F'U_L - E_t)(T_n - T_a)] \quad (3.26)$$

Let $B_L = F'U_L - E_t$ and $\eta_{o,e} = F'(\tau\alpha)_e - E_0$, then the above equation can be written as:

$$q_{useful} = A_n[\eta_{o,e} G - E_L(T_n - T_a)] \quad (3.27)$$

The new parameters BL and o, e indicate the effective heat loss coefficient and effective optical efficiency, respectively. These are the key equations for developing analytical models of collector performance. The useful energy given by a collector to storage or load may also be determined experimentally by measuring the intake and output collector temperatures, heat transfer fluid properties, and mass flow rate of that fluid through the collector; thus

$$Q_{useful} = \dot{m} C_p (T_o - T_i) \quad (3.28)$$

Where (m) is the fluid mass flow rate through the absorber, (C_p) is the fluid's specific heat capacity, (T_o) is the outlet fluid temperature, and (T_i) is the intake fluid temperature.

3.4.6. The Efficiency of Collector

The PV/T collector's thermal and electrical efficiency should be assessed individually. Thermal efficiency is tested using the ISO 9806-1 standard, while electrical efficiency is determined by measuring I-U curves with a capacitive load [43]. A flat-plate solar collector's thermal efficiency is defined as the ratio of usable heat provided by the collector to total solar energy received by the collector. The collector efficiency increases because of replacement.:

$$\eta = (\tau\alpha)_e - U_L(T_p - T_a)/G \tag{3.29}$$

The problem with applying this equation is that the average temperature of the absorber plate, T_p , is frequently unknown. However, the system designer knows or may reasonably predict the temperature of the fluid entering the collector, T_i, because the fluid temperature approximates that which comes from storage or the supply water main. Whillier modified this equation to offer a more practical formula for collector efficiency, replacing T_i for T_p and including the collector heat removal factor, F_r, to compensate for the decreased heat losses [50, 51]. Hence,

$$\eta = F_r[(\tau\alpha)_e - U_L(T_i - T_a)/G] \tag{3.30}$$

(F_r) denotes the proportion of actual useful energy gain to maximum achievable useful energy gain. When the whole collector is at the incoming fluid temperature T_i, the maximum feasible usable energy gain occurs. Heat losses to the surroundings are kept to a minimum in such an ideal circumstance. Obviously, F_r cannot be more than one; water collectors typically have F_r values between 0.7 and 0.9. Similarly, if we use the mean collector fluid temperature, the efficiency increases [52]:

$$\eta = F'[(\tau\alpha)_e - U_L(T_m - T_a)/G] \quad (3.31)$$

Where

$$T_{m=} - T_i + \frac{T_o - T_i}{2} \quad (3.32)$$

If (F'), (Fr), (UL), and $(\tau\alpha)_e$ If the collector efficiency were constant, it would be a linear function of the reduced temperature difference. T*,

$$\eta = \eta_0 - F'U_L T^* \quad (3.33)$$

Where,

$$T^* = \frac{T_m - T_a}{G} \quad (3.34)$$

This is not quite accurate since UL fluctuates with fluid and air temperature, (τα) e is affected by the relative amount of beam, diffuse, and ground-reflected radiation, and Fr is affected by UL on a weekly basis. As a result, a higher order connection between η_0 and T* is more likely [53].

$$\eta = \eta_0 - a_1 T^* - a_2 G T^{*^2} \quad (3.35)$$

Where a_1 and a_2 are fitting constants. The ordinate intercept, η_o, represents a measure of the ability of the collector to absorb solar energy and to transfer it to the collector fluid. If electrical energy is extracted from collector, this ability is reduced to $\eta_{o,e}$ in accordance with the first law of thermodynamics [54]. The slope of the equation is a measure of the collector's capacity to avoid heat losses to the environment. This ability is increased to BL if electrical energy is taken from the collector.

PART 4

EXPERIMENTAL WORK

4.1. CHAPTER OVERVIEW

This chapter describes the major research plan as well as the tools employed in the study, namely CFD modelling and experimental examination. A new experimental model of FPC was devised and built to validate the prediction and CFD simulation findings. The model was submitted to a measurement procedure, which will be explained further in the chapter. The entire experimental facility is separated into sections. These sections investigate the use of nano material additives to water in an open circle. FPC system and how it affects photovoltaic panel (PV) cooling, description of FPC analysis used, nanofluid preparations measurement system concerning the characterization of collector performance, data collection. While the last section illustrates the uncertainty analysis.

4.2. THE PV/T SYSTEM LAYOUT

The FPC's performance is influenced by the working environment. The new FPC model developed and built in this thesis has been put at the University of Technology in Iraq's solar research location. The latitude is N33.3123o, the longitude is 44.446 E, and the height is 21.23m. Meteorological data measured inside the University for the Dawn Portion of the day (7 am - 7 pm); as a working time of the flat plate collector are as follows:

- The average wind velocity was (1.7 m/s).
- The solar radiation intensity range was (24 to 1112 W/m2).
- The average ambient air temperature was (34 ℃) and range was (26~43 ˚C).

- The average ambient air pressure was (100200 Pa) and range was (99891~100540 Pa).

Model-SS is the main shape of the new FPC model. The FPC's conceptual design outlines are explained in the following sections.

4.3. DESIGN OF FLAT PLATE COLLECTOR (FPC)

The temperature drop from the flat plate collector surface is determined by the amount of solar radiation reaching the back surface of the PV panel, the area of the collector, and the absorber materials. Because the future goal is to increase the amount of electricity generated by the PV panel by using FPC, it is suggested that it be installed in an open environment and use water as a solar radiation absorbing medium.

As a result, the absorber material would be flowing water mixed with various types of nano particles, while the collector cover material could be high conductivity plates of aluminum, preferably for investigation objectives. The collector area could be calculated based on the size of the PV panel and the amount of heat that reaches this cover in the model location. The collector has a slope angle of 30° to improve the solar radiation projection model within its daily range [55].

4.3.1. Specification of New Design of Flat Plate Collector

The function of the FPC is to subtract the heat from the back surface of the photovoltaic panel to the water flowing into it. The parameters involved in the collector are the tangential and vertical parts of internal geometry, and the increasing of contact area between the heat transfer material and hot surfaces, furthermore, temperature difference between water entering FPC and ambient air.

The new design utilizes aluminum uniform bulges connected with collector cover from bottom to provide powerful heat transfer and water movement with slow streamlined manner. This can be achieved because the velocity components of water flow are more valuable when the collector cover was without bulges. In the new design of the present

work, new model of bulges utilized sphere shape (Model-SS). The FPC geometry for this model could be described as below:

- Design and fabricate Model-SS: this model has a number 120 sphere bulges, a 25 mm diameter, and is made of aluminum to allow powerful heat transfer. These bulges were distributed uniformly on the bottom surface of the collector cover so that they were 8 spheres within one row, while the number of rows was 15, as shown in Figure 4.1.

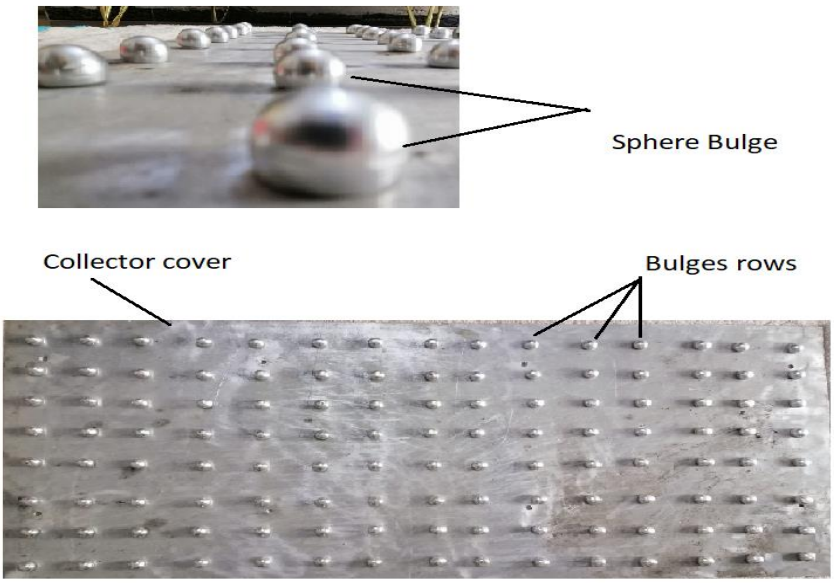

Figure 4.1. Structural pictures of a Model-SS.

4.3.2. Collector Geometry

Figure 4.2 shows a photo of the collector section for the investigation of water flow passing through inlet pipe to outlet pipe. The collector body has dimensions of 600×1100×30 mm, a 13 mm inlet and outlet diameter, it is made of steel. To connect collector cover was used number of screws and rubber band used to prevent water leakage from the edges of the collector.

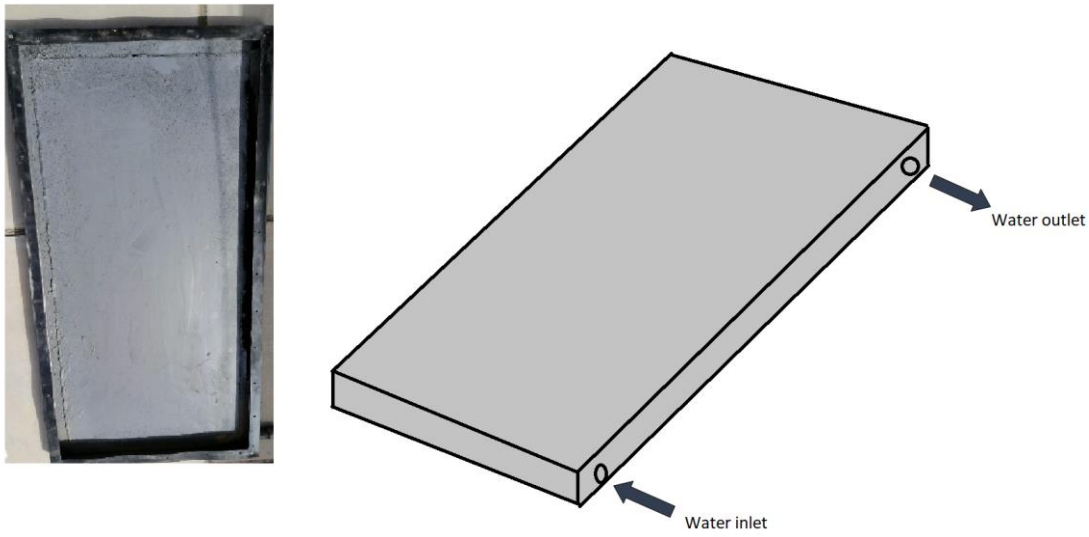

Figure 4.2. Flat plate collector body.

4.4. PREPARATIONS OF NANOFLUIDS

The nano material mixture is simply not a liquid- solid mixture. Preparation of nano fluid is the first key step in applying nano phase particles to change the heat transfer performance of conventional fluids. To get clear, describe, durable suspension, with low agglomeration of particles, a two-step method was selected to prepare the nano fluids [56]:

- The first step is that the nano particles and distilled water are mixed directly.
- The second step is the use ultrasonic vibrator for preparation of mixed aqueous nano fluid, but longer time of high energy sonication can introduce defects, as shown in Figure (4.3).

Nanofluid samples were prepared for different concentrations by dispersing pre-weighed quantities of dry particles and pure water. The all mixtures were then subjected to ultrasonic mixing (500 Watts, 70 Hz, German) for 15 to 20 minutes to break up any particle aggregates. The process results in uniform dispersions for the duration of the experiments. The concentrations used in the experiments are Cn= 1, 2, and 3% by volume.

Figure 4.3. Ultrasonic vibrator.

The volume concentration is evaluated from the following equations.

$$\mathrm{Cn} = \frac{\boldsymbol{volume\ of\ nanopartical}}{\boldsymbol{volume\ of\ nanopartical + volume\ of\ water}} \times 100 \tag{4.1}$$

$$\mathrm{Cn} = \frac{(m/\rho)_{nanopartical}}{(m/\rho)_{nanopartical} + (m/\rho)_{water}} \times 100 \tag{4.2}$$

Noting that the volume of pure water used in the test setup is 25 L. The nano particles used in the preparation of nano fluids are copper oxide nano particles (CuO, 99%, 40nm) and aluminum oxide nano particles (γ Al_2O_3, gamma, 99%, and 20nm). The properties (density, viscosity, and specific heat) for the two types of nano particle used are shown in Appendix A as provided from the manufacturer and are listed in Table 4.1.

Table 4.1. The properties of two type's nano particles used.

Property	**CuO diameter 40 nm**	**Al_2O_3 diameter 20 nm**
Cp (kJ/kg. K)	535.6	765
Density (kg/m^3)	6400	3970
K (W/m. K)	76.5	40

4.4.1. Measurement of Nanofluid Density

The measurement of nanofluid density was carried out by weighing a sample volume of 500 ml with different concentrations for each type of nano fluid and dividing the values of weight by volume. Table 4.2 shows the results of measurements.

Table 4.2. The experimental results of nano fluids density.

	Pure water	CuO (40 nm)-Water		
Nano particles concentration (Vol. %)	0	1	2	3
Density (kg/m^3)	995.7	1049.7	1103.8	1157.8
	Pure water	Al_2O_3 (20 nm)- Water		
Nano particles concentration (Vol. %)	0	1	2	3
Density (kg/m^3)	995.7	1025.4	1055.2	1084.9

4.4.2. Measurement of Nanofluid Specific Heat

The used instrument for measurement of Nanofluid specific heat is ESD-201 type manifested in Figure (4.4). This instrument consists of a steel container with a capacity of 10 liters which is isolated from outside by air gap. Inside this container, there is a mixer that operates by an electric motor to move the nanofluid and to distribute the temperature. At the top of box, a small hole to put the thermometer to measure the temperature of nanofluid in the container. The specific heat can be calculated on two stages, as follows:

Energy balance in the first stage can be calculate:

$$Q_H = Q_V + Q_W \tag{4.3}$$

Energy balance in the second stage can be calculated.

$$Q_H = Q_V + Q_{nano} \quad (4.4)$$

$$Volt \times current \times time = m\,Nano \times C\,Nano \times \Delta T + mV \times CV \times \Delta T \quad (4.5)$$

m_V = 0.5 kg, C_V = 0.46 kJ/kgK, m_{nano}= equivalent to 3 litters. The results of measurement are given in Table 4.3.

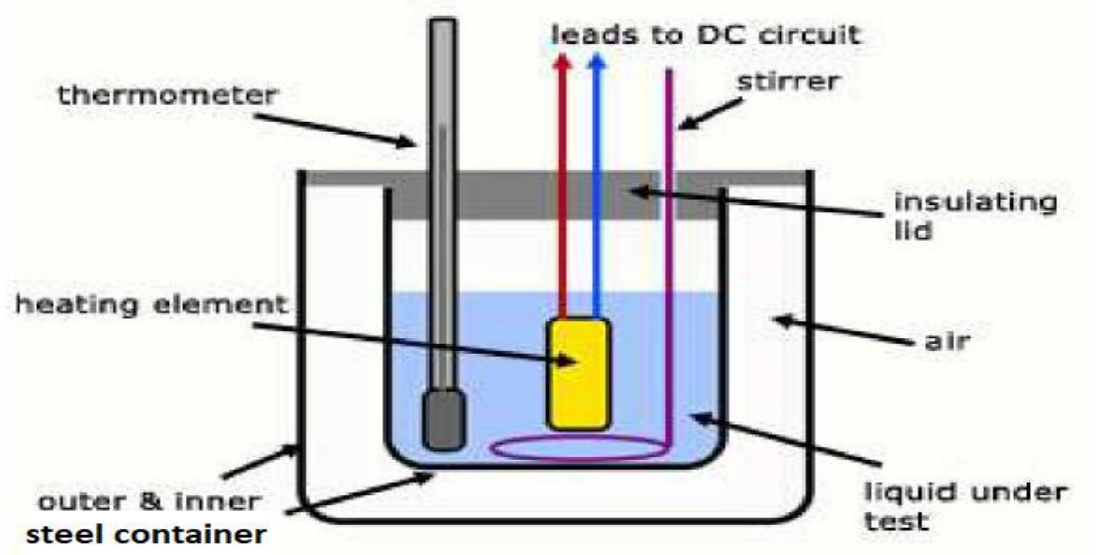

Figure 4.4. Specific heat instrument ESD-201.

Table 4.3. Results of experimental measurements of specific heat.

	Pure water	CuO (40 nm)-Water		
Nano particles concentration (Vol. %)	0	1	2	3
Specific heat (kJ/kg.K)	4.183	3.961	3.760	3.578
	Pure water	Al_2O_3 (20 nm)- Water		
Nano particles concentration (Vol. %)	0	1	2	3
Specific heat (kJ/kg.K)	4.183	4.051	3.926	3.808

4.4.3. Measurement of Nano fluids Viscosity

In this study, the viscometer type Brookfield digital viscometer model DV-E, as given in Figure (4.5). It offers the 'dynamic viscosity' value) was used. It works on the premise of shearing the fluid whose viscosity is being measured between two surfaces.

One of the surfaces of these viscometers is fixed, while the other is spun by an external motor, with fluid filling the area in between. The measurements are carried out by either delivering a constant torque and measuring the changes in rotation speed or applying a constant speed and measuring the changes in torque. The produced samples with various nanofluid concentrations were evaluated, and the findings are shown in Table 4.4. Figure 4.14 shown Nanofluid preparing for different concentrations.

Figure 4.5. Digital viscometer model DV-E.

Table 4.4. Experimental results of the measured viscosity.

	Pure water	CuO (40 nm)-Water		
Nano particles concentration (Vol. %)	0	1	2	3
Viscosity (N.s/m2)	$0.998*10^{-3}$	$1.0253*10^{-3}$	$1.0964*10^{-3}$	$1.23*10^{-3}$
	Pure water	Al_2O_3 (20 nm)- Water		
Nano particles concentration (Vol. %)	0	1	2	3
viscosity (N.s/m2)	$0.998*10^{-3}$	$1.0827*10^{-3}$	$1.18*10^{-3}$	$1.26*10^{-3}$

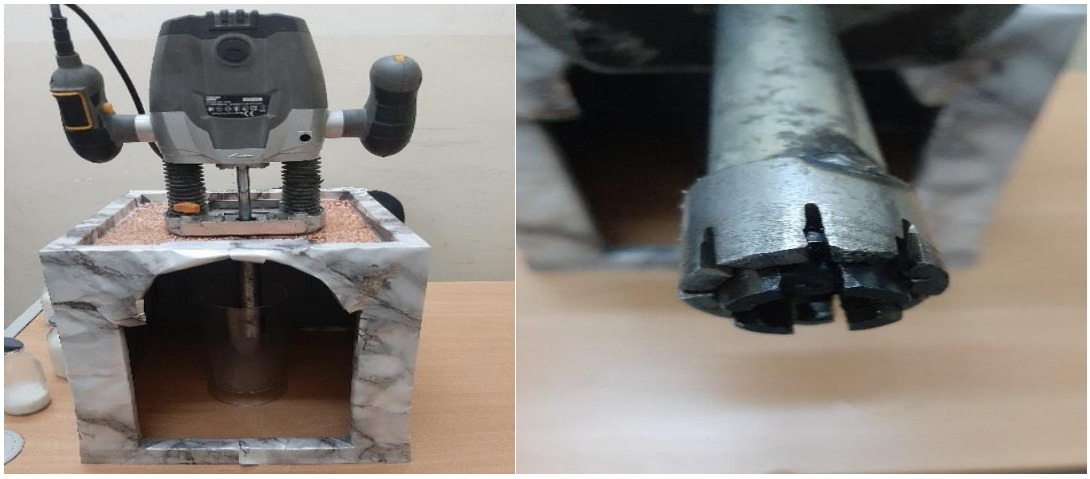

a) b)

c) d)

e) f)

Figure 4.6. a), b), c), d), e), f) Nanofluid prearranging for all different concentrations.

4.4.4. Measurement of nanofluids Thermal Conductivity

KD2Pro thermal conductivity meter was used to measure nano fluids thermal conductivity, as shown in Figure 4.6. The experimental results of measured thermal conductivity are presented in Table 4.5.

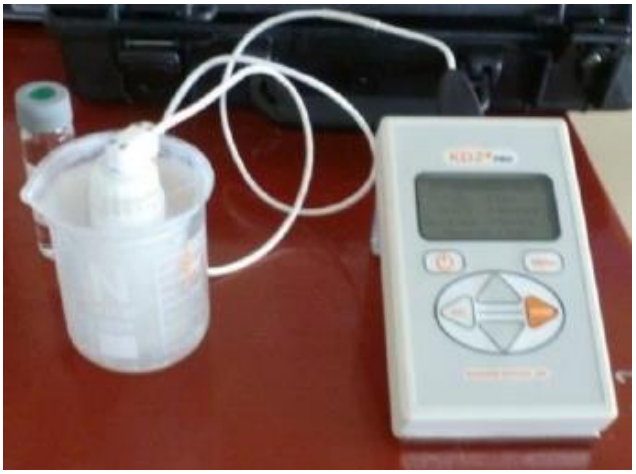

Figure 4.7. Thermal conductivity device.

Table 4.5. Experimental results of the measured thermal conductivity.

	Pure water	CuO (40 nm)-Water		
Nano particles concentration (Vol. %)	0	1	2	3
Thermal cond. (W/m.K)	0.599	1.01	1.95	2.56
	Pure water	Al_2O_3 (20 nm)- Water		
Nano particles concentration (Vol. %)	0	1	2	3
Thermal cond. (W/m.K)	0.599	0.867	1.11	1.78

4.5. EXPERIMENTAL SETUP

Experimental investigation of PV panel cooling system design for power generation is an objective of the present study. The subtract heat energy was done using FPC system by depending on closed circle water flow. The thermal collector (absorber) is attached to the back of an off-the-shelf PV panel. To get a first estimate of the characteristics of PV/T system, all experiments were carried out by comparing with PV system and a part of the collected energy is extracted as electricity instead of heat, as illustrated in Figure (4.7). Both the PV panel and PV/T system inclined with 30^o from the horizontal plane. Temperatures for different regions of the PV/T system were measured by temperature measurement unit and the water flow rate was measured by flow rate

device before entering the collector. To control the water flow rate accurately, one-way valves were used. Calibration curve for these devices is shown in Appendix B.

Figure 4.8. Experimental setup of the PV and PV/T system.

4.5.1. Photovoltaic PV Panels

A photovoltaic system is made up of several photovoltaic solar cells. An individual small PV cell can generate about 1 to 2 Watt of power approximately depends on the type of material used. For higher power output, PV cells can be connected to form higher power modules. Traditional single-crystalline silicon (Si) solar modules are produced using silicon cells, are normally flat-plate, and are the most efficient solar modules. In this investigation, two PV panels with a maximum power capacity of 150 Watt (model MSM150S for MAGNZON firm) were employed, as indicated in Figure (4.8), one of them was used in PV system side while the other used in PV/T system side, and Table 4.6 list the main technical specifications of the PV panel.

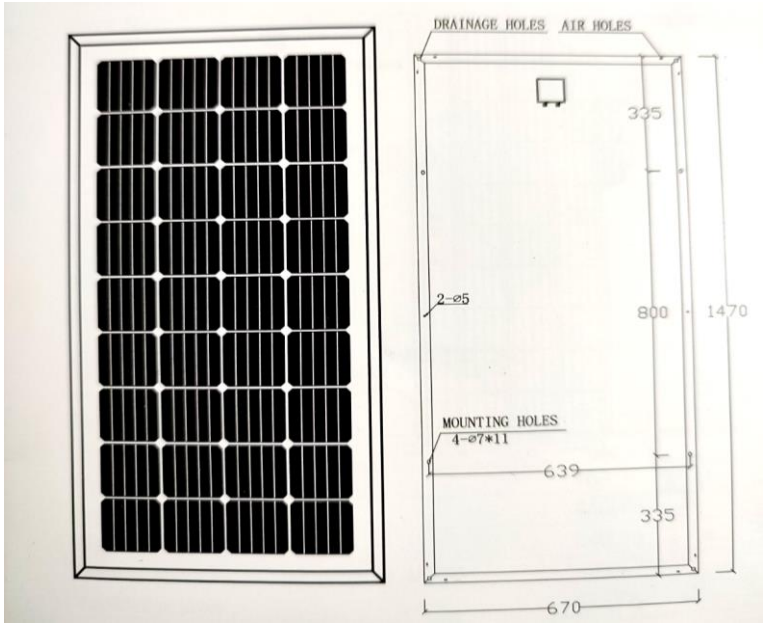

Figure 4.9. Schematic of photovoltaic panel.

Table 4.6. The main technical PV panel specifications.

Model of PV panel	MSM150S
Type of cells (mm)	Mono (156×104)
NO. of cells and connections	4×9=36
Dimensions (mm) (L×W×H)	1470×670×30
Weight (kg)	11.0
Glass	3.2mm Tempered glass
Encapsulation	EVA
Rated maximum power (Mp)	150 W
Cell efficiency	17.7%
Open circuit voltage (Voc)	22.4 V
maximum power voltage (Vmp)	17.5 V
Short circuit current (Isc)	9.05 A
maximum power current (Imp)	8.63 A

4.5.2. Instruments for Measuring

Various tools were used to measure tests in order to conduct experimental research on this subject. A measurement examination was carried out for the previously reported experimental model of the FPC. Testing positions of thermocouples type K and roto-meter will be explained to capture varied measurements. The following devices were used to record the experimental measurement variables:

- Temperature measurement unit.
- Water flow rate measurement unit.
- Solar power meter instrument.
- An anemometer instrument.

4.5.2.1. Temperature Measurement Unit

This study's experimental examination was carried out employing a temperature measurement device. Experiment methods were carried out on sunny days, avoiding overcast days or clouds. All temperature testing on the FPC model were performed to become acquainted and confident with the measuring process. Experiment measurements were carried out at the solar research facility, where two PV panels were built, one of which included the FPC model. Temperature measurements are classified into numerous categories.; Group-A was used three thermocouples for measuring PV panel surface, Group-B was used two thermocouples for measuring inlet and outlet water temperature, and Group-C was used three thermocouples for measuring collector surface, as shown in Figure (4.9). All thermocouples were used by Type-K with selector switch and digital thermometer, as shown in Figure 4.10. All specific properties for all parts of the temperature measurement system are shown in Table 4.7. Calibration of temperature measurement system is explained as described in Appendix (B).

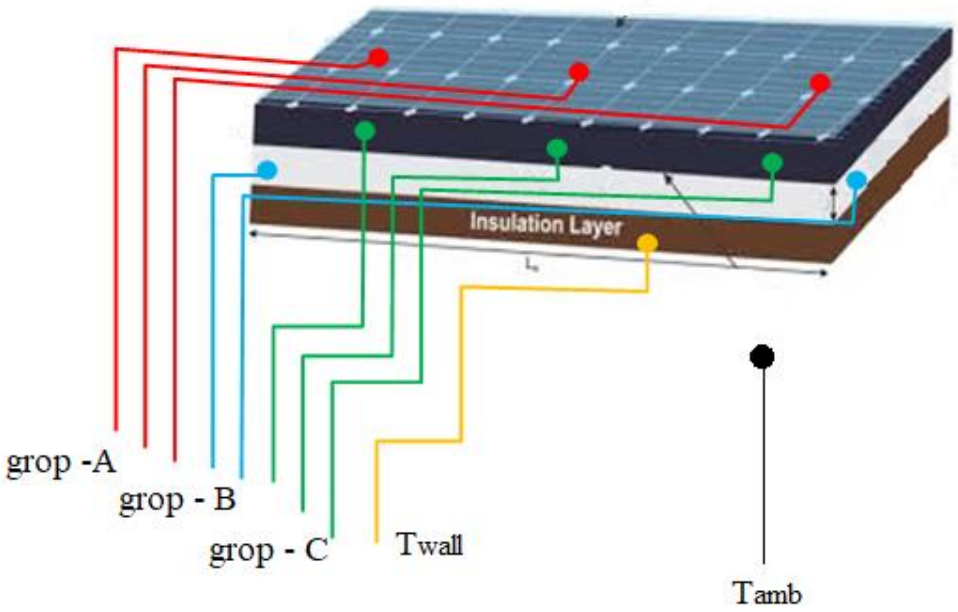

Figure 4.10. Positioning schematic of temperature measurement in the PV/T system.

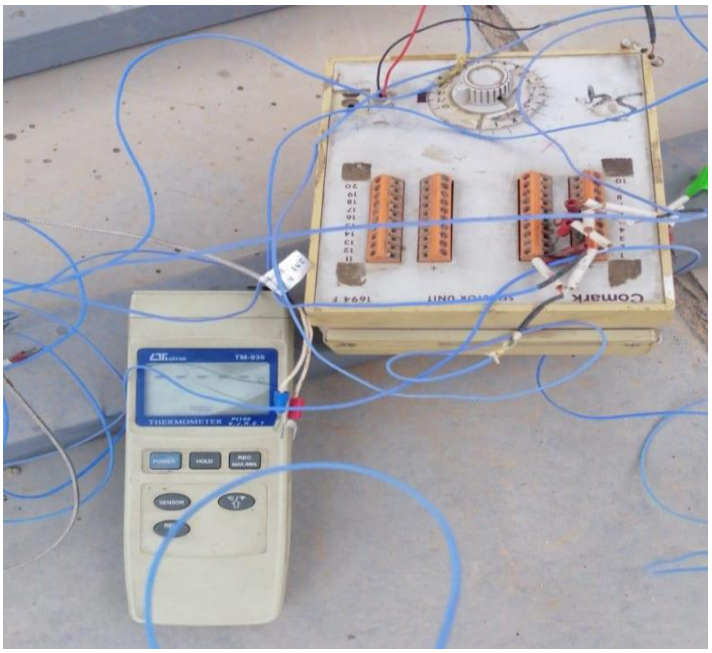

Figure 4.11. Temperature measurement instruments.

Table 4.7. All specific properties for all parts of temperature measurement system.

No.	Type of Thermocouples	position	Accuracy	Reader Thermometer – Tm-936
1	Probe type-K	2 points, inlet and outlet collector	± 0.3	Accuracy ± (0.2 % + 0.5 ℃)
2	Wire type -K	6 points, on PV panel and PV/T system	± 0.2	
3	Wire type-K	3 points, on Collector cover	± 0.2	
4	Wire type-K	4 points, to measuring Ambient temperature, collector body	± 0.2	

4.5.2.2. Water Flow Rate Measurement Unit

Flow meter Rotameter model M-15 measuring range 1-7 LPM) instrument, shown in Figure (4.11), is connecting with water flow line can measure and volumetric flow rate in LPM (litter per minute). Specifications of rotameter instruments were described in Table 4.8.

Figure 4.12. Rotameter instrument.

Table 4.8. Specifications of Rotameter instrument.

Specifications	Quantity
Internal Hole Diameter:	12mm
Overall Size:	21 x 3.2cm (L*D)
Accuracy	± 0.5% of reading
Material:	Plastic Metal

4.5.2.3. Solar Power Meter Instrument

Figure 4.13. Solar power meter instrument.

Figure 4.12 shows a portable solar power meter (model: SPM-1116 SD) that can measure and display irradiance for spot check measurements in W/m2. The energy intensity released by solar radiation at a specific location on the planet can be processed by solar-meter equipment. The sun-meter equipment was developed to measure the total of direct and diffuse solar radiation, which is known as global solar radiation. Table 1 describes the specifications of a solar-meter apparatus (4.9). Its sensor is a stretched silicon cell that is not highly sensitive to heat fluctuations. Through a diffusor and a correction filter, it collects solar light. The sensor's output voltage is proportional to the amount of radiation received. Following a specified measurement shutdown, data is automatically recorded and systematically displayed

to the operator prior to the start of a new measurement. On a timed basis, the maximum/minimum values, average irradiance, and cumulative energy in W/m2 are all provided in a solar-meter device.

Table 4.9. Specifications of solar power meter instrument.

Specifications	**Quantity**
Solar Irrigation Range	1 W/m^2 to 1200 W/m^2
Calculation Frequency (W/m^2)	1/ min
Accuracy	± 5% of reading
Operating Temperature	from -10°C to +50°C
Frequency of The Measure	2 Hz

4.5.2.4. Wind Speed Instrument (Anemometer)

Wind speed instrument (Anemometer model: AM-4826), shown in Figure (4.13), is a portable instrument which can measure wind speed or air flows in channel in m/sec (km/hr). Specifications of Anemometer instrument was described in Table 4.10.

Figure 4.14. Anemometer instrument.

Table 4.10. Specifications of anemometer instrument.

Specifications	Quantity
Wind speed Range	0.3–30 m/s,1.4-108 km/h
Accuracy	± 0.7% of reading+ 2 digit
Operating Temperature	from 10°C to +60°C
Power Supply	4×1.5V Battery

4.6. DATA COLLECTION

This section describes the experimental approach used in the outside measuring technique for the PV/T system research. Experiment methods were carried out on sunny days, with overcast days or clouds avoided throughout testing. To become acquainted with and satisfied with the measuring technique, simple tests of water temperature, surface temperatures, wind speed, water/nano particles flow rate, and solar intensity were performed at various sites of the PV/T system. Also, the period time ranges were chosen from 7:00 am to 7:00 pm provide a range for study effect of PV panel heating due to solar radiation on its performance.

The experimental procedure used in this study is described as follows. The first set of experiments for Model-SS collector was conducted by temperature measurement system and water circling system for recording PV panel surface temperature, collector surface temperature and water inlet and outlet temperatures from collector with varied water flow rates at several days, also solar meter was used to solar intensity measuring through daily time, as mentioned in Table 4.10. In the following experiments, the temperature measurement system was coupled with a Model-SS thermal collector cooled by water/nano particles (at different volumetric concentrations 1%, 2% and 3% of CuO and Al2O3) to record the surface temperature of the PV panel, the surface temperature of The collector and the temperatures of the inlet and outlet of the water from the collector at various water flow rates in several days, and the solar meter was used to measure the intensity of the sun during the daily time, as mentioned in Table 4.11.

Table 4.11. Data collected for PV/T system.

Model-SS with Water						
No.	Water flow (l/min)	T PV.	T col.	G Watt/m2	T_{amb}	Tw_{in}, Tw_o
1	1.5	3 points	3 points	24-1112	1	2 points
2	2.0 l	3 points	3 points	24-1112	1	2 points
3	2.5	3 points	3 points	24-1112	1	2 points
4	3.5	3 points	3 points	24-1112	1	2 points
Model-SS with Water/Cuo (1%, 2% and 3%)						
5	1.5	3 points	3 points	24-1000	1	2 points
6	3.5	3 points	3 points	24-1000	1	2 points
Model-SS with Water/Al_2O_3 (1%, 2% and 3%)						
7	1.5	3 points	3 points	24-1000	1	2 points
8	3.5	3 points	3 points	24-1000	1	2 points

4.7. UNCERTAINTY ANALYSIS

Uncertainty analysis in the tests is very important to provide a high level of confidence in all results. It is obtained by determining the repeatability and increasing interest in the results. All tests were repeated thrice. The variants of the predicted values of water flow rates, temperatures and solar intensity were used to calculate the uncertainty using the percent relative standard error. The error components are unlikely to be at their maximum value and same polarity at the same time. A more realistic method is to use the root-sum-of-squares method, that is, by taking the square root of the sum of the individual errors, as shown in Equations (4.6 and 4.7) [52].

$$\delta_{total} = \sqrt{(\delta_{sensor})^2 + (\delta_{instrument})^2} \tag{4.6}$$

$$Min.\,\&\,Max.\,Uncer.\,(\%) \;=\; 100 \times \left(\frac{\delta_{total}}{Min.\,\&\,Max.\;Reading}\right) \tag{4.7}$$

$$\delta_{k=} \sqrt{\delta_{q1}{}^{2} + \delta_{q2}{}^{2} + \cdots . \delta_{qn}{}^{2}} \quad (4.8)$$

Where, δ_{total} is the total uncertainty for the device. δ_k is the overall experimental uncertainty and δ_q is the uncertainty for the devices. All values for the maximum and minimum uncertainty percentage was calculated from: water flow meter, thermocouple system, solar power meter, and anemometer. Table (4.12) shows the uncertainty percentage error of the experimental yield values measured.

Table 4.12. Uncertainties of the measured parameters.

Parameter	Max. value	Min. value	Min. Uncertainty	Max. Uncertainty
Water flow rate	3.5 l/min	1.5l/min	± 0.62	± 0.56
Temperatures	71 ºC	20 ºC	± 1.16	±1.05
Solar intensity	1112 W/m^2	24 W/m^2	± 1.91	±1.7
Wind speed	2.4 m/s	1.2 m/s	± 0.11	±0.08
I (amp)	3.19 A	0.01 A	±0.11	± 0.09
V (Volt)	15,79 V	0.06 V	±0.63	±0.47
Total Uncertainty			±2.4	±2.13

PART 5

RESULTS AND DISCUSSION

5.1. CHAPTER OVERVIEW

The results obtained from the numerical simulation and experimental measurement of the PV/T system are elaborated and discussed. This chapter also includes comparison between practical and theoretical results (simulation). In the practical part, we first explain the effect of fluid flow rate on the PV/T system. The second part is the effect of the type of nano material used. The third part we explain the effect of concentration of nano materials on the PV/T system. The last section of the chapter is a comparison between the performances of the system practically and mathematically. Multiple parameters were considered (temperature, wind speed, solar radiation, and ambient temperature) from 7 A.M. - 7 P.M. in studying the PV/T system as shown in Appendix. C. This study was done from the 7th of April until the 2nd of May, excluding the days with challenging weather such as rain and dust storms. In Figure (5.1) we have illustrated the measured results of two very important parameters that affect the efficiency of PV/T systems which are solar radiation and the ambient temperature. Solar radiation reaches a peak at around 12-2 P.M and ambient temperature too.

The overall performance of the PVT is analyzed depending on the values of solar radiation, cell temperature, mass flow rate as well as the type and concentration of nano fluids. Then we calculate the thermal power, thermal efficiency, and electrical efficiency of the PV/T system and compare them.

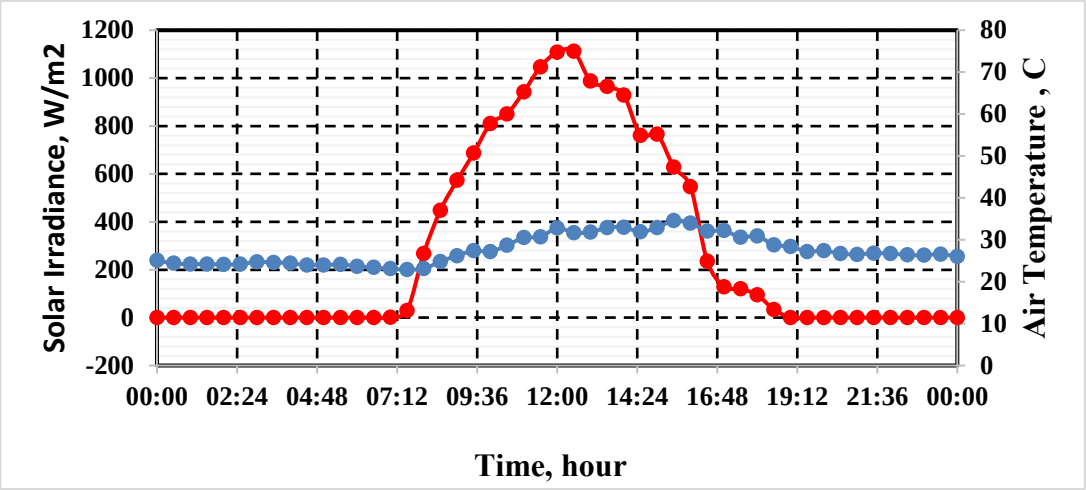

Figure 5.1. The change in solar radiation and air temperature during daylight hours.

5.1.1. The Effect of Coolant Flow Rate on the PV/T System

The flow rate is one of the main factors affecting the PV/T system.

5.1.1.1. The Effect of Coolant Flow Rate on the Panel Surface Temperature

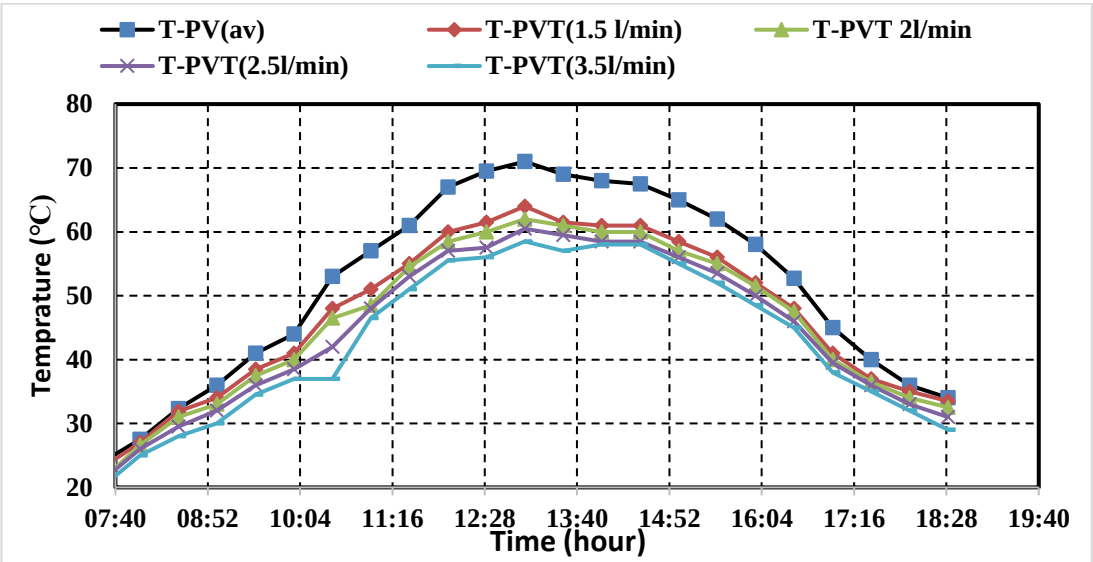

Figure 5.2. The effect of coolant flow rate on the panel surface temperature during the hours of the day.

By recording the surface temperatures of the photovoltaic cell during daylight hours with flow rates (1.5, 2, 2.5, and 3.5)l/min , we obtained a decrease in the cell surface

temperature with increasing in flow rate as shown in Figure (5.2) and comparing it with a photovoltaic cell without cooling at (13:00) where the percentage of temperature decrease was (10%) at flow rate (1.5l/min) but it was (12.6%, 14.7%, 17.6%) at (2 ,2.5 and 3.5l/min) respectively. Figure 5.3 shows a decrease in the collector temperature with an increase in the flow rates of the coolant.

The highest temperature of the collector surface was at one o'clock in the afternoon (53) ℃ at a flow rate of 1.5 liters per minute, which decreased by 2.5% when using a flow rate of 2 liters per minute, and decreased to (5.6%, 9.4%) when using (2.5 and 3.5 liters per minute) respectively.

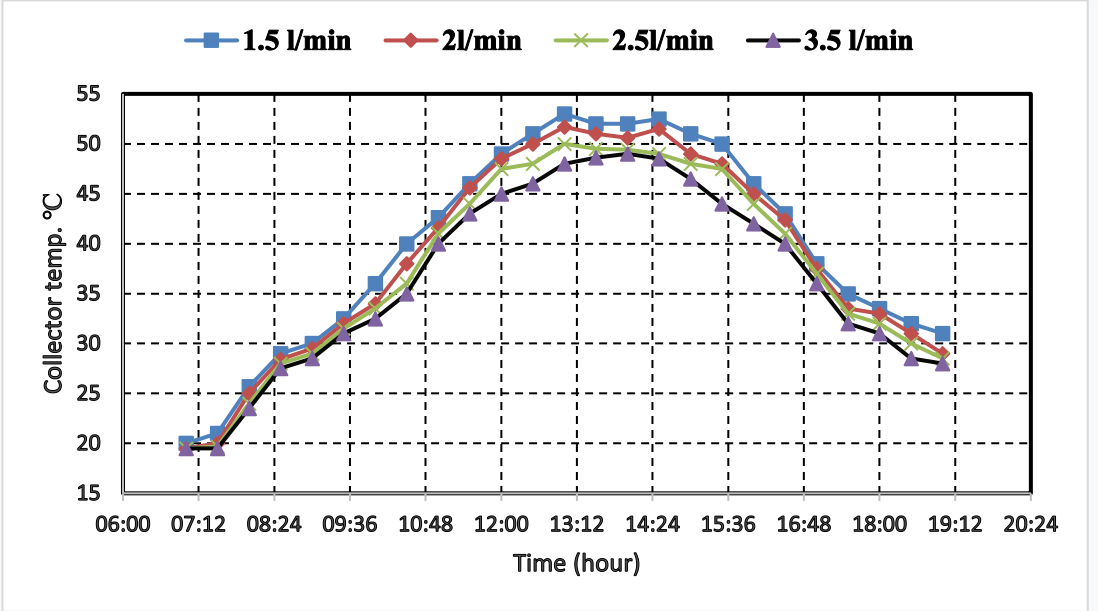

Figure 5.3. The change in the temperature of the collector during the day for different flow rates collector temp.

5.1.1.2. The Effect of Coolant Flow Rate on the PV/T Electrical Efficiency

The Evans DL (1981) equation was used to calculate electrical efficiency based on the recorded temperature [58].

$$Electrical\ efficiency = \eta\_(elec.) = \eta\_ref \times [1 - \beta\_ref\ (T\ p - T\ ref)] \qquad (5.1)$$

The temperature of the cell surface is one of the important parameters in calculating the efficiency of the electrical cell. The ideal electrical efficiency of the cell is calculated under standard conditions (solar radiation = 1000 Watts / m ^{2}, cell temperature = 25 ℃), where the electrical efficiency of the cell decreases with an increase in cell temperature of 25 ℃. The ideal efficiency that was calculated for the cell = η_{ref} = (17.1%) decreased to 13.5 % at one o'clock in the afternoon to increase by 3.7% when cooled with 1.5l/minin. of water and when the flow rate is increased to (2, 2.5 and 3.5l/min) the electrical efficiency increases by 5.6%, 6.4% and 7.5%, respectively, the highest electrical efficiency at a flow rate of (3.5l/min) as shown in Figure 5.4.

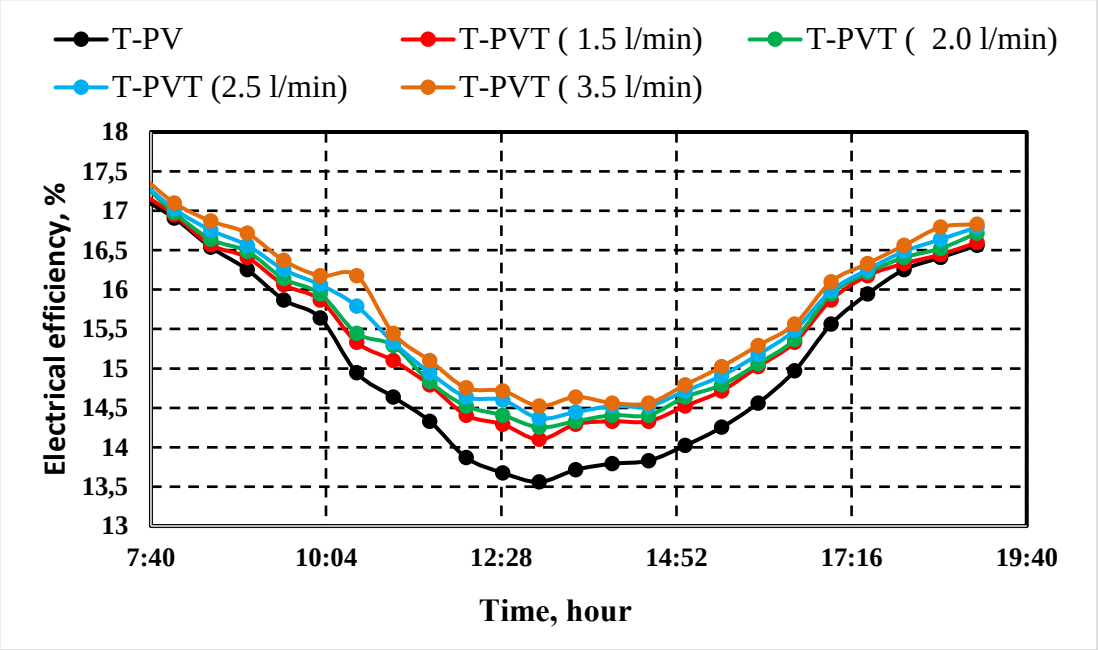

Figure 5.4. The effect of coolant flow rate on the panel electrical efficiency during the hours of the day.

5.1.1.3. Effect Coolant Flow Rate on the Absorbed Power

We calculate the thermal energy by using the eq. (3.7) for different flow rates during daylight hours as shown in Figure 5.5 where we notice an increase in the thermal energy absorbed with an increase in the flow rate. The absorbed thermal energy increased by (16%) when using a flow rate (2l/min) than that when using a flow rate

(1.5l/min), and increased by (33% ,41%) when using a flow rate (2.5 and 3.5l/min), respectively.

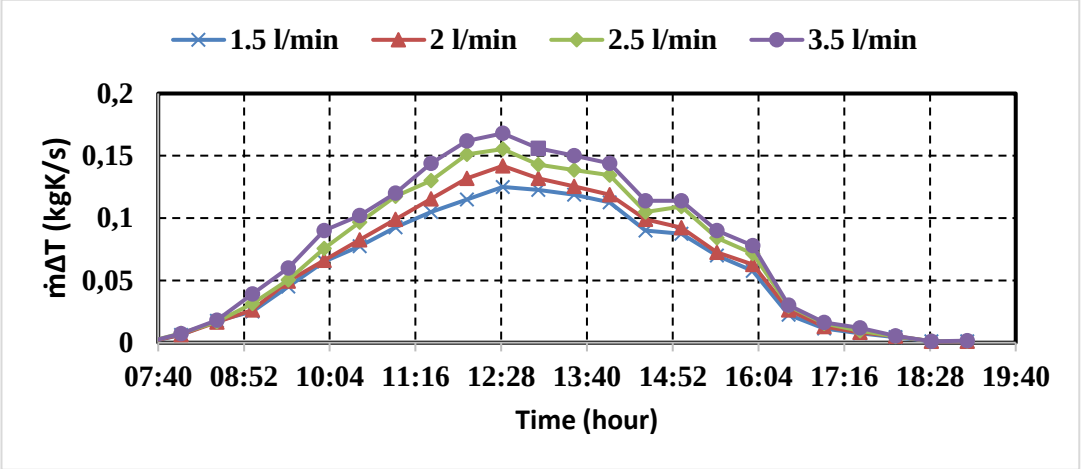

Figure 5.5. Effect of flow rate on the absorbed thermal energy during daylight hours.

5.1.1.4. Effect Coolant Flow Rate on the Coolant Temperature Difference Between the Collector Inlet and Outlet

Figure 5.6 shows the effect of the coolant flow rate on the temperature difference between the inlet and outlet of the coolant during daylight hours for the new collector. We notice a decrease in the (ΔT) with an increase in the flow rate. Where we notice the highest value of (ΔT) at 12:30 p.m. (at the highest value of solar radiation and cell surface temperature) when we use flow rate (1.5l/min) 5 ℃compared to flow rates (2, 2 .5, 3.5) at the same time we get (4.3, 3.7, 2.8 ℃) respectively.

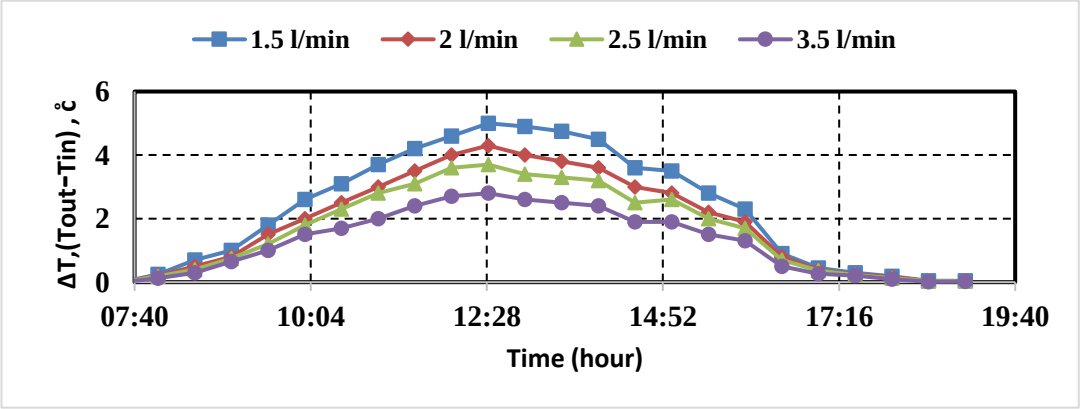

Figure 5.6. The temperature difference between the inlet and outlet of the coolant during daylight hours for different flow rates.

5.1.1.5. Effect Coolant Flow Rate on PV/T Thermal Efficiency

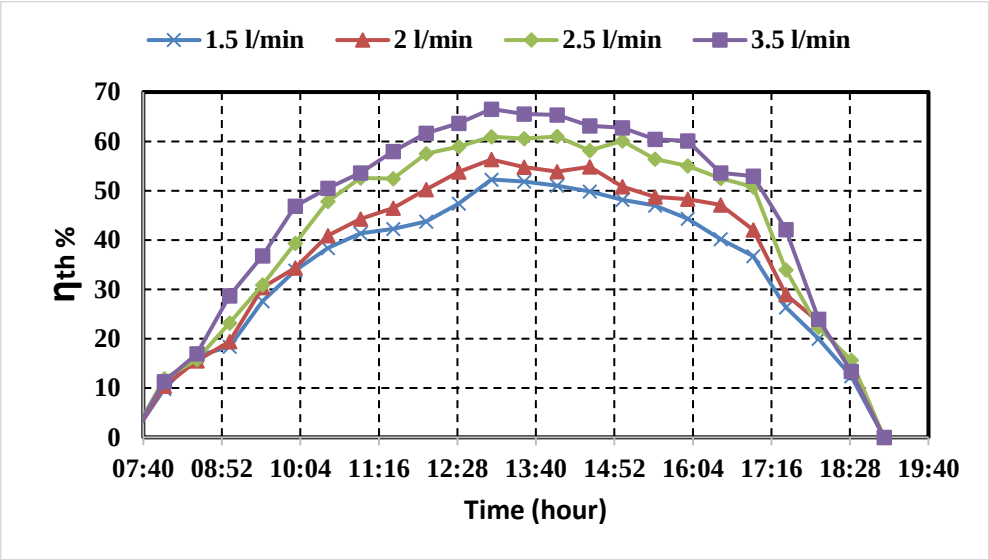

Figure 5.7. Effect of flow rate on thermal efficiency.

The thermal efficiency of the system was calculated through the equation (3.7) when using flow rates (1.5, 2, 2.5, and 3.5l/min) as shown in Figure 5.7, where we notice an increase in thermal efficiency with an increase in the flow rate. The thermal efficiency was compared for the different flow rates at maximum radiation, where the thermal efficiency increased at the flow rate (2l/min) by (7.7%) than the thermal efficiency when we used (1.5l/min) and also increased by (16.5%, 27.4%) when we used the flow rates (2.5, and 3.5l/min) respectively.

5.1.2. Effect of Nano Materials on the PV/T System

Nanofluid was used instead of water as a cooling fluid for the system. We used two materials (CuO and Al_2O_3) at concentrations of (1%, 2%, 3% V%) and at a flow rate of 1.5l/min and 3.5l/min and recorded the following observations as shown in Appendix C.

5.1.2.1. Effect of Nano Materials Type on the PV/T System

Nanofluid was used instead of water as a cooling fluid, where (CuO) was used with volumetric concentrations of 1%, 2% and 3%, as well as (aluminum oxide Al_2O_3) with the same volumetric concentrations. and the following points were studied:

5.1.2.1.1. Effect of Nano Materials Type on the PV/T Temperature

Figure 5.8 represents the cell surface temperature during daylight hours for different types of nanofluids, at one o'clock we note that using (CuO/water) at volumetric concentrations3% reduces the cell temperature (16%), while it decreased by (14%,10%) when using (Al_2O_3 / water) at volumetric concentrations of 3% and water alone, respectively. While Figure 5.9 represents the cell surface temperature during daylight hours for different types of nanofluids, at one o'clock we note that using (CuO /water) at a volumetric concentration 3% reduces the cell temperature (24%), while it decreased by (22.5%,17.6%) when using (Al_2O_3 / water) at volumetric concentrations of 3% and water alone, respectively.

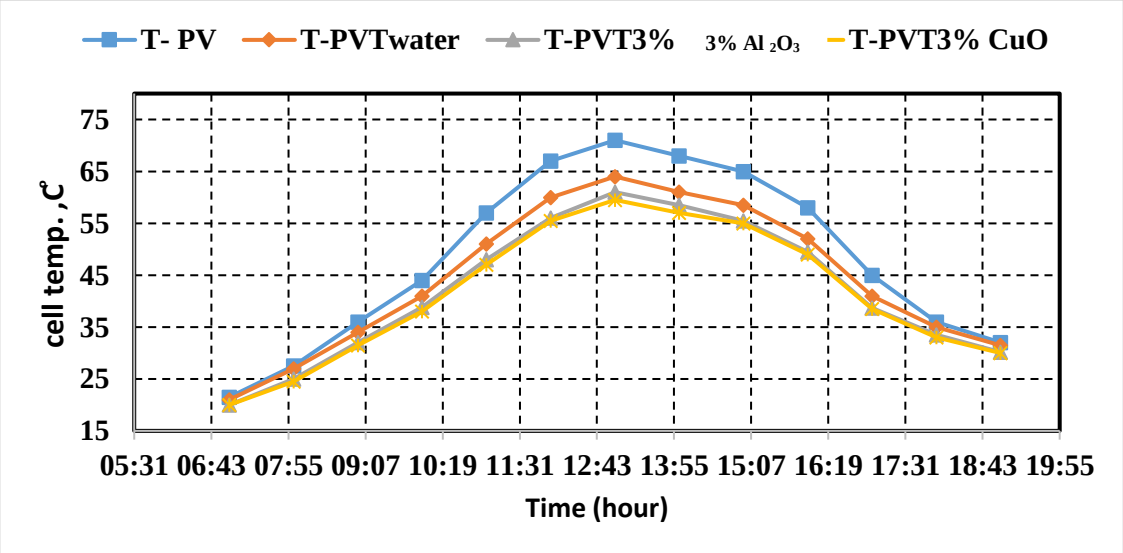

Figure 5.8. Cell surface temperature during daylight hours for different types of nanofluid at concentration 3% flow rate (1.5l/min).

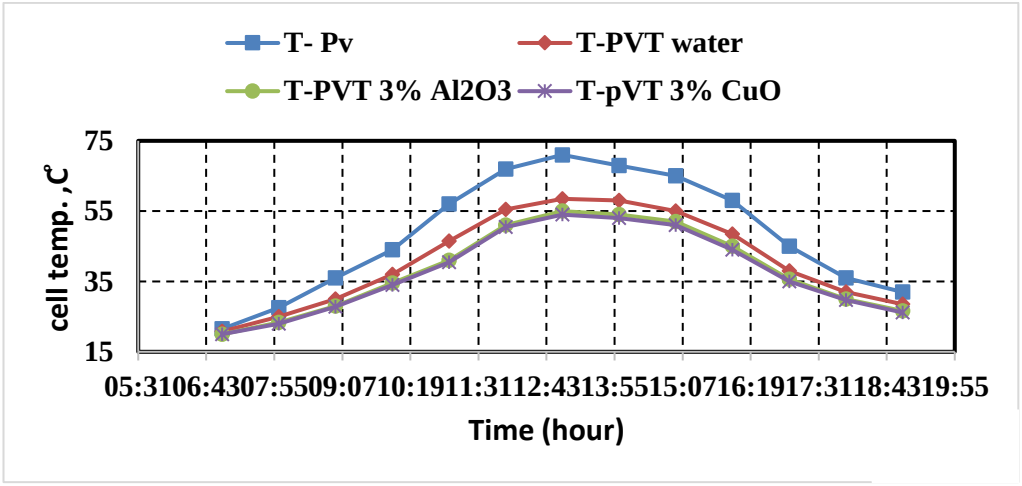

Figure 5.9. Cell surface temperature during daylight hours for different types of Nanofluid at at concentration 3% flow rate (3.5l/min).

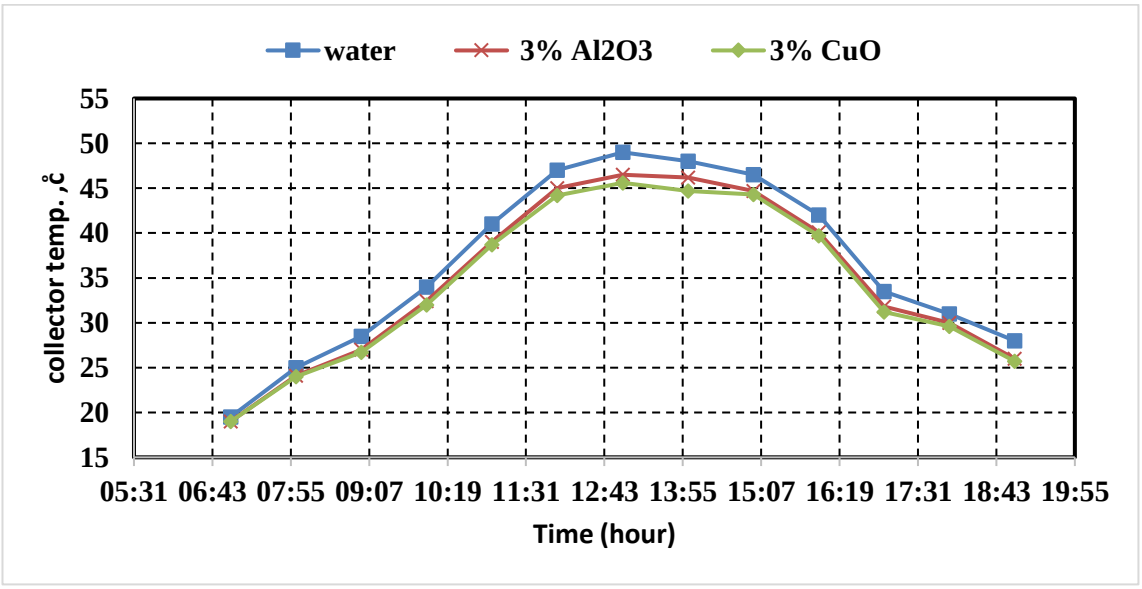

Figure 5.10. Surface temperature of the collector during daylight hours for different types of Nanofluid at at concentration 3% flow rate(3.5)l/min.

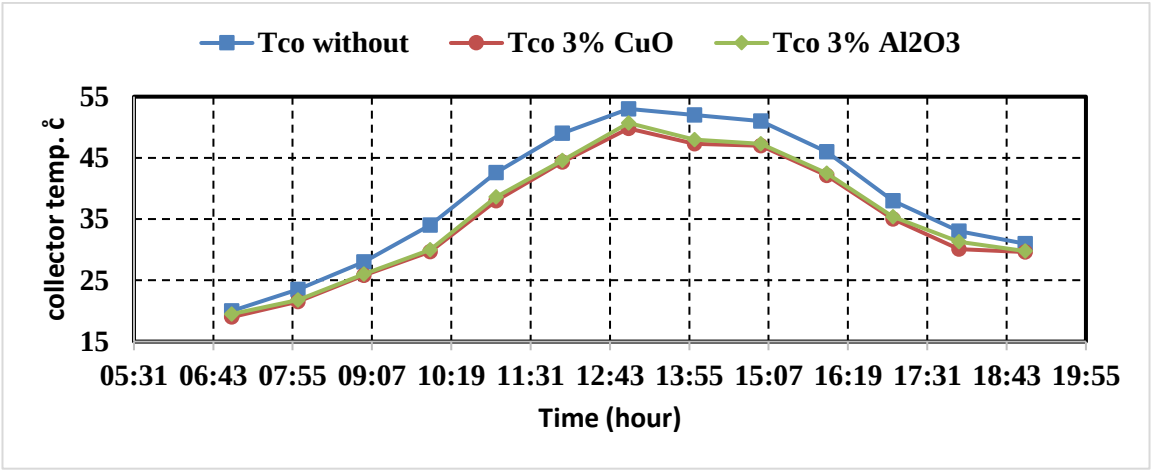

Figure 5.11. Surface temperature of the collector during daylight hours for different types of Nanofluid at at concentration 3% flow rate (1.5)l/min.

Figure 5.10 represents the surface temperature of the collector during daylight hours for different types of nanofluids, where we note that the use of (CuO) at a volumetric concentration of 3% reduces the temperature of the collector (7%), while it decreased by (5%) when using (Al_2O_3) by volumetric concentration 3% for a flow rate of 3.5 liters per minute. Figure (5.11) represents the surface temperature of the collector during daylight hours for different types of nanofluids, where we note that the use of (CuO) at a volumetric concentration of 3% reduces the temperature of the collector (6%), while it decreased by (4.3%) when using (Al_2O_3/water) by volumetric concentration 3% for a flow rate of 1.5 liters per minute.

5.1.2.1.2. Effect of nano -Materials Type on the PV/T Electrical Efficiency

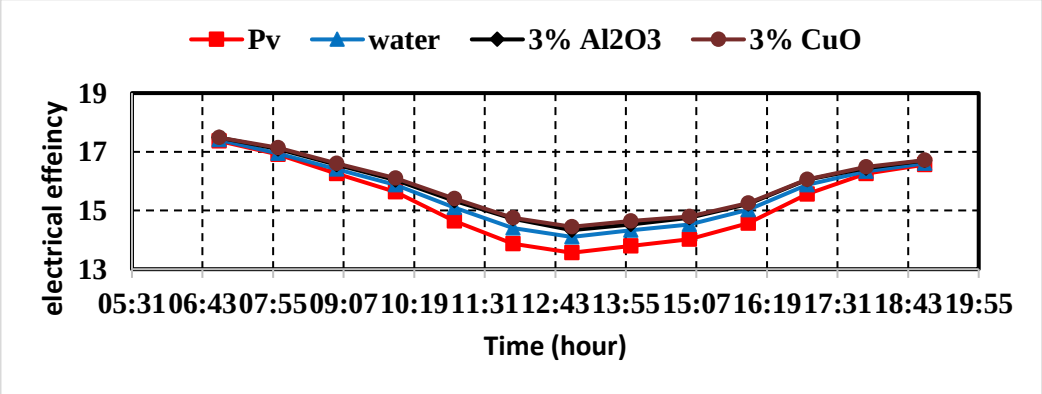

Figure 5.12. Electrical efficiency of PV during daylight hours for different types of nanofluid at at concentration 3% flow rate (1.5)l/min.

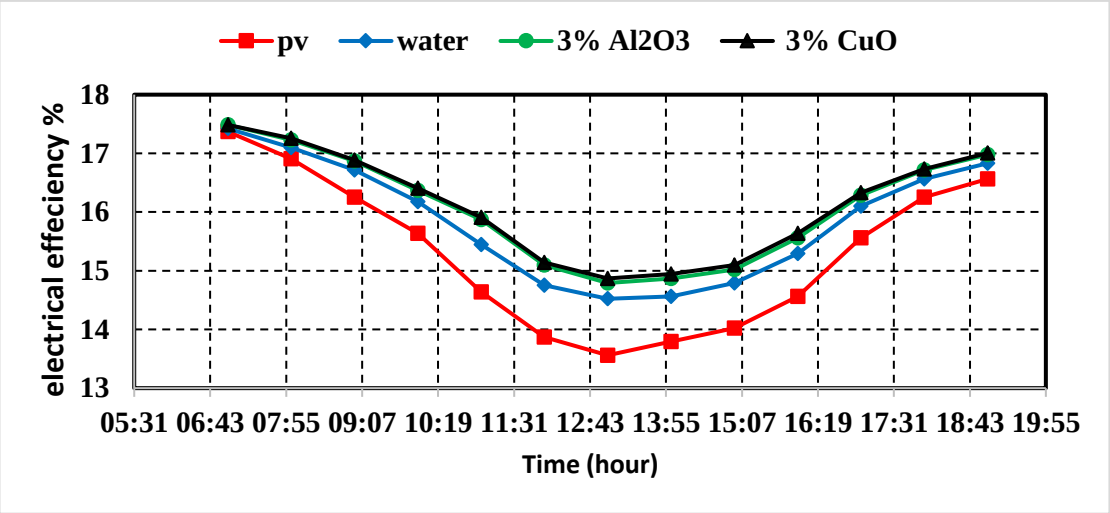

Figure 5.13. Electrical efficiency of PV during daylight hours for different types of nanofluid at concentration 3% and flow rate (3.5)l/min.

Figure 5.12 and 5.13 show the electrical efficiency of the photovoltaic cell which cooled by (CuO/water)3% volumetric concentration and (Al_2O_3/ water)3% volumetric concentration recorded during daylight hours and compare them with the uncooled cell efficiency, where we clearly see an increase in the efficiency when using (CuO /water) nanofluid as a coolant with volumetric concentration of (3%) by (6.5%) while we get increasing by (5.6%) and (3.2%)when we use (Al_2O_3/water) and (water) respectively at flow rate (1.5l/min). Increase in the efficiency when using (CuO /water) nanofluid as a coolant with volumetric concentration of (3%) by (10%) while we get increasing by (9.1%) and (7%) when we use (Al_2O_3/water) and (water) respectively at flow rate (3.5l/min).

5.1.2.1.3. Effect of nano -Materials Type on the Coolant Temperature Difference Between the Inlet and Outlet of the Collector

Figure 5.14 show the coolant temperature difference between the inlet and outlet of the collector which cooled by (CuO/water)3% volumetric concentration and ($Al_2 O_3$/ water)3% volumetric concentration recorded during daylight hours and compare them with that when we use water only, where we clearly see an increase (Δ T) when using(CuO /water) nanofluid as a coolant with volumetric concentration of (3%) by (47 %) than when using only water while we get increasing by (40.8%) when we use

(Al2O3/water) at flow rate (1.5l/min) and (5.15) show the Coolant temperature difference between the inlet and outlet of the collector which cooled by (CuO/water)3% volumetric concentration and (Al_2 O_3/ water)3% volumetric concentration recorded during daylight hours and compare them with that when we use water only, where we clearly see an increase (Δ T) when using(CuO /water) nanofluid as a coolant with volumetric concentration of (3%) volumetric concentration by (40.7 %) than when using only water while we get increasing by (37%) when we use (al2o3/water) at flow rate (3.5l/min) .

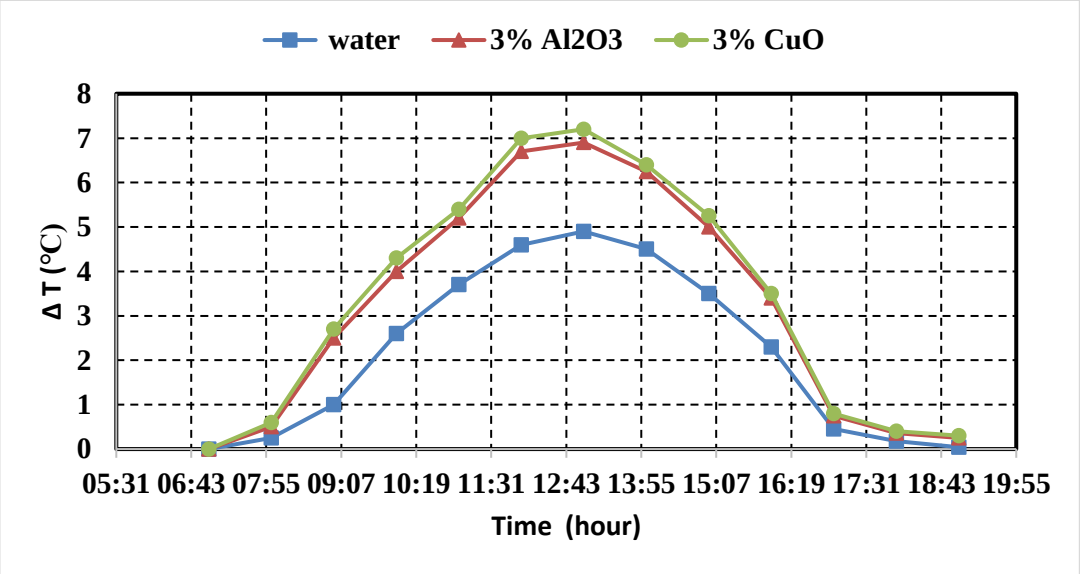

Figure 5.14. The effect of nanofluid type on the (Δ T) with volumetric concentration =3% and flow rate=1.5l/min.

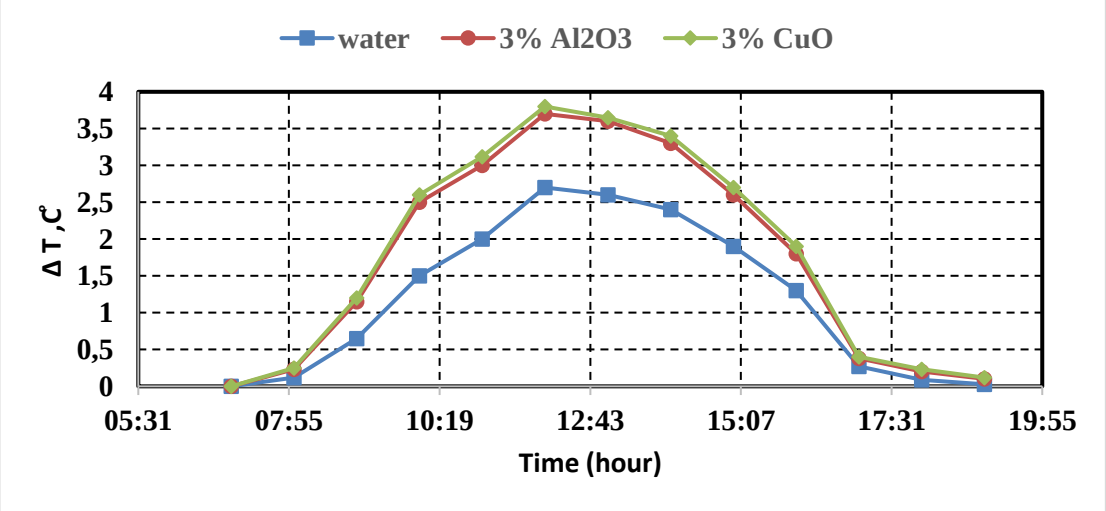

Figure 5.15. The effect of nanofluid type on the (Δ T) with concentration =3% and flow rate=3.5l/min.

5.1.2.1.4. Effect of Nano -Materials Type on the Thermal Efficiency of the Collector

Figure 5.16 and 5.17 show the thermal efficiency of the collector which calculated when we used (CuO/water)3% volumetric concentration and (Al2 O3/ water)3% volumetric concentration during daylight hours and compare them with that when we use water only, where we clearly see an increase in thermal efficiency when using(CuO /water) Nanofluid as a coolant with mixing ratios of (3%) volumetric concentration by (47 %) than when using only water while we get increasing by (40.8%) when we use (Al_2O_3/water) at flow rate (1.5l/min) and (5.17) show the thermal efficiency of the collector which calculate when we use (CuO/water)3% volumetric concentration and (Al_2O_3/ water)3% volumetric concentration recorded during daylight hours and compare them with that when we use water only, where we clearly see an increase in thermal efficiency when using(CuO /water) nanofluid as a coolant with volumetric concentration of (3%) by (40.7 %) than when using only water while we get increasing by (38%) when we use (Al_2O_3/water) at flow rate (3.5l/min) .

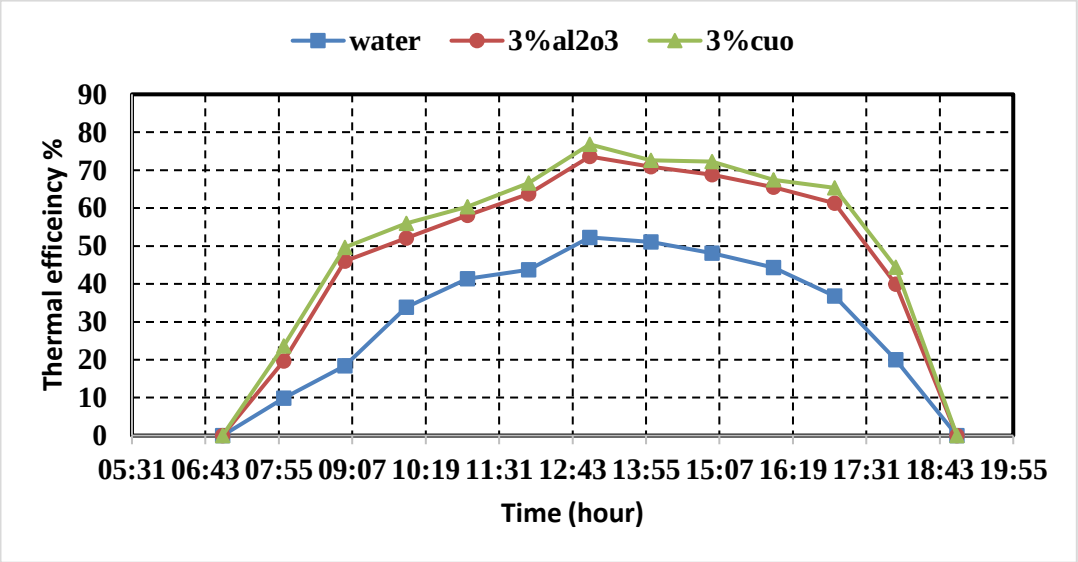

Figure 5.16. The effect of nanofluid type on the thermal efficiency with concentration =3% and flow rate=1.5l/min.

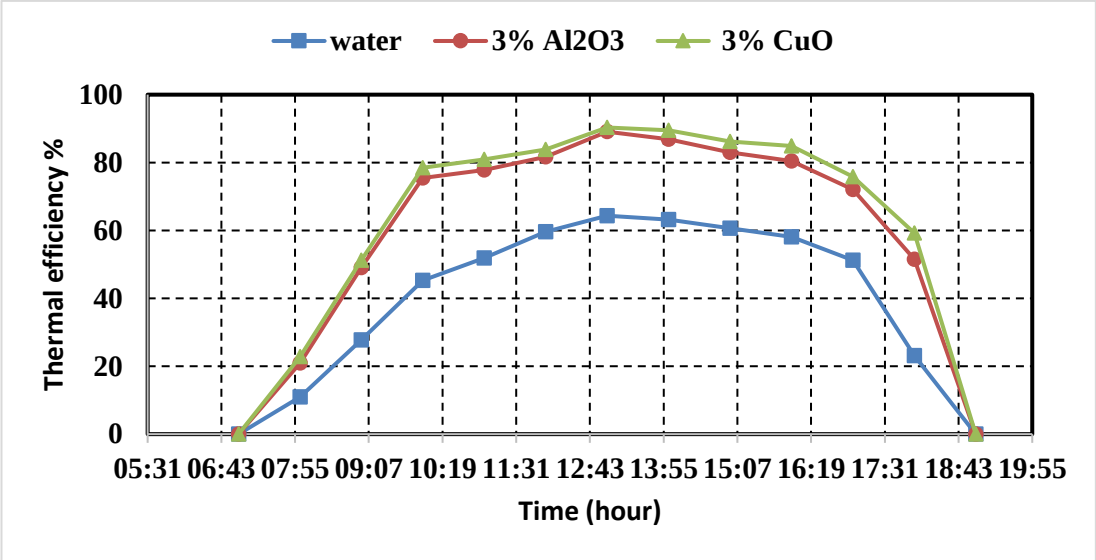

Figure 5.17. The effect of nanofluid type on the thermal efficiency with concentration =3% and flow rate=3.5 l/min.

5.1.2.2. Effect of nano -Materials Concentration on the PV/T System

5.1.2.2.1. Effect of nano -materials concentration on the PV/T temp.

Figure (5.18), (5.19), (5.20) and (5.21) represent the cell surface temperature during daylight hours for different concentrations of (CuO and Al_2O_3) nanofluids. In general, we notice a decrease in the temperature of the cell surface with an increase in the concentration of nano material's when the flow rate is fixed for both nano materials. For example, in figure (5.20) at one o'clock we note that using (CuO/water) at a volumetric concentration 3% reduces the cell temperature (16%), while it decreased by (13%,11.8%) when using (2%) and (1%) volumetric concentration ratio respectively. While (5.22), (5.23), (5.24) and (5.25) represent the collector surface temperature during daylight hours for different concentration of (CuO and Al_2O_3) nanofluids. In general, we notice a decrease in the temperature of the collector surface with an increase in the concentration of nano material's when the flow rate is fixed for both nano materials. For example, in figure (5.23), at one o'clock we note that using (CuO/water) at a volumetric concentration 3% reduces the cell temperature (9.6%), while it decreased by (5.8%,2.2%) when using (2%) and (1%) mixing ratio respectively.

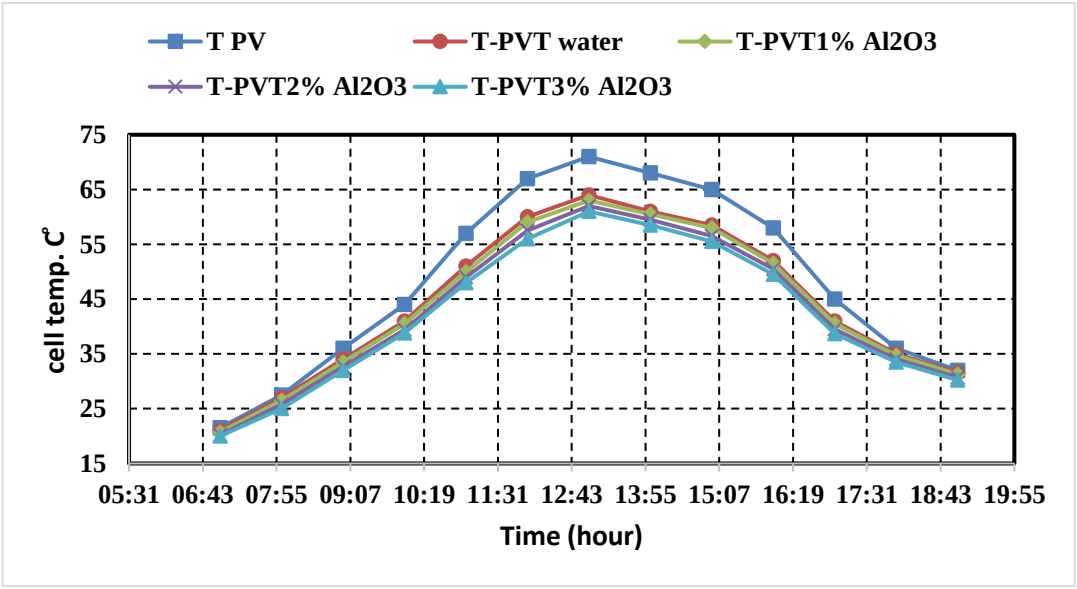

Figure 5.18. The effect of Nanofluid concentration on the cell temp, flow rate=1.5l/min.

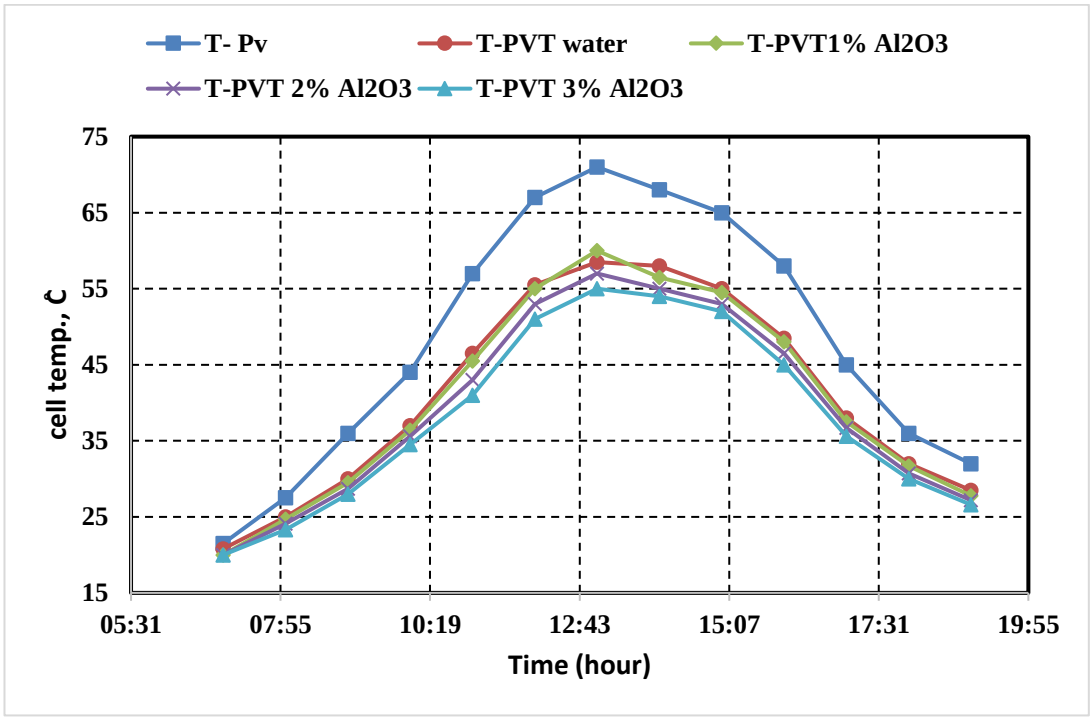

Figure 5.19. The effect of Nanofluid concentration on the cell temp. flow rate=3.5l/min.

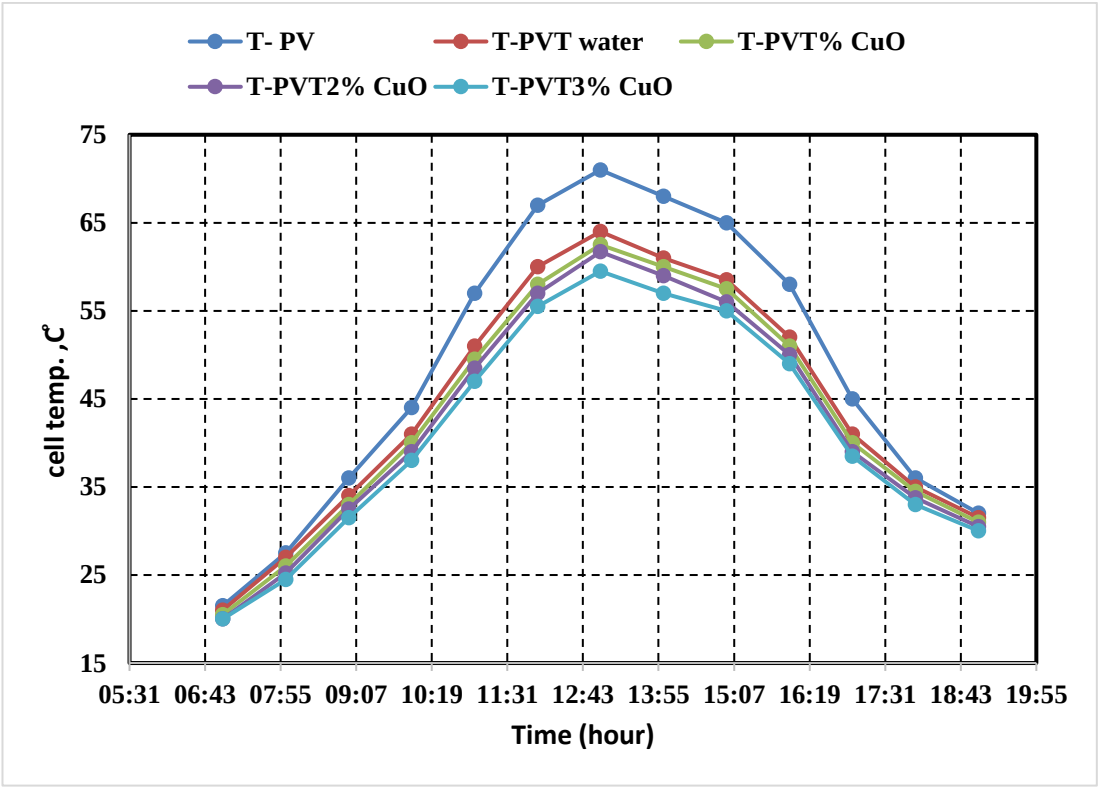

Figure 5.20. The effect of Nanofluid concentration on the cell temp. flow rate=1.5l/min.

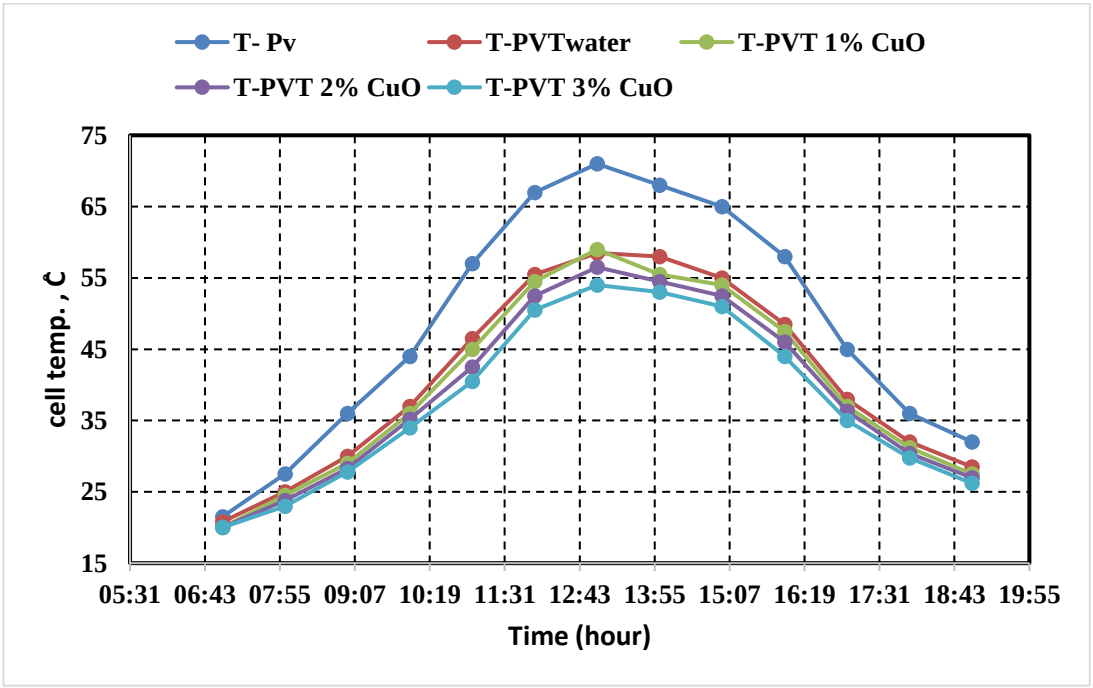

Figure 5.21. The effect of Nanofluid concentration on the cell temp. flow rate=3.5l/min.

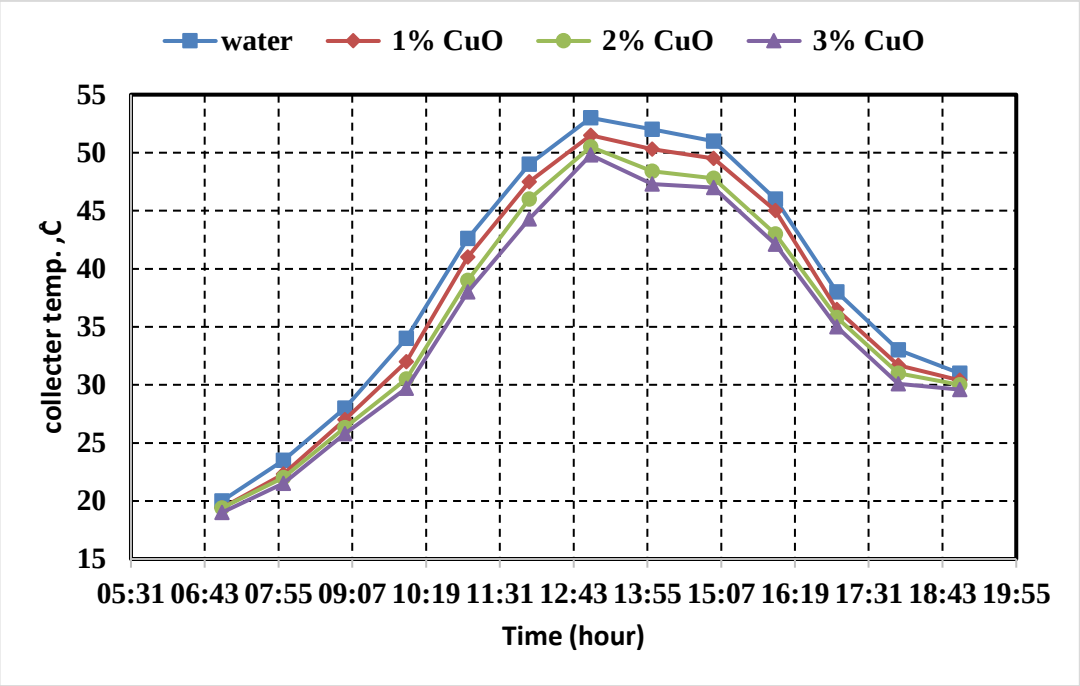

Figure 5.22. The effect of Nanofluid concentration on the collector temp flow rate=1.5l/min.

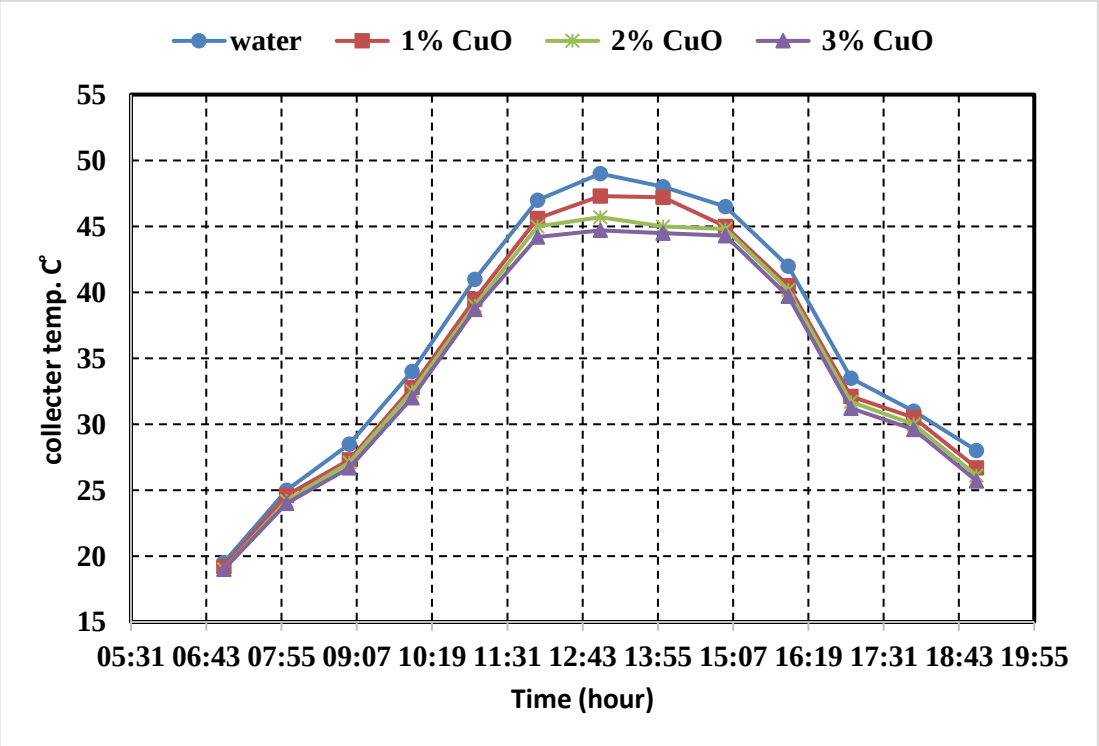

Figure 5.23. The effect of Nanofluid concentration on the collector temp flow rate=3.5l/min.

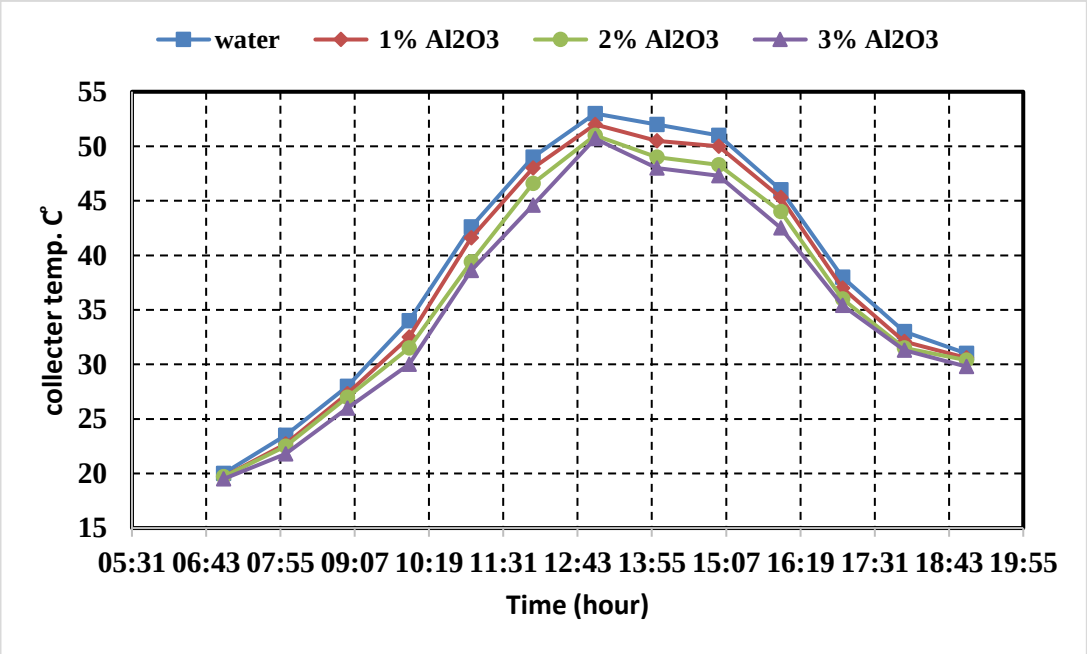

Figure 5.24. The effect of Nanofluid concentration on the collector temp. flow rate=1.5l/min.

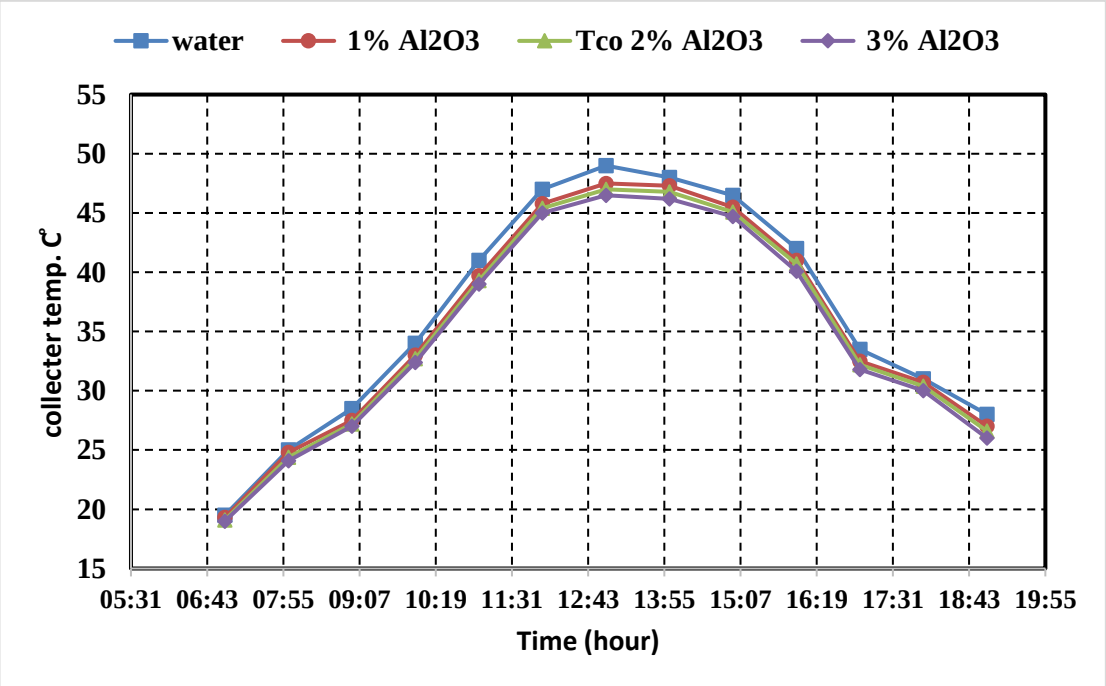

Figure 5.25. The effect of Nanofluid concentration on the collector temp., flow rate=3.5l/min.

5.1.2.2.2. Effect of Nano -Materials Concentration on the PV/T Electrical Efficiency

Figure (5.26), (5.27), (5.28) and (5.29) represent the electrical efficiency during daylight hours for different concentrations of (CuO and Al2O3) Nanofluids. In general, we notice an increase in electrical efficiency with an increase in the concentration of nano materials when the flow rate is fixed for both nano materials. For example, in figure (5.29) at one o'clock we note that using (cuo/water) at a mixing ratio 3% V% increase the electrical efficiency (16%), while it decreased by (13%, 11.8%) when using (2%) and (1%) mixing ratio respectively.

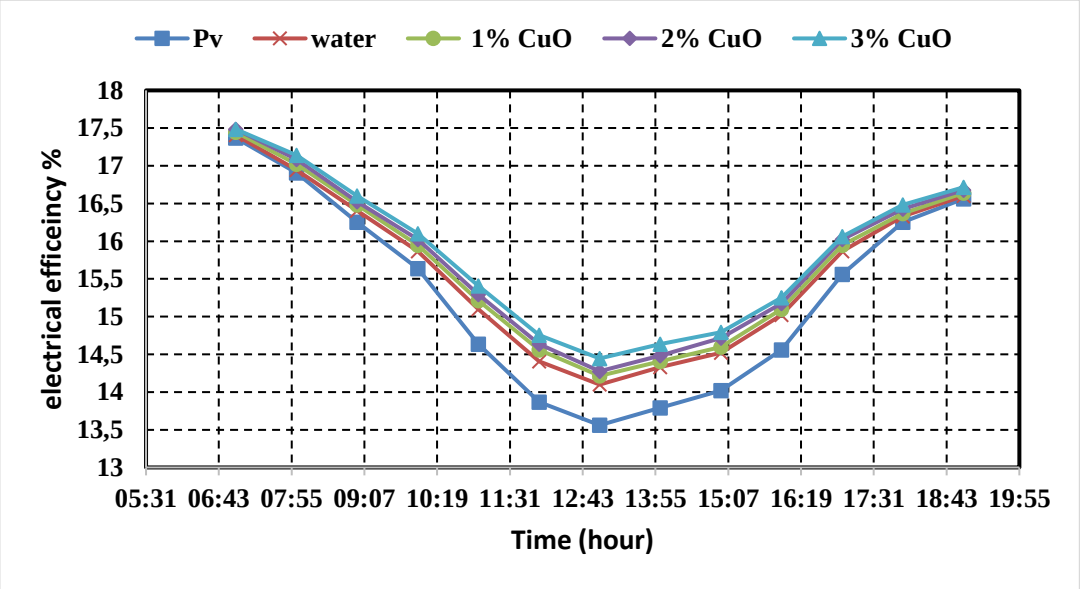

Figure 5.26. The effect of Nanofluid concentration on electrical efficiency, flow rate=1.5l/min.

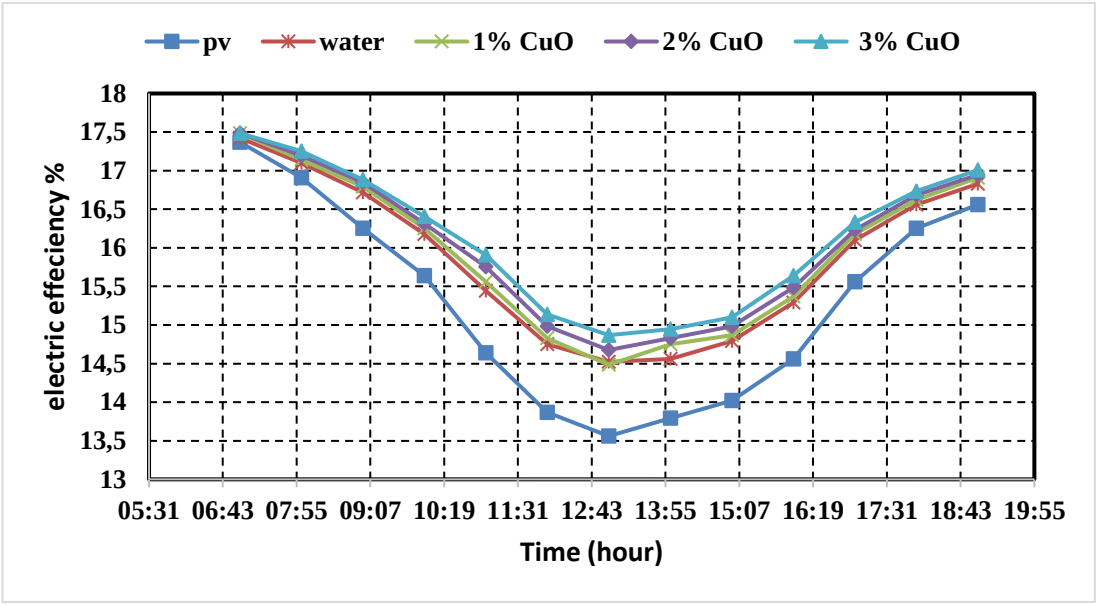

Figure 5.27. The effect of Nanofluid concentration on electrical efficiency, flow rate=3.5l/min.

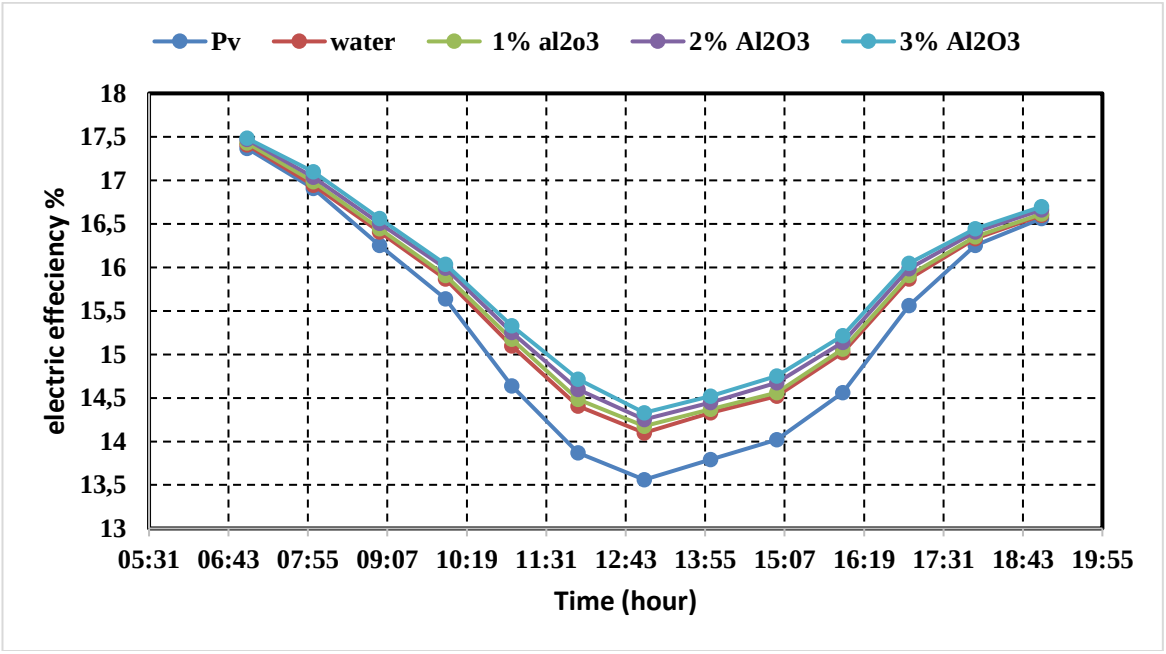

Figure 5.28. The effect of Nanofluid concentration on electrical efficiency, flow rate=1.5l/min.

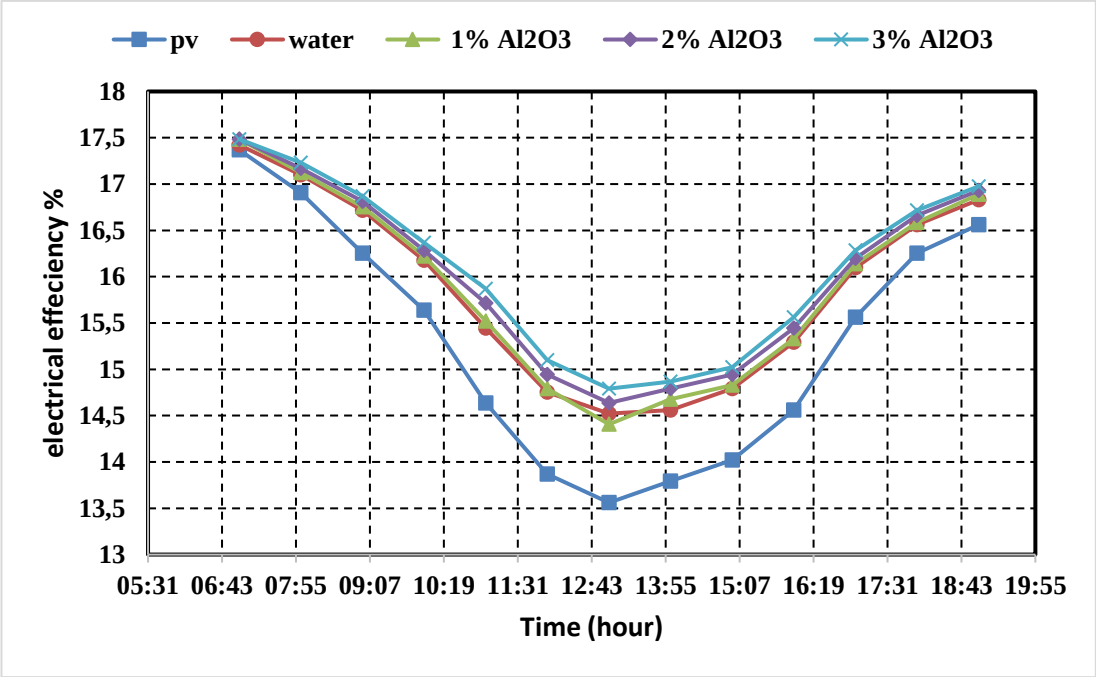

Figure 5.29. The effect of Nanofluid concentration on electrical efficiency, flow rate=3.5l/min.

5.1.2.2.3. Effect of Nano -materials Concentration on the Coolant Temperature Difference Between the Inlet and Outlet of the Collector

Figure (5.30), (5.31), (5.32) and (5.33) represent the Coolant temperature difference between the inlet and outlet of the collector during daylight hours for different concentrations of (CuO and Al2O3) Nanofluids. In general, we notice an increase in the (Δ T) with an increase in the concentration of nano material's when the flow rate is fixed for both nano materials. For example, in figure (5.31) at one o'clock we note that using (cuo/water) at a mixing ratio 3% V% increase (Δ T) (16%), while it decreased by (13%, 11.8%) when using (2%) and (1%) mixing ratio respectively

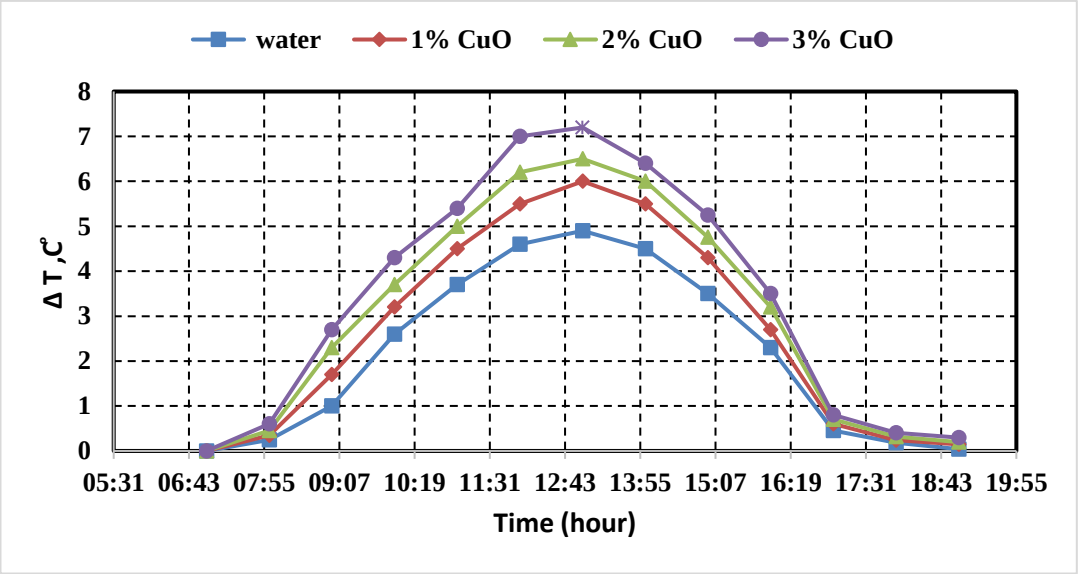

Figure 5.30. The effect of Nanofluid concentration on Δ T, flow rate=1.5l/min.

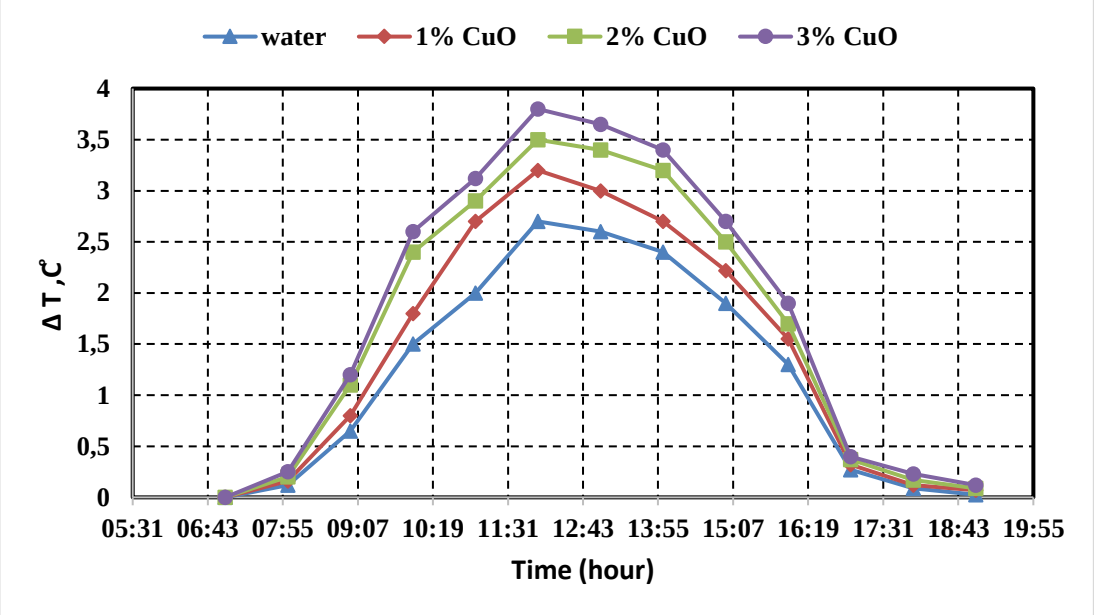

Figure 5.31. The effect of Nanofluid concentration on Δ T, flow rate=3.5l/min.

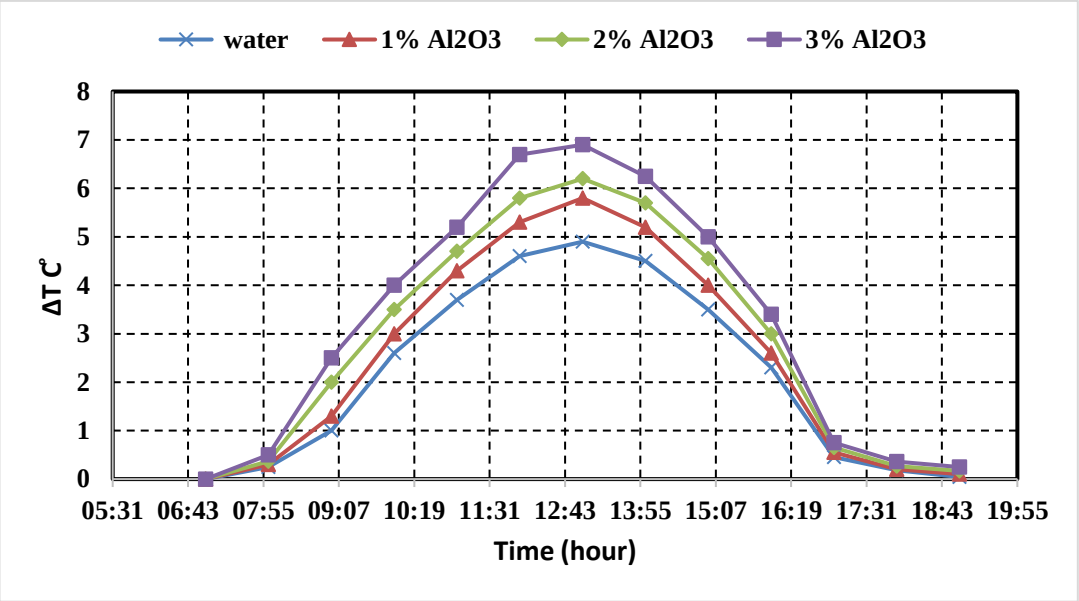

Figure 5.32. The effect of Nanofluid concentration on Δ T, flow rate=1.5l/min.

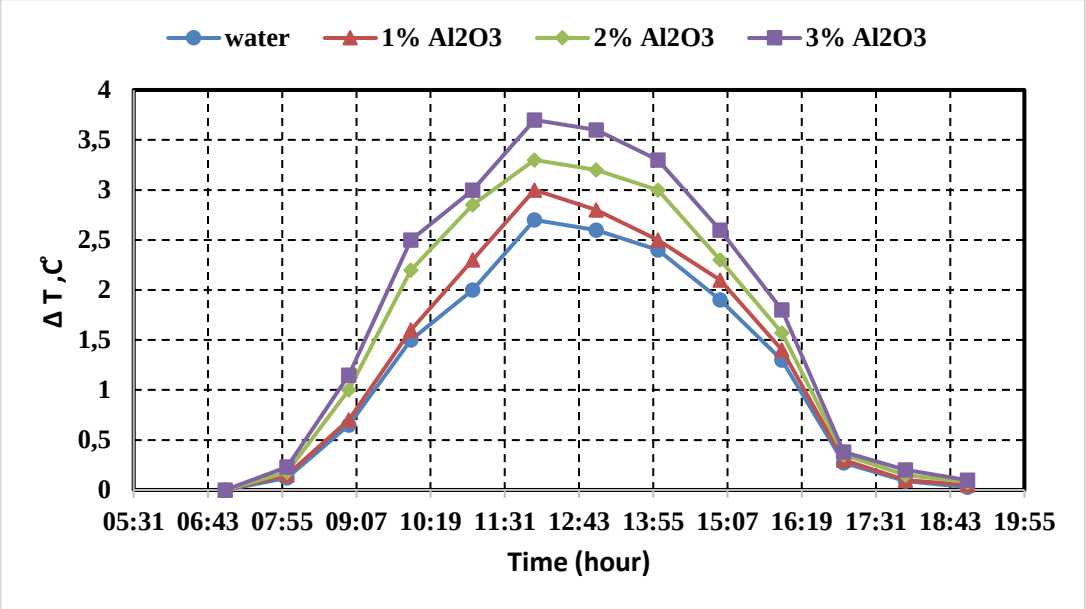

Figure 5.33. The effect of nanofluid concentration on Δ T, flow rate=3.5l/min.

5.1.2.2.4. Effect of Nano -Materials Concentration on the Thermal Efficiency of the PV/T System

Figure (5.34), (5.35), (5.36) and (5.37) represent thermal efficiency during daylight hours for different concentrations of (CuO and Al2O3) nanofluids. In general, we notice an increase in thermal efficiency with an increase in the concentration of nano

materials when the flow rate is fixed for both nano materials. For example, in figure (5.37) at one o'clock we note that using (cuo/water) at a volumetric concentration 3% increase the thermal efficiency (40.4%), while it increased by (30.8%, 15.4%) when using (2%) and (1%) volumetric concentration respectively.

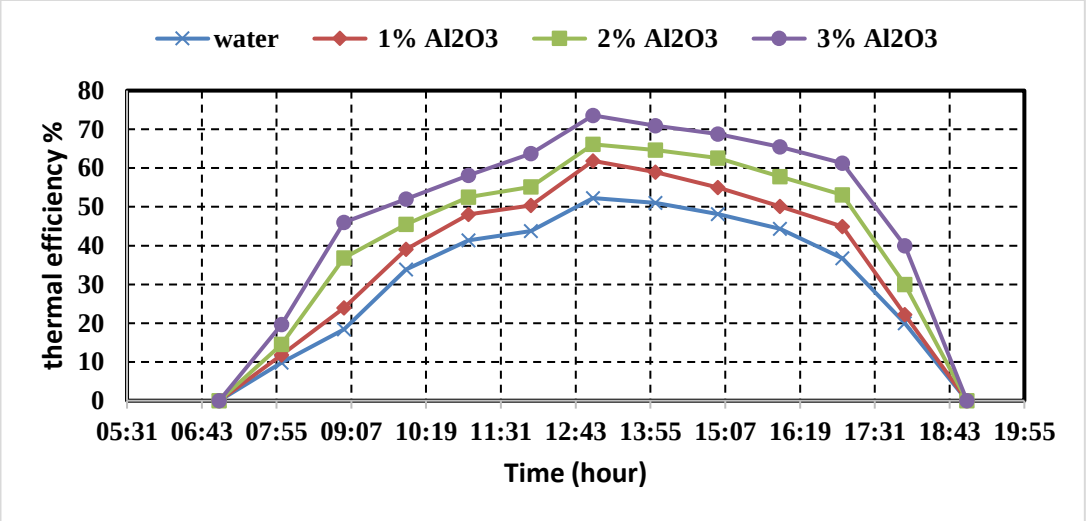

Figure 5.34. The effect of nanofluid concentration on the thermal efficiency, flow rate=1.5l/min.

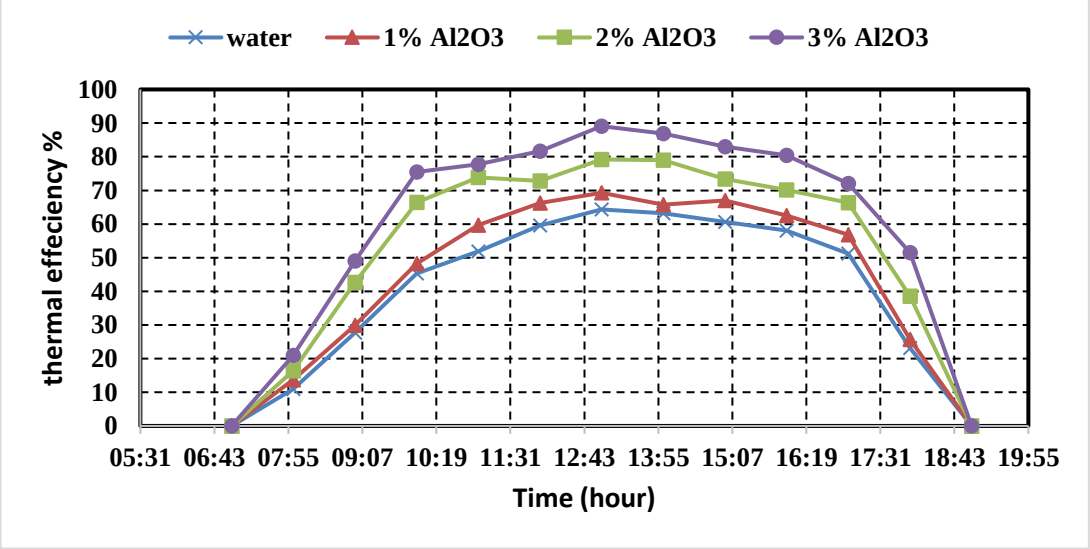

Figure 5.35. The effect of nanofluid concentration on the thermal efficiency, flow rate=3.5l/min.

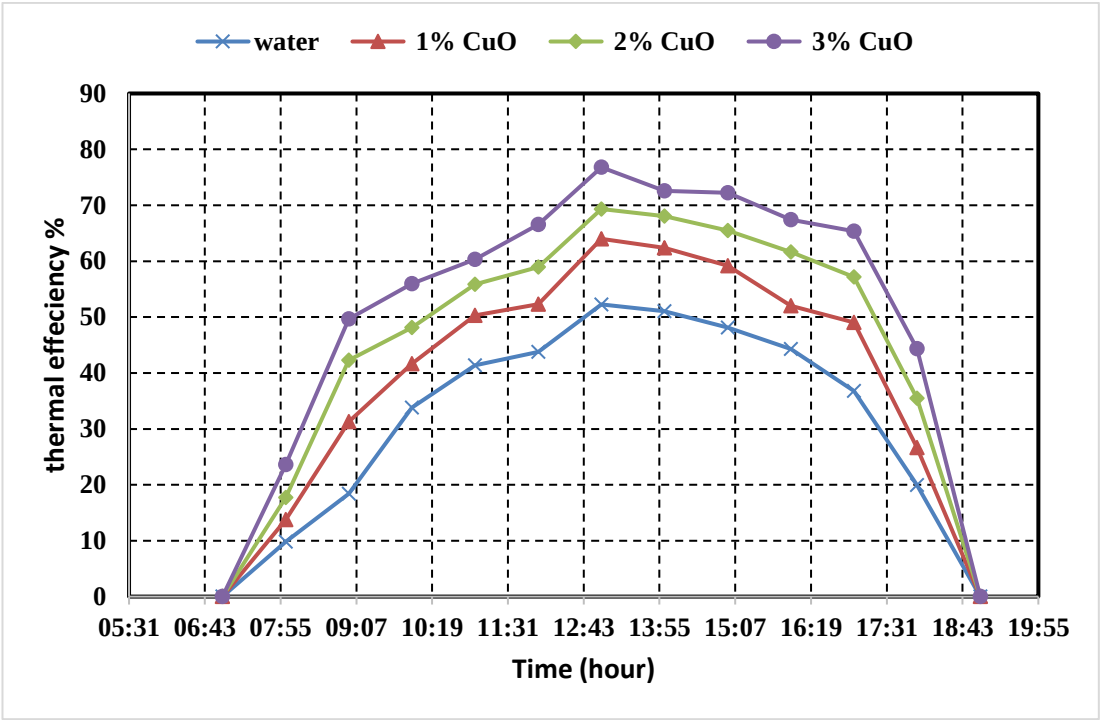

Figure 5.36. The effect of nanofluid concentration on the thermal efficiency. flow rate=1.5l/min.

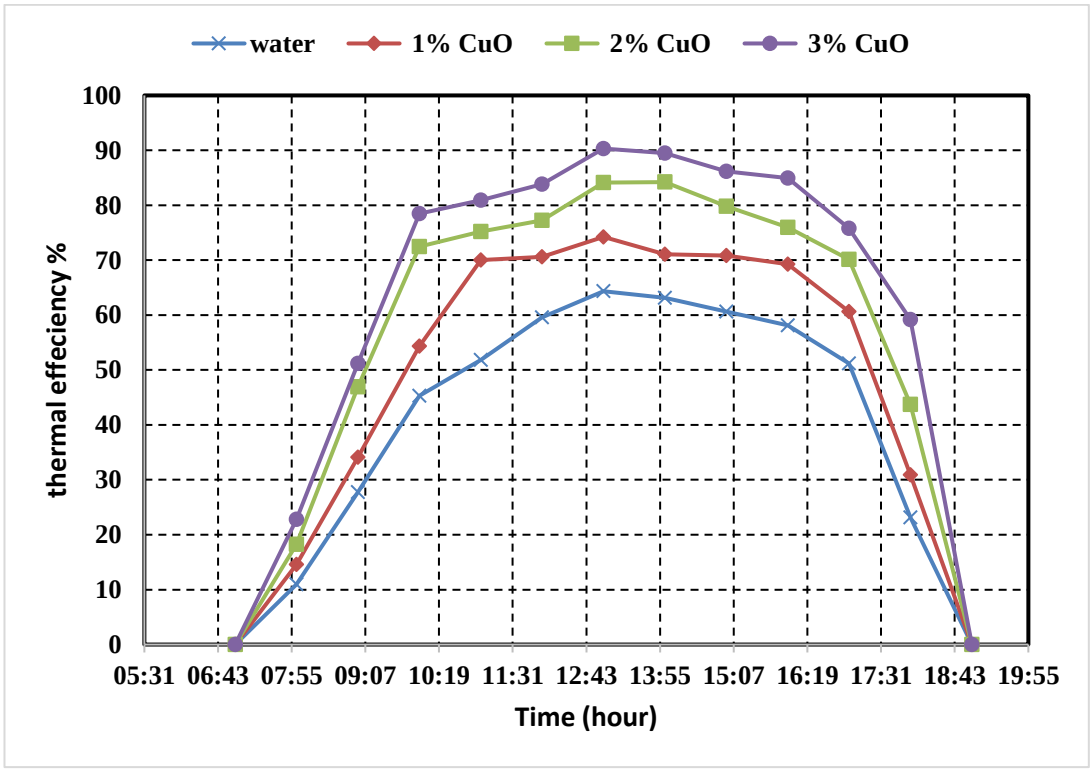

Figure 5.37. The effect of nanofluid concentration on the thermal efficiency. flow rate=3.5l/min.

5.2. NUMERICAL SIMULATION RESULTS

We have studied the effect of nano material's type and nano material concentration on the PV/T system, especially the surface temperature of the collector, as well as the difference in the temperature of the nanofluid when it enters the collector and when it exits.

5.2.1. Result of PV/T Model (SS) with (Water) Only

The figures (5.38) and (5.39) show the temperature distribution on the surface of the collector, where it is low at the inlet of the collector due to the presence of a new coolant with a low temperature, and it rises relatively towards the outlet of the collector, where the temperature of the coolant increases when it absorbs heat from the collector cover, which is in contact with the back of the panel. We also note the temperature decrease at connection points (sphere bulge) due to the increase in the surface area for heat transfer at these points, as is evident in all contours (5.38) and (5.39). We also note the temperature decrease in the morning and evening hours when the amounts of solar radiation are few. We also noticed a decrease in the surface temperatures of the collector when using a higher flow rate.

The Figure 5.41 shows the decrease in the surface temperature of the collector with an increase in the flow rate, and the maximum decrease in the surface temperature of the collector when using (3.5)l/min by(5.9 %) than when using (1.5l/min) but it decrease by(4.8% and 3.2 %) when we use (2.5l/min and 2l/min)respectively , Because of The coolant absorbs a greater amount of heat from the collector cover which supported by (sphere bulge), which helps to Increase the rate of heat transfer between the absorption plate and the coolant.

Figure 5.40 shows the difference in coolant temperature between the inlet and outlet of the collector with a change in the flow rate, where the largest difference in the coolant temperature was at a flow rate of (1.5)l/min It increases by (11.9%) than when using (3.5l/min) while it increases by (10.7% and 9.8%) when using (2.5 and 2l/min) respectively.

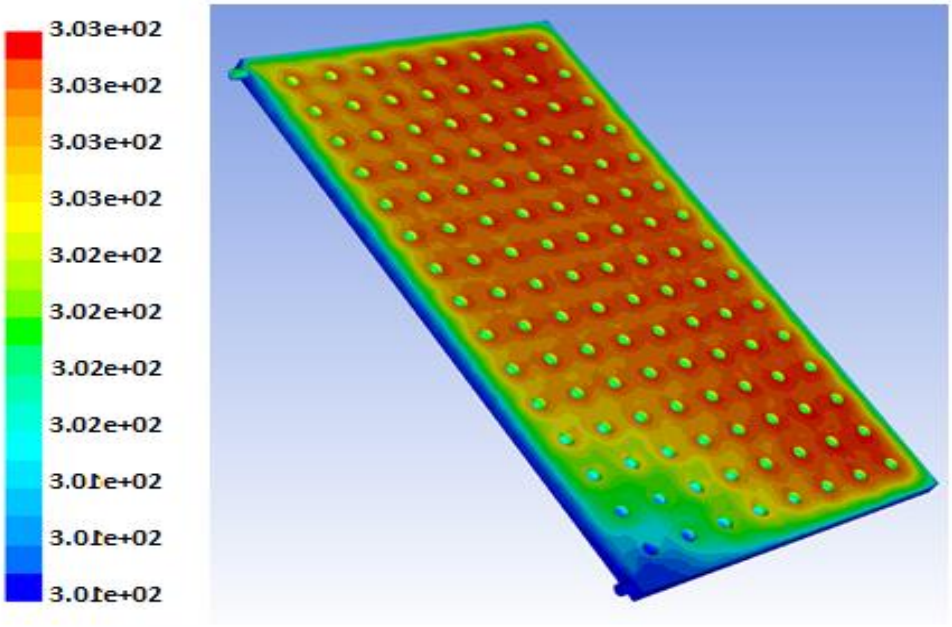

(a) at 8:00 Am

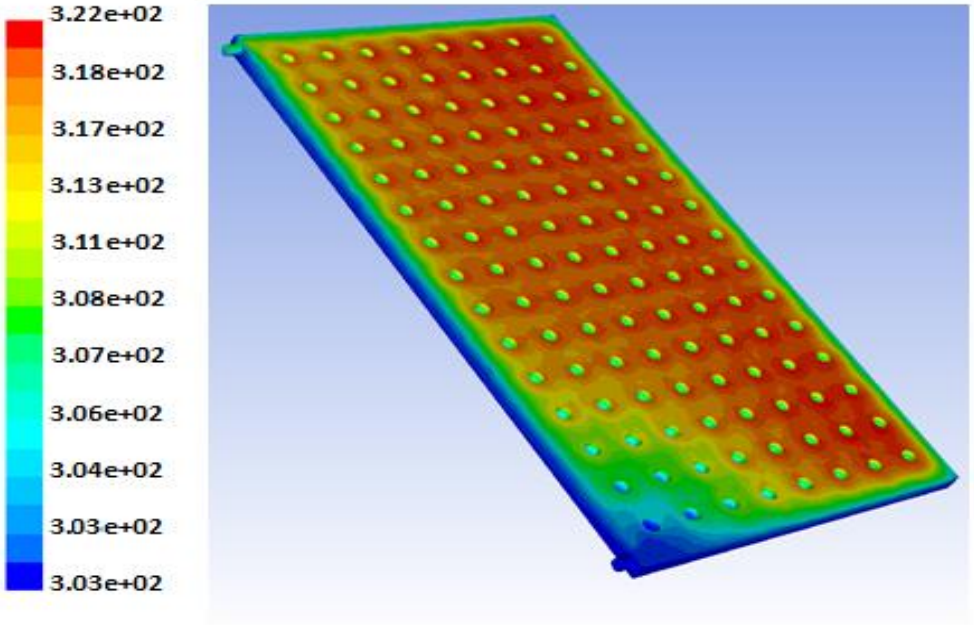

(b) at 10:00 Am

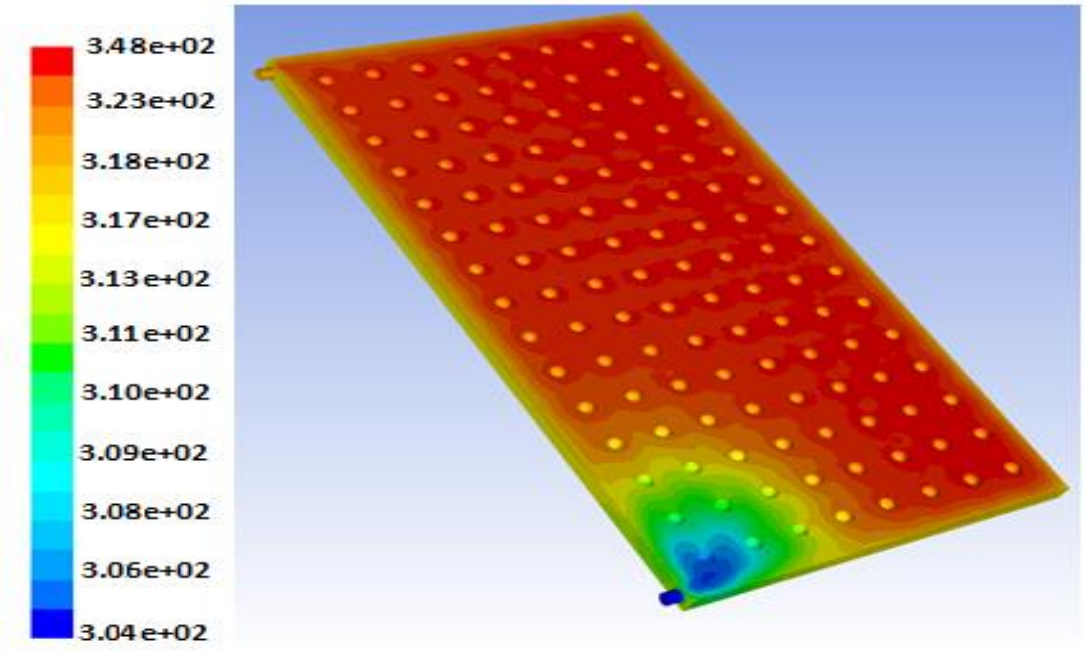

(c) at 1:00 Pm

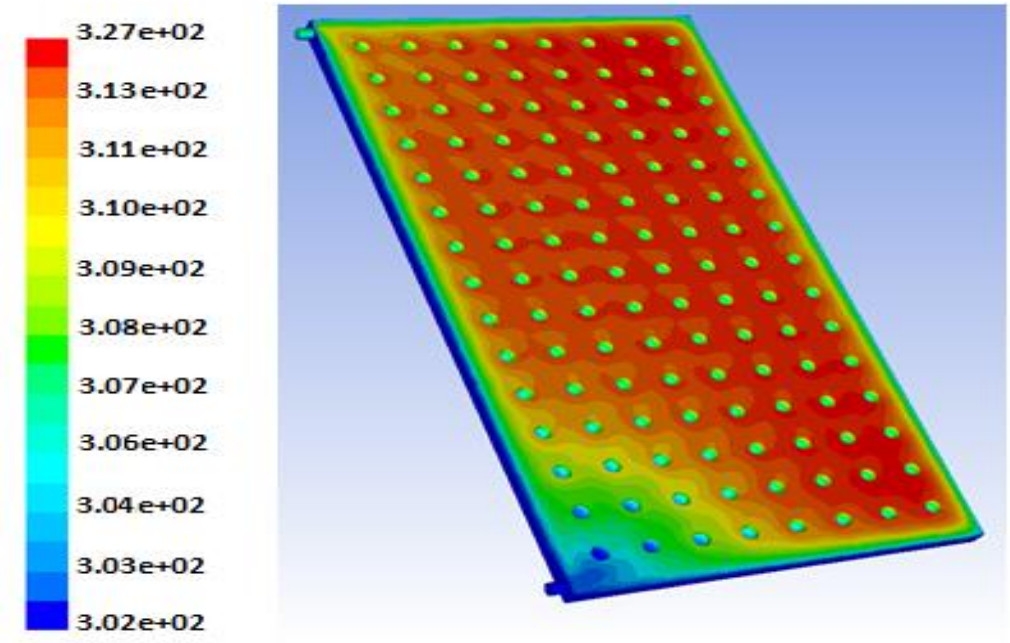

(d) at 6:00 Pm

Figure 5.388. Contours of temperature distribution for Model-SS collector (1.5l/minin flow rate); (a) at 8 a.m., (b) at 10 a.m., (c) at 1 p.m., (d) at 6 p.m.

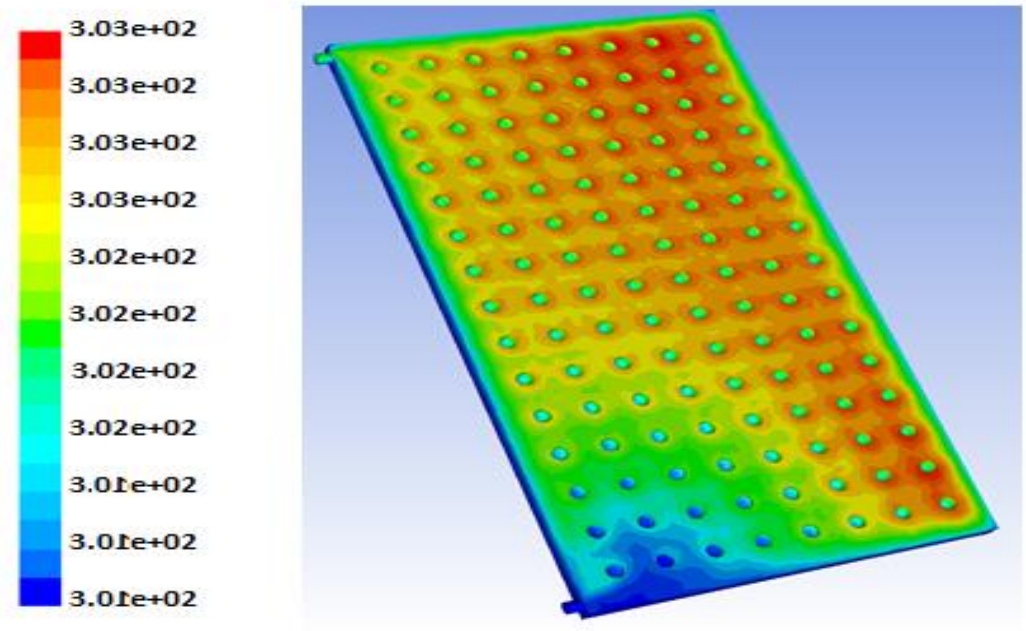

(a) at 8:00 Am

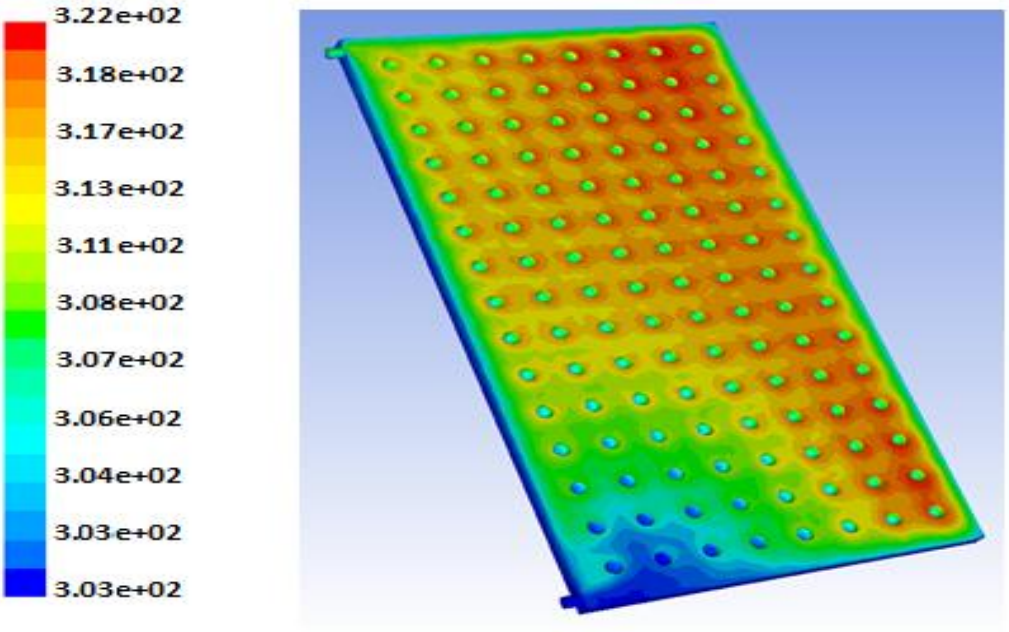

(b) at 10:00 Am

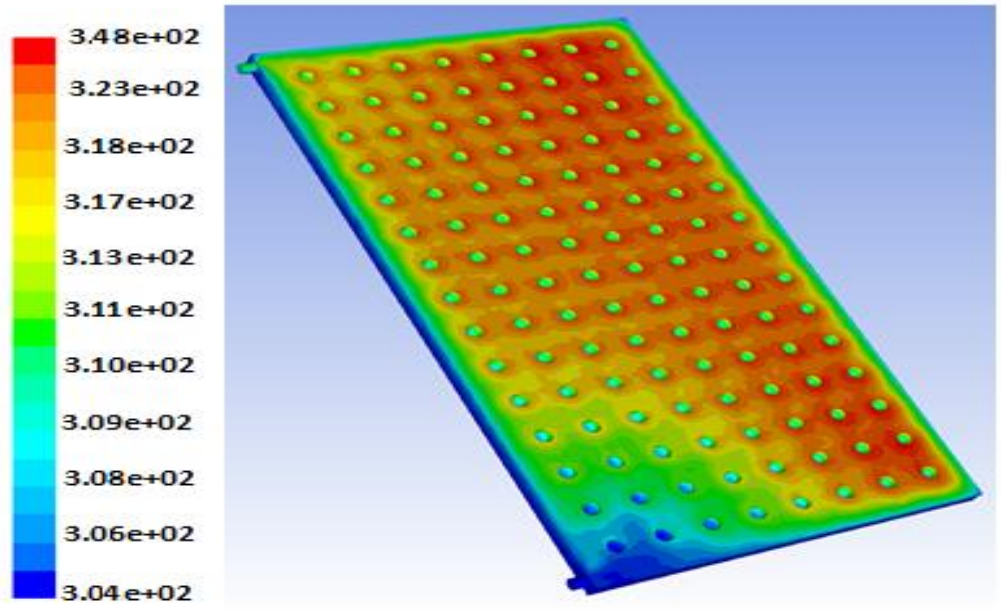

(c) at 1:00 Pm

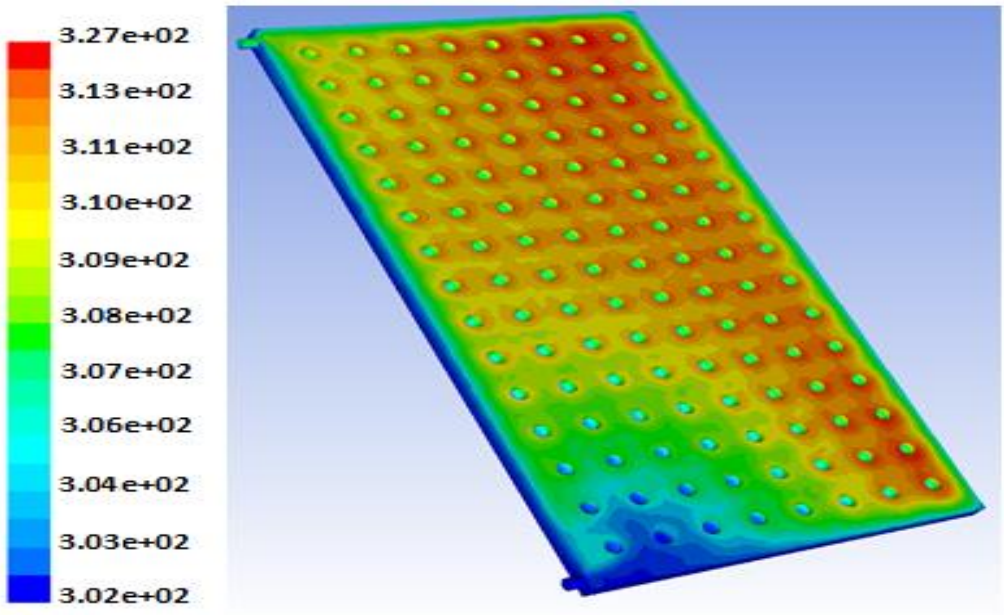

(d) at 6:00 Pm

Figure 5.39. Contours of temperature distribution for Model-SS collector (3.5l/minin flow rate); (a) at 8 a.m., (b) at 10 a.m., (c) at 1 p.m., (d) at 6 p.m.

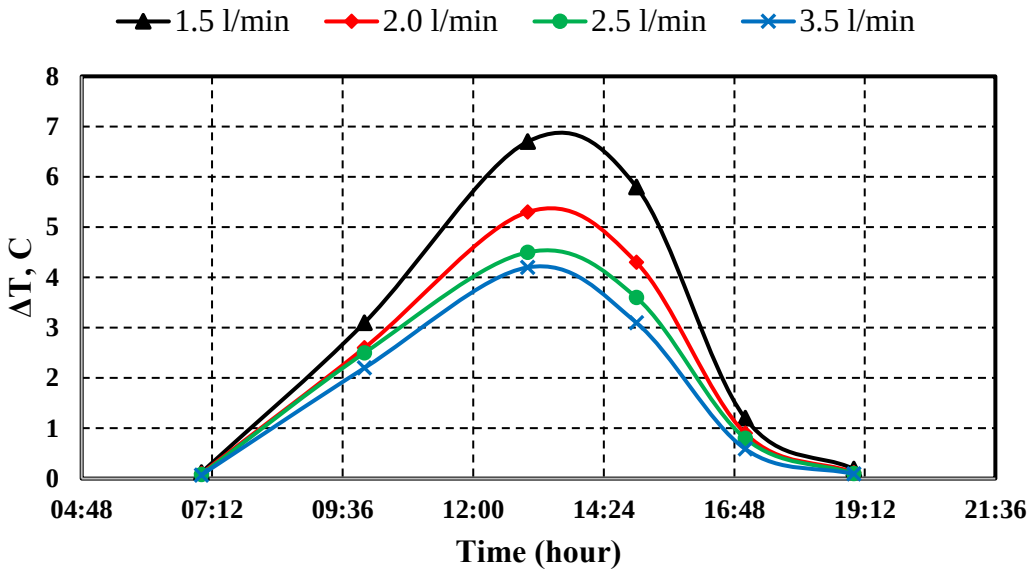

Figure 5.390. Simulated results of difference water temperature between the inlet and output for Model-SS collector at different flow rates.

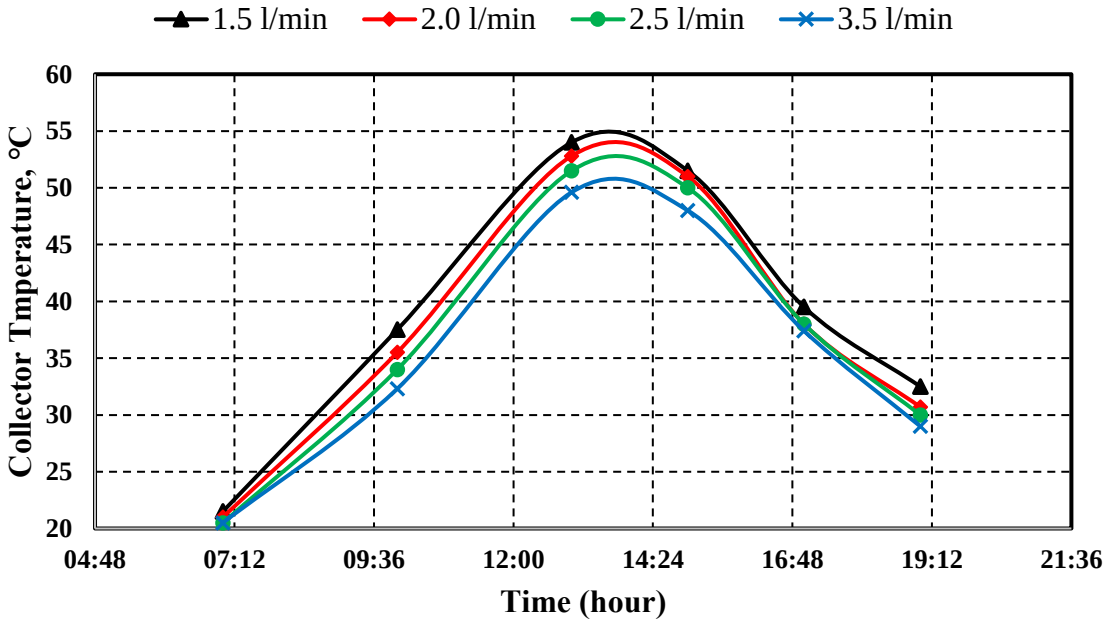

Figure 5.401. Simulated results of average temperature of collector cover for Model-SS at different flow rates.

5.2.2. Result of PV/T Model (SS) with (Al_2O_3/Water) Nanofluid

The figures (5.42) and (5.43) show the temperature distribution on the surface of the collector, at(1:00 PM)when we use (Al_2O_3/water) Nanofluid with deferent concentration (1%,2% and 3% Vt) and with flow rate (1.5l/min and 3.5l/min)We notice a decrease in the surface temperature of the collector with an increase in the mixing ratio (concentration) at a constant flow rate Where we notice a decrease in the surface temperature of the collector by (4.1%) when using a nano -liquid with a concentration (1%) compared to its temperature when using water only, while it decreases by (6.8% ,8.4%) when using concentrations (2% and 3%) at flow rate (1.5l/min)respectively as shown in figure (5.45.a and b), We also note the temperature decrease when we using a higher flow rate(3.5l/min) with the same concentration as shown in figure (5.45.b) Where we notice a decrease in the surface temperature of the collector by (5.1%) when using a Nano -liquid with a concentration (1%) compared to its temperature when using water only, while it decreases by (6.2% and 7.8%) when using concentrations (2% and 3%) respectively and as is evident in the contours (5.42)and(5.43). where it is low at the inlet of the collector due to the presence of a new coolant with a low temperature, and it rises relatively towards the outlet of the collector, where the temperature of the coolant increases when it absorbs heat from the collector cover, which is in contact with the back of the panel.

We also note the temperature decrease at connection points (sphere bulge) due to the increase in the surface area for heat transfer at these points, as is evident in all contours (5.42) and (5.43).

Figure (5.44 a and b) shows the difference in coolant temperature between the inlet and outlet of the collector with a change in the concentration, where the largest difference in the coolant temperature was at a concentration of (3%) This is due to the increase in the heat transfer coefficient of the liquid after increasing the proportion of mixing nano material's Where we notice an increase in (Δ T) by (3.8) when using a Nanoliquid with a concentration (1%) compared to when using water only, while it increases by (5.9% and 10.3%) when using concentrations (2% and 3%) respectively at a flow rate (1.5l/min) as shown in Figure (5.44.a).

When using a flow rate (3.5l/min) we notice a decrease in (Δ T) in general compared to using a flow rate (1.5l/min) where we recorded the following percentages of increases for (Δ T) with an increase in concentration (3.2% at 1% concentration, 4.7% at 2% concentration and 7.8 at 3% concentration) as show in figure (5.44.b).

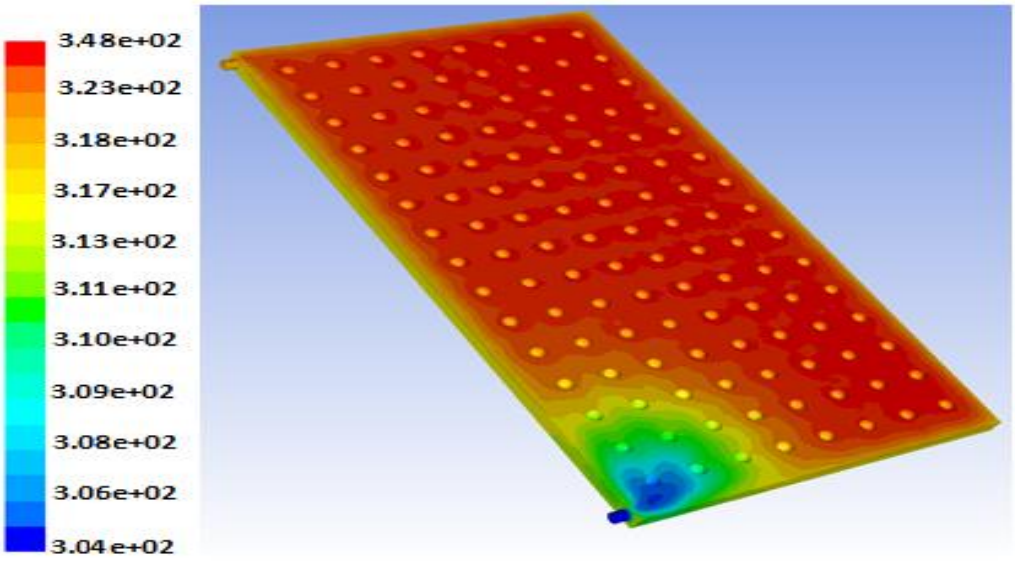

(a) Without Nano

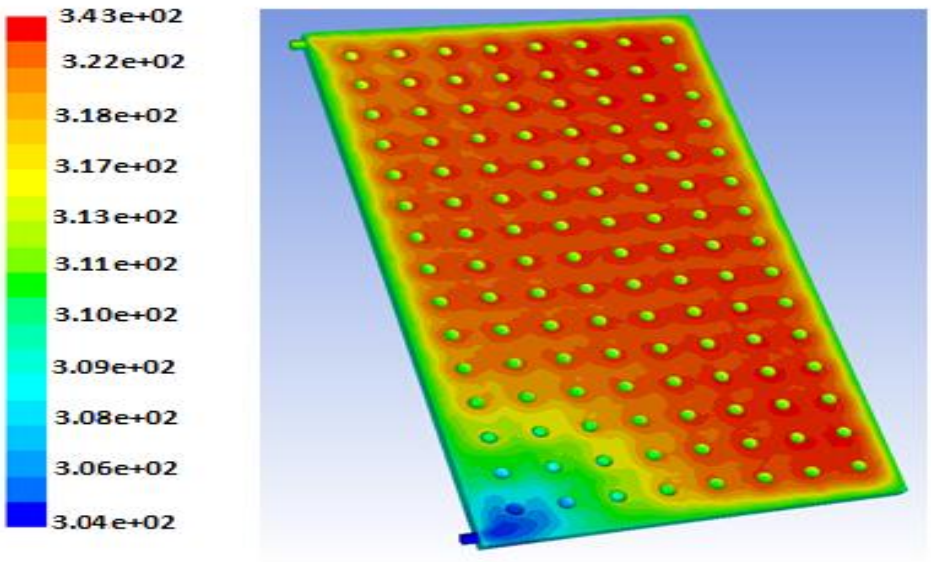

(b) at 1 % Al_2O_3

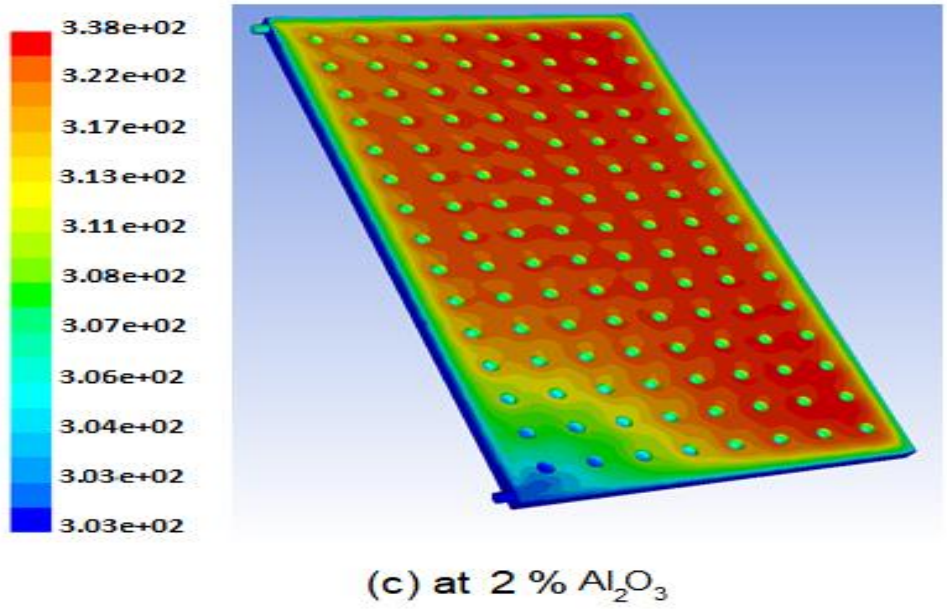

(c) at 2 % Al_2O_3

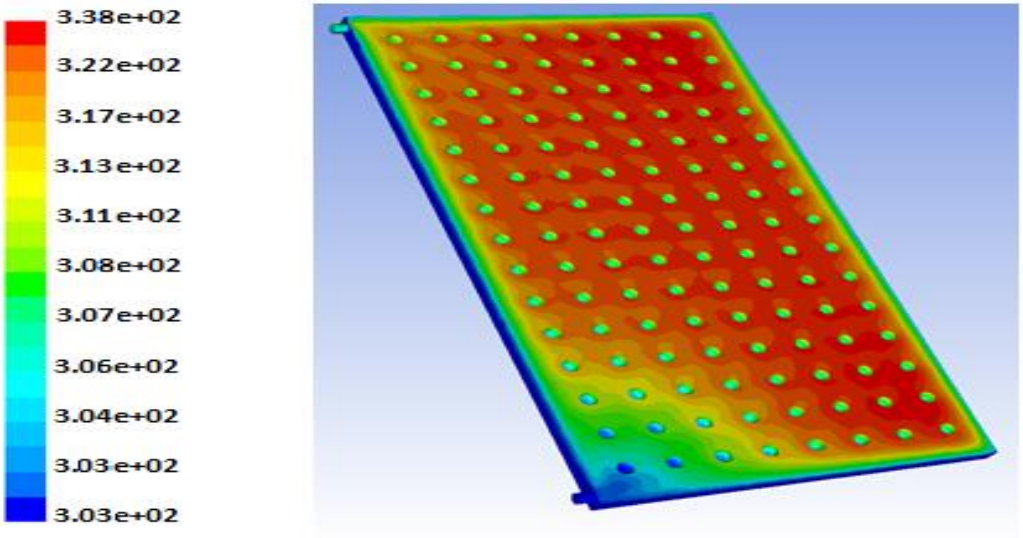

(d) at 3 % Al_2O_3

Figure 5.412. Contours of temperature distribution for Model-SS collector with 1.5l/minin flow rate at 1:00 pm; (a) without Nano , (b) with 1% Al_2O_3, (c) with 2% Al_2O_3, (d) with 3% Al_2O_3

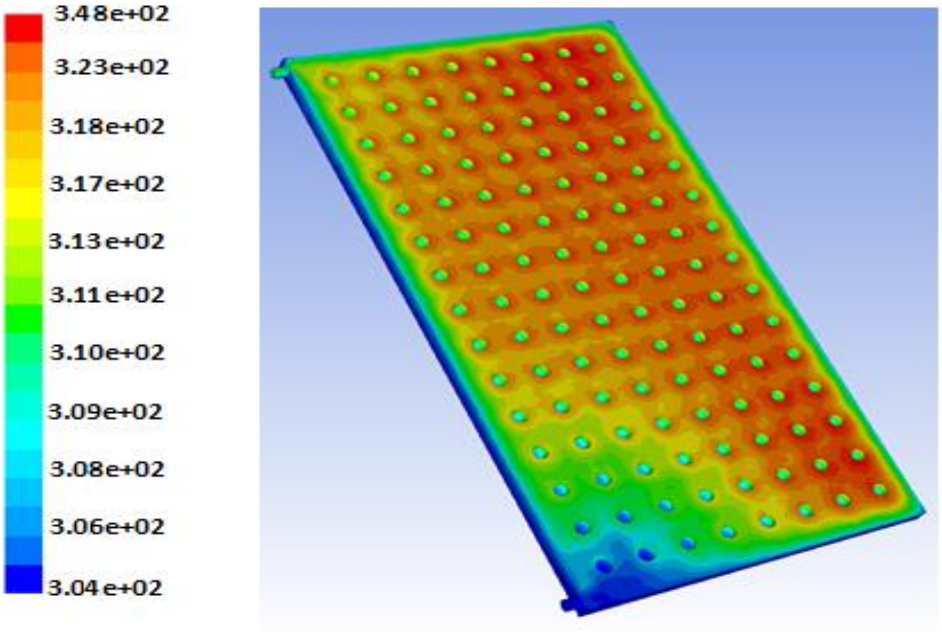

(a) Without Nano

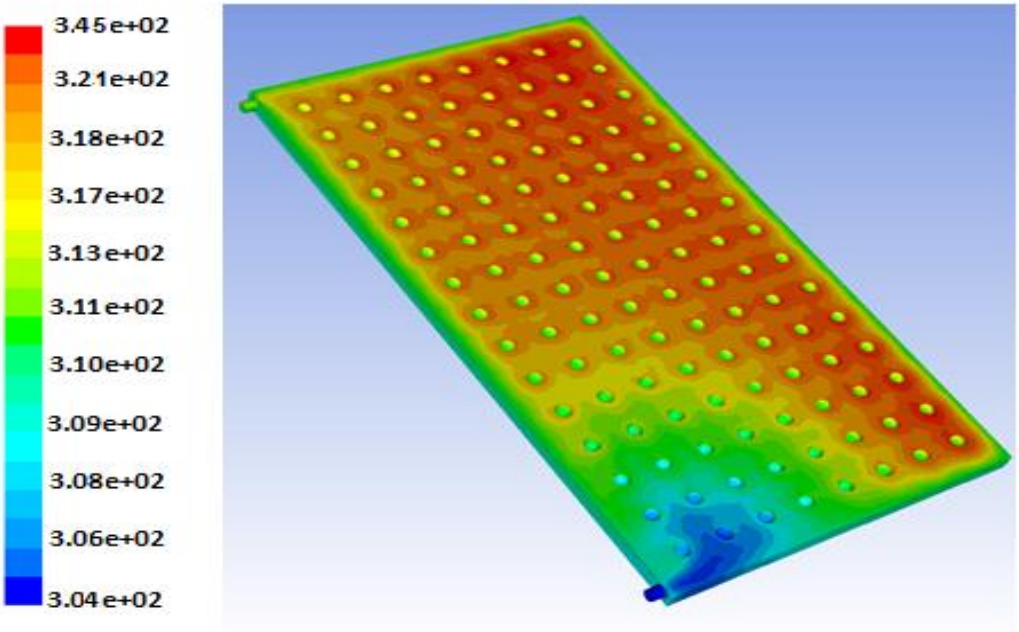

(b) at 1% Al_2O_3

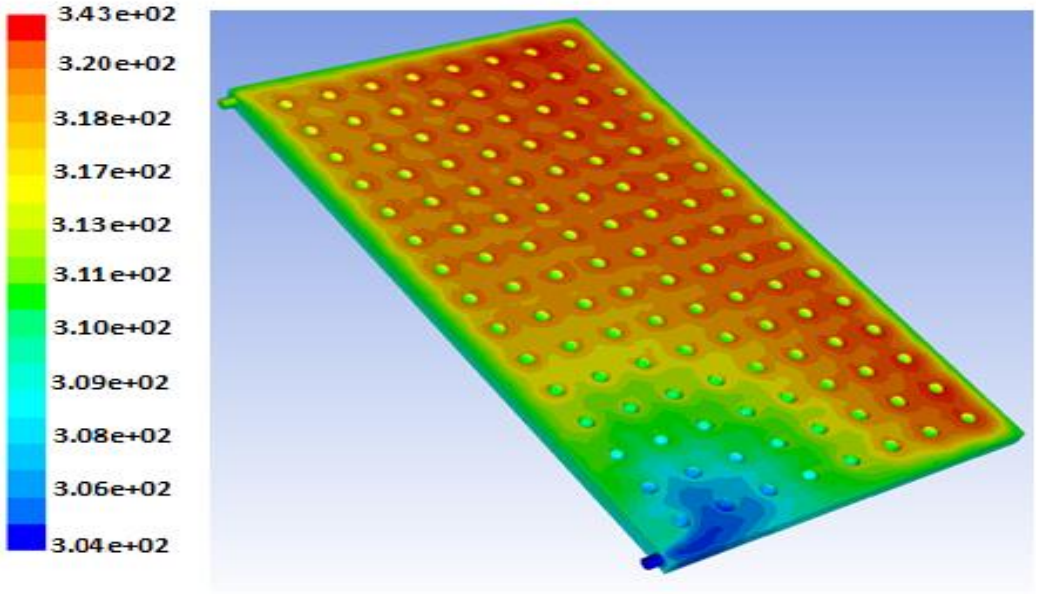

(c) at 2 % Al_2O_3

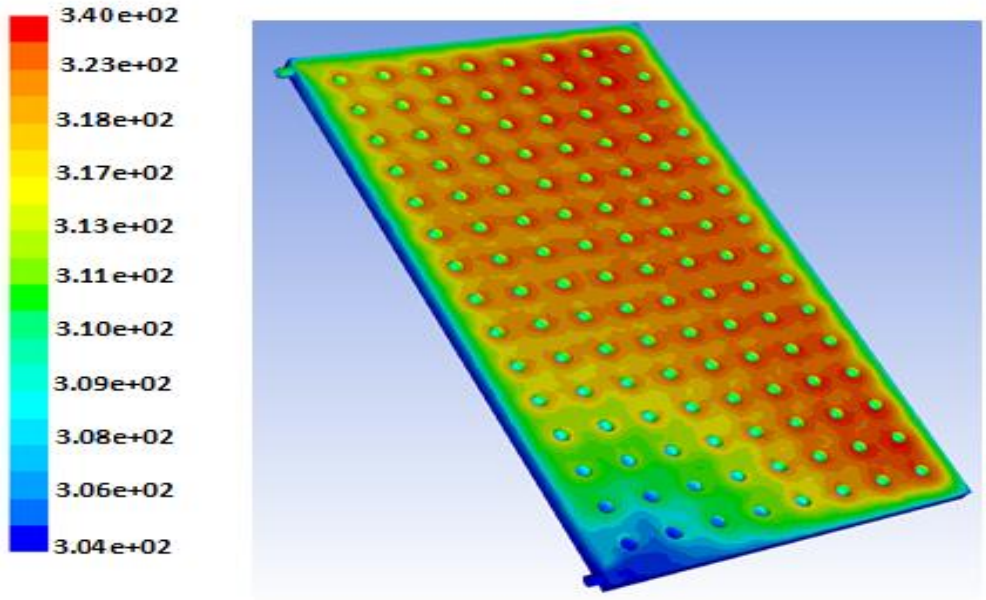

(d) at 3% Al_2O_3

Figure 5.423. Contours of temperature distribution for Model-SS collector with 3.5l/minin flow rate at 1:00 pm; (a) without Nano , (b) with 1% Al_2O_3, (c) with 2% Al_2O_3, (d) with 3% Al_2O_3.

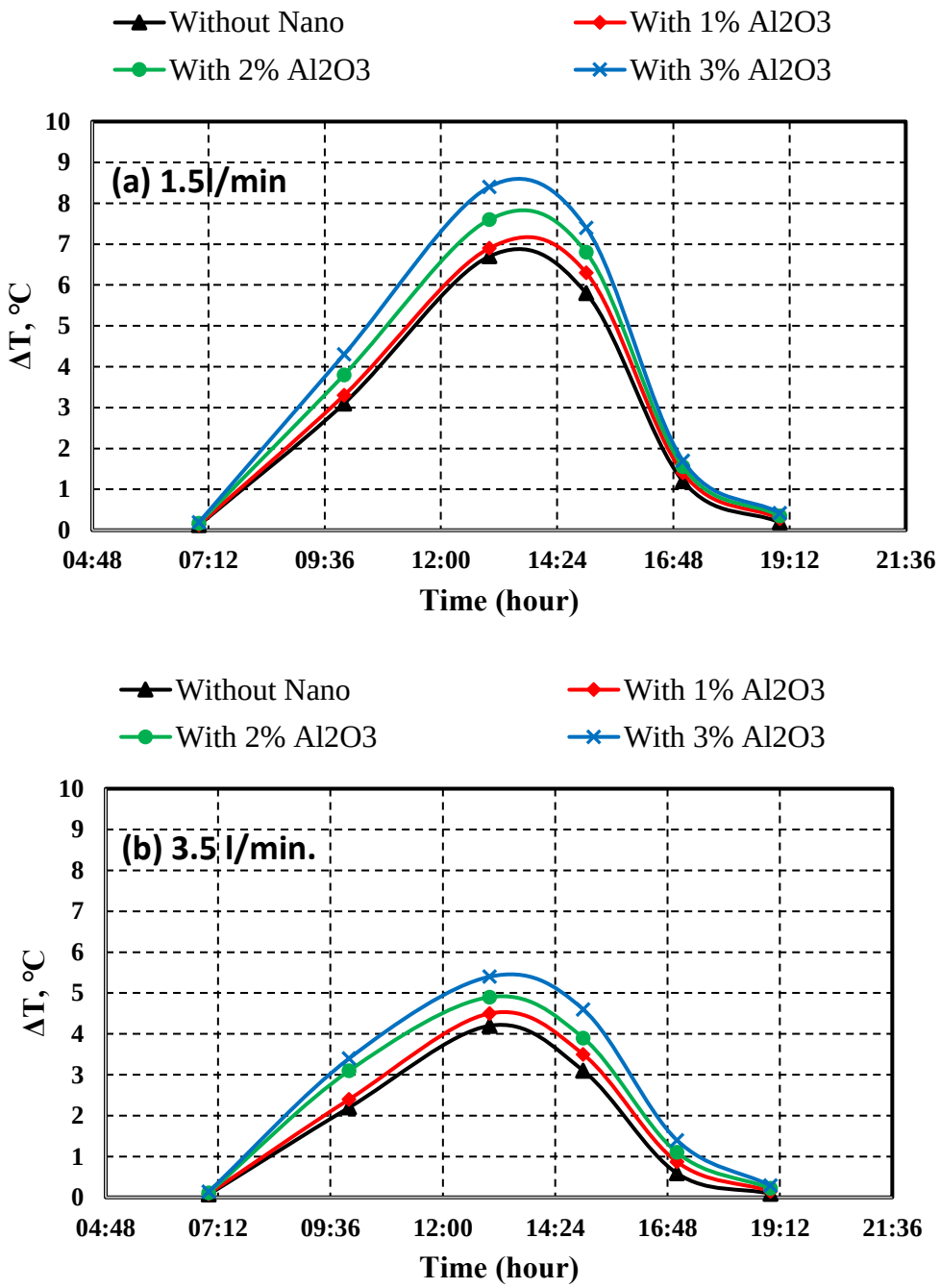

Figure 5.434. Simulated results of difference water temperature between the inlet and output for Model-SS collector at different concentrations of Al_2O_3 nano particles.

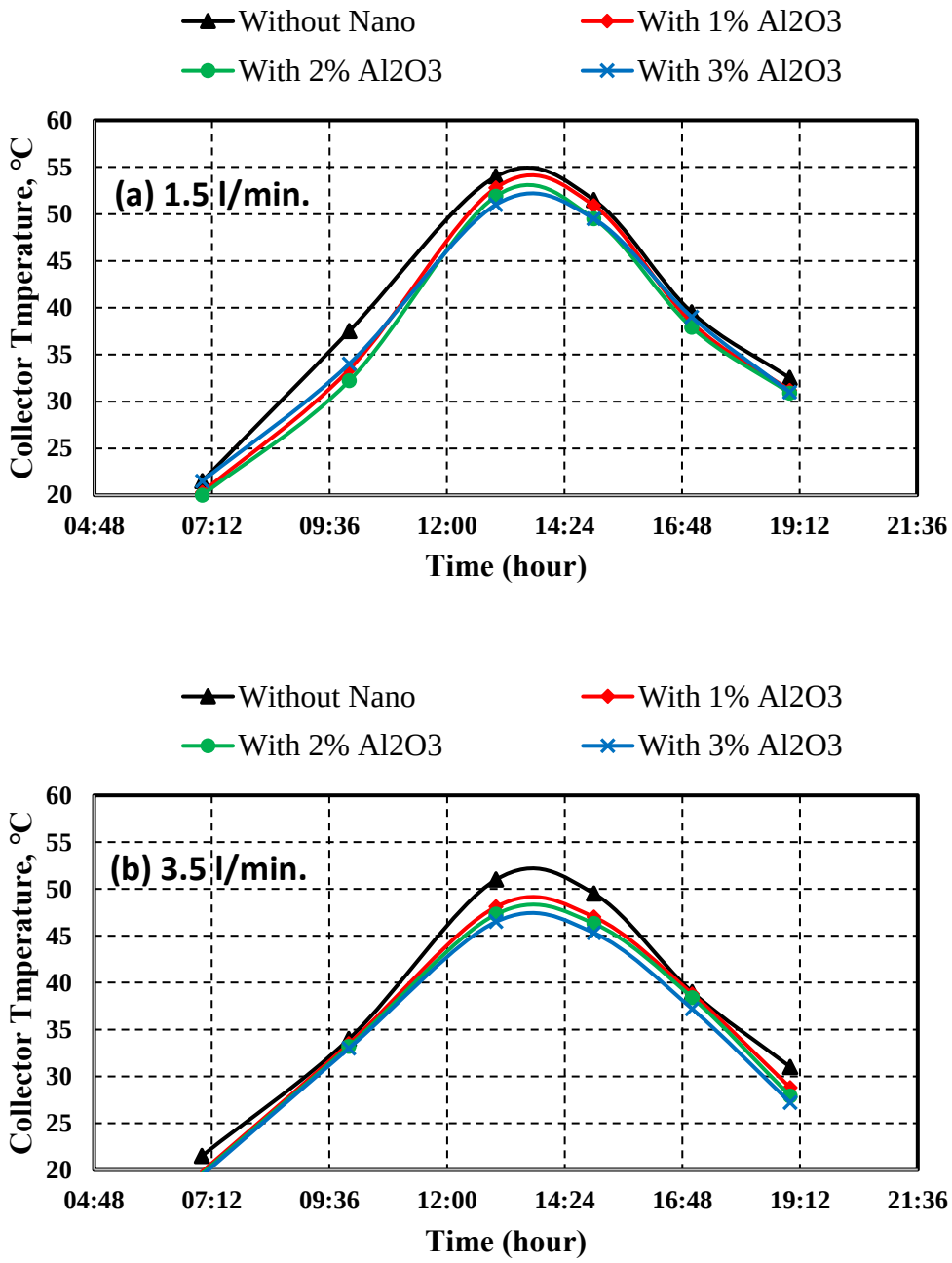

Figure 5.445. Simulated results of average temperature of collector cover for Model-SS collector at different concentrations of Al2O3 nano particles.

5.2.3. Result of PV/T Model (SS) with (CuO/Water) Nanofluid

The figures (5.46) and (5.47) show the temperature distribution on the surface of the collector, at(1:00 PM)when we use (CuO/water) Nanofluid with deferent concentration (1%,2% and 3% Vt) and with flow rate (1.5l/min and 3.5l/min)We notice a decrease in the surface temperature of the collector with an increase in the

mixing ratio (concentration) at a constant flow rate Where we notice a decrease in the surface temperature of the collector by (5.3%) when using a nano -liquid with a concentration (1%) compared to its temperature when using water only, while it decreases by (6.6% ,6.9%) when using concentrations (2% and 3%) at flow rate (1.5l/min)respectively as shown in figure (5.49.a), We also note the temperature decrease when we using a higher flow rate(3.5l/min) with the same concentration as shown in figure (5.49.b) Where we notice a decrease in the surface temperature of the collector by (9.4%) when using a Nano -liquid with a concentration (1%) compared to its temperature when using water only, while it decreases by (10.3% and 11.2%) when using concentrations (2% and 3%) respectively and as is evident in the contours (5.46.a,b,c and d). where it is low at the inlet of the collector due to the presence of a new coolant with a low temperature, and it rises relatively towards the outlet of the collector, where the temperature of the coolant increases when it absorbs heat from the collector cover, which is in contact with the back of the panel.

We also note the temperature decrease at connection points (sphere bulge) due to the increase in the surface area for heat transfer at these points, as is evident in all contours (5.46) and (5.47). Figure (5.48 a and b) shows the difference in coolant temperature between the inlet and outlet of the collector with a change in the concentration, where the largest difference in the coolant temperature was at a concentration of (3%) This is due to the increase in the heat transfer coefficient of the liquid after increasing the proportion of mixing nano material's Where we notice an increase in (Δ T) by (6.8%) when using a Nanoliquid with a concentration (1%) compared to when using water only, while it increases by (10.5% and 13.2%) when using concentrations (2% and 3%) respectively at a flow rate (1.5l/min) as shown in Figure (5.48.a)

When using a flow rate (3.5l/min) we notice a decrease in (Δ T) in general compared to using a flow rate (1.5l/min) where we recorded the following percentages of increases for (Δ T) with an increase in concentration (5.4% at 1% concentration, 6.2% at 2% concentration and 9.2 at 3% concentration) as show in figure (5.48.b)

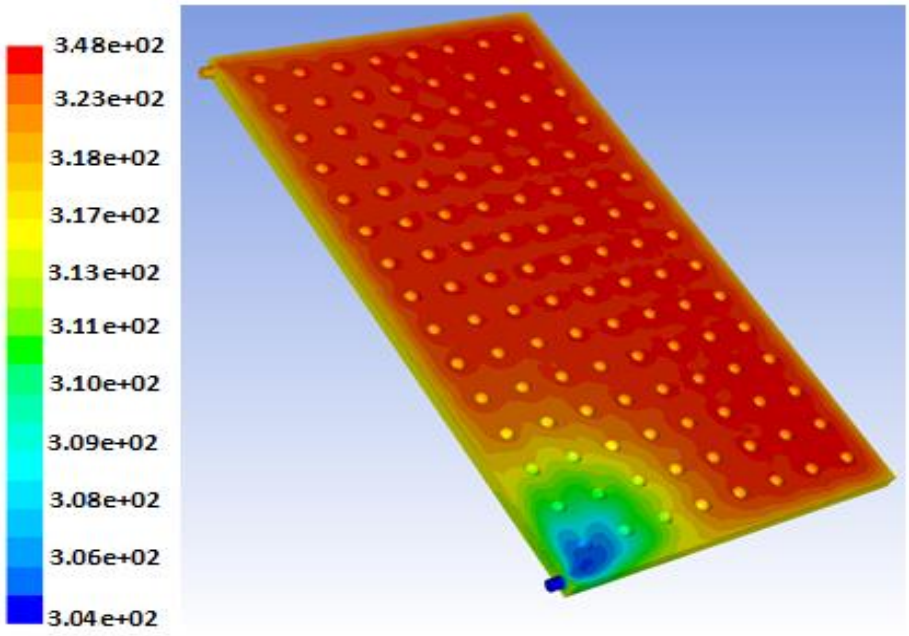

(a) Without Nano

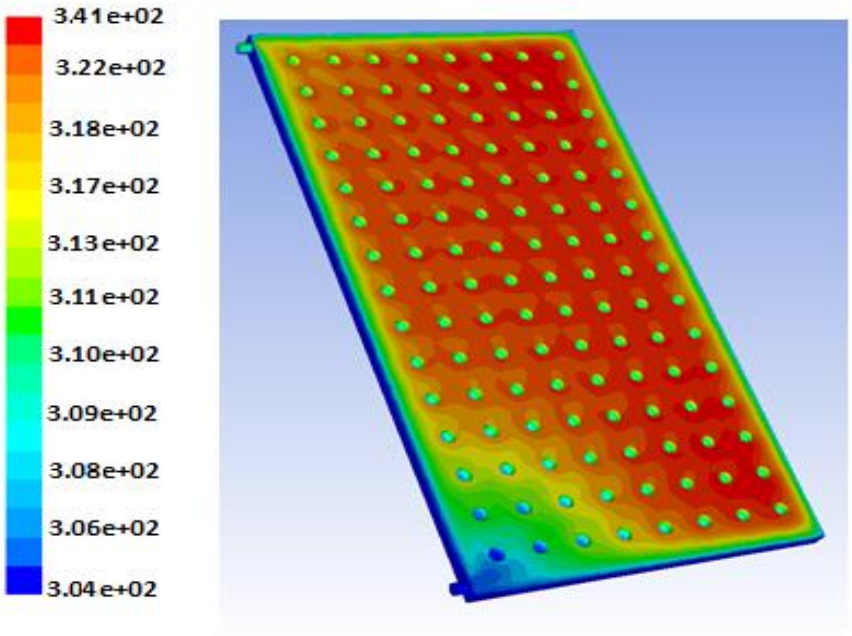

(b) at 1% **CuO**

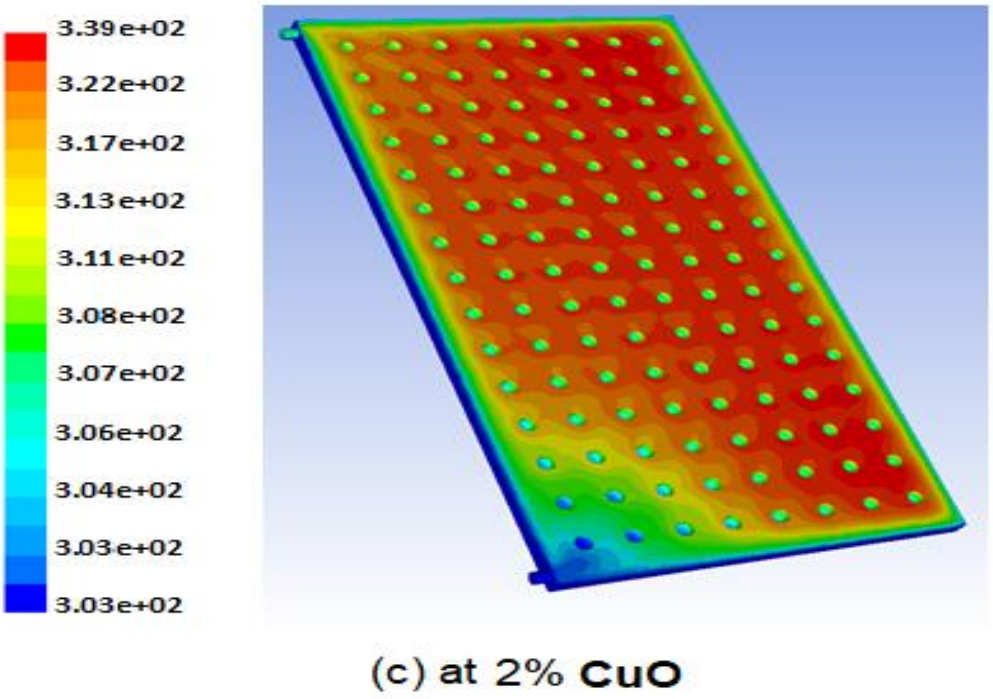

(c) at 2% CuO

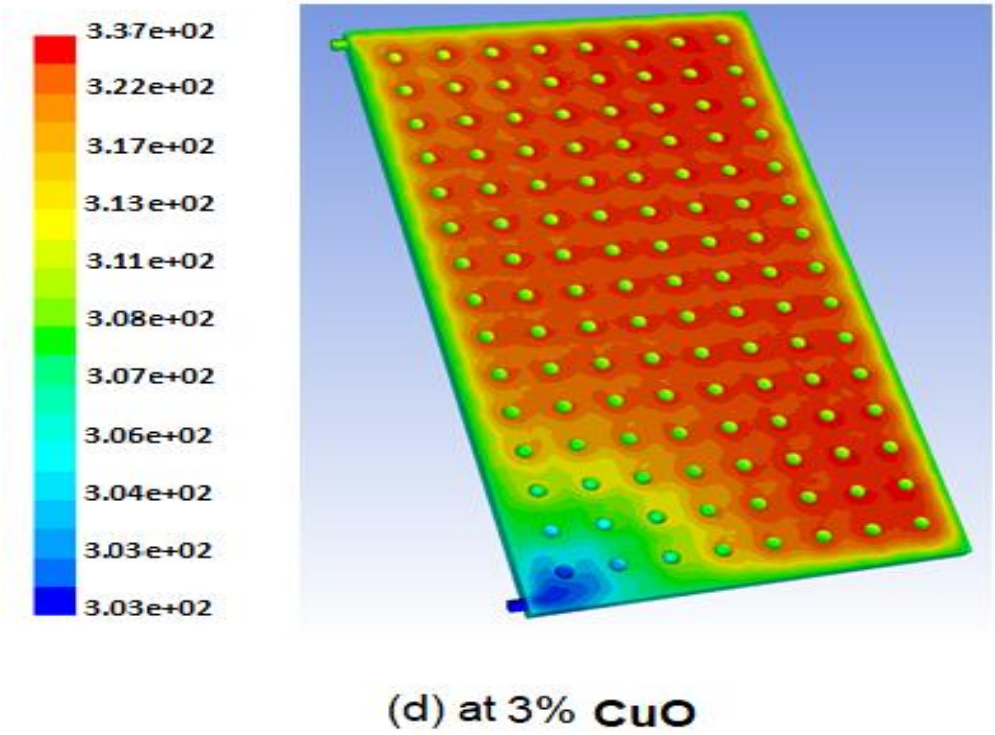

(d) at 3% CuO

Figure 5.456. Contours of temperature distribution for Model-SS collector with 1.5l/minin flow rate at 1:00 pm; (a) without Nano , (b) with 1% CuO, (c) with 2% CuO, (d) with 3% CuO.

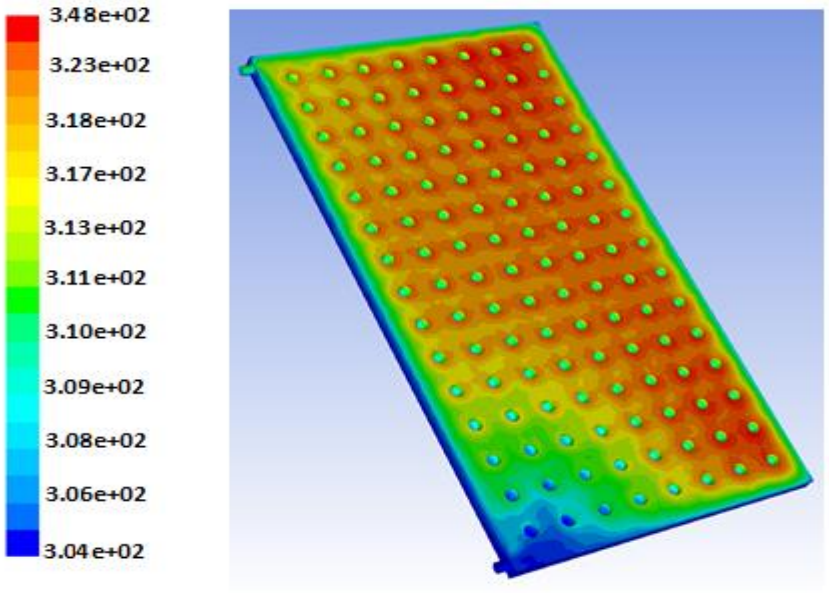

(a) Without Nano

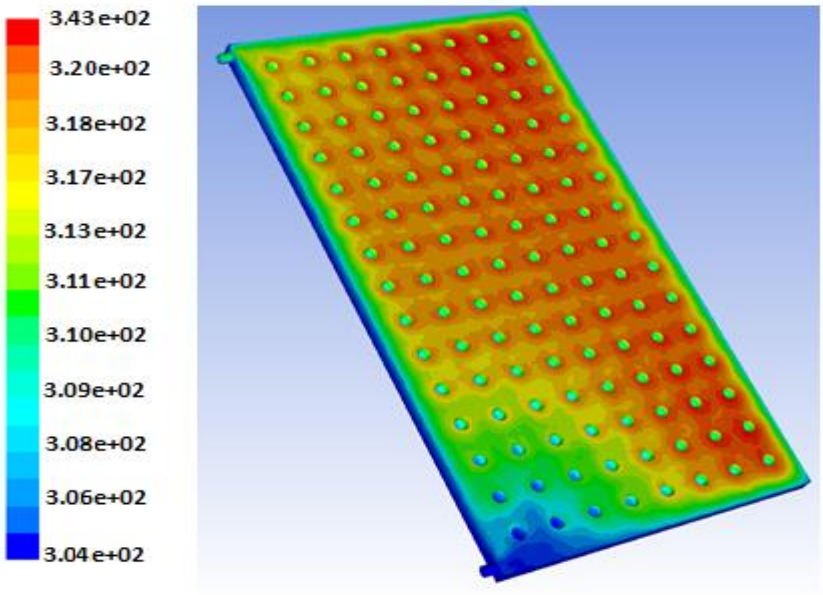

(b) at 1% CuO

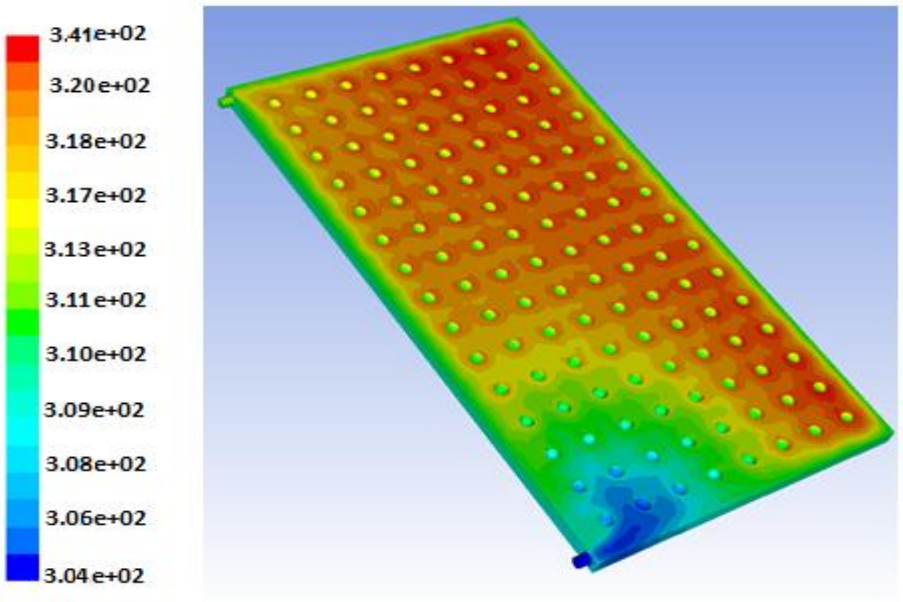

(c) at 2% CuO

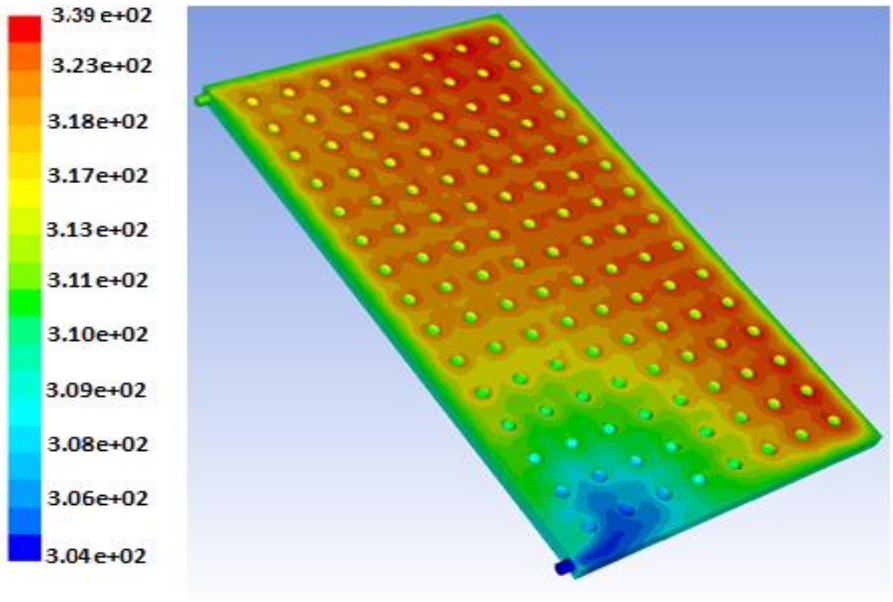

(d) at 3% CuO

Figure 5.467. Contours of temperature distribution for Model-SS collector with 3.5l/minin flow rate at 1:00 pm; (a) without Nano , (b) with 1% CuO, (c) with 2% CuO, (d) with 3% CuO.

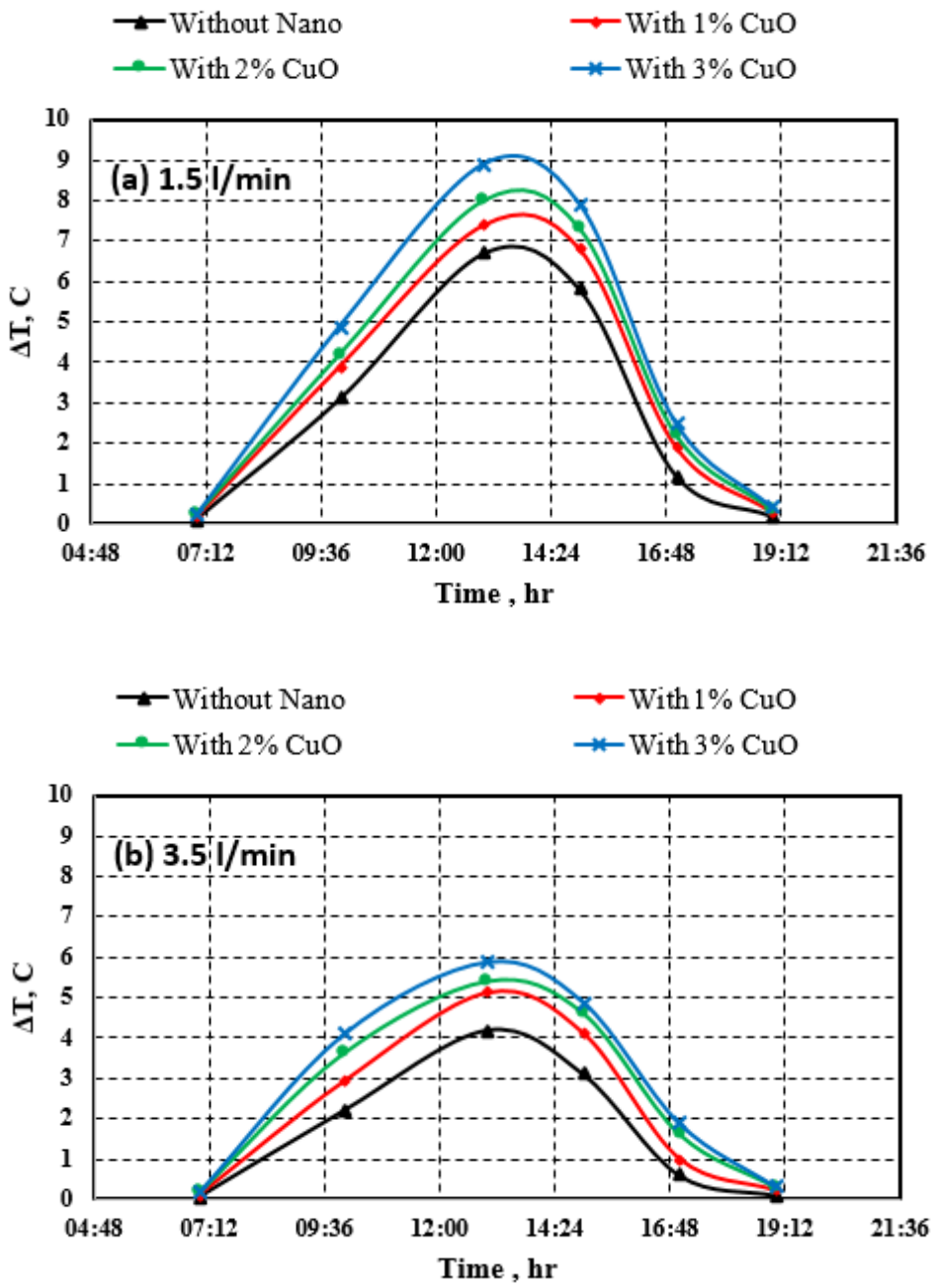

Figure 5.478. Simulated results of difference water temperature between the inlet and output for Model-SS collector at different concentrations of CuO nano particles.

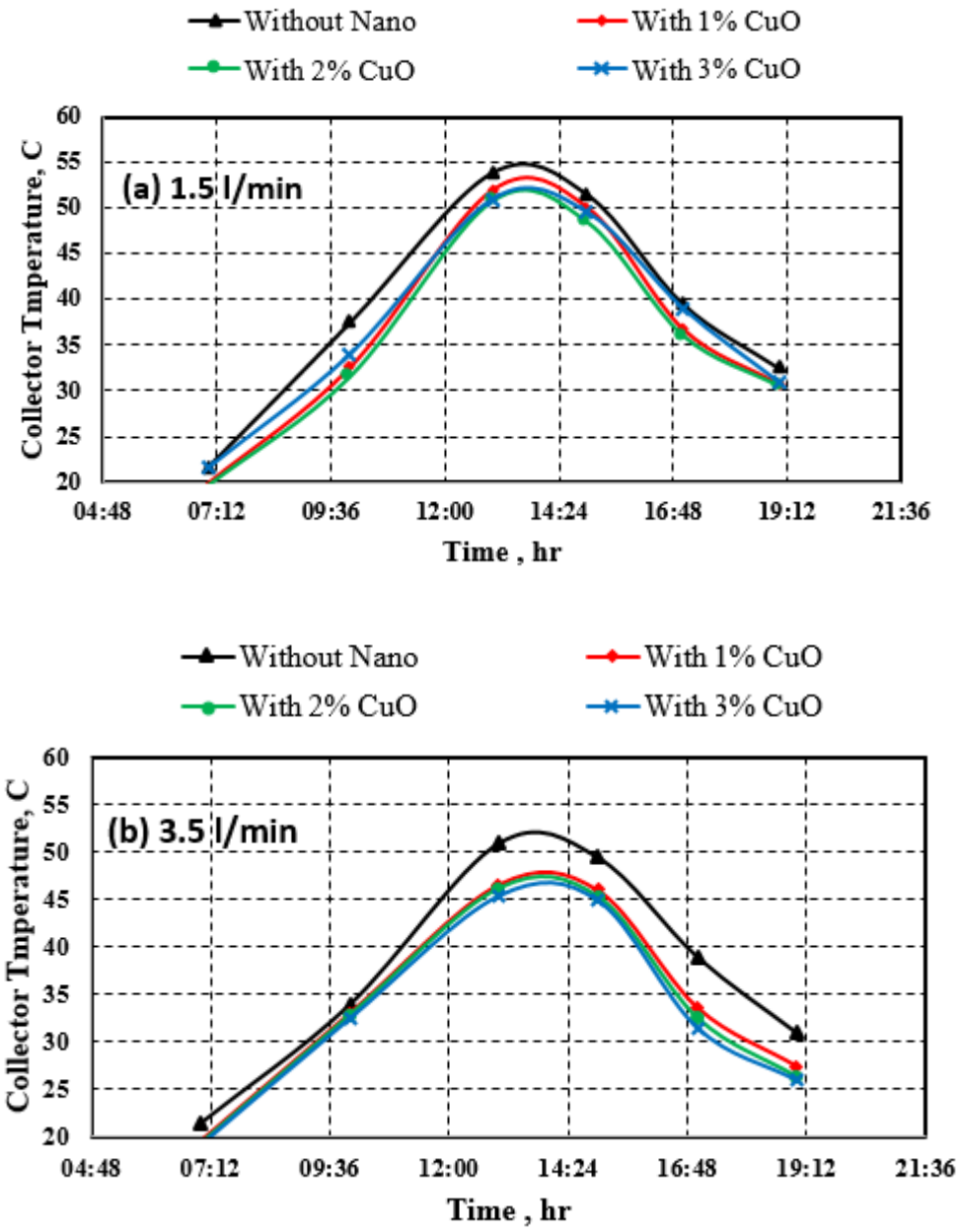

Figure 5.49 Simulated results of average temperature of collector cover for Model-SS collector at different concentrations of CuO nano particles.

5.3. VALIDATION OF NUMERICAL MODELLING

The results showed a closeness between the practical and theoretical results within the permissible limits, as indicated by the following points:

5.3.1. Validation Results of PV/T Model-SS

The figures (5.50) and (5. 51) shows the practical results with the results obtained from the simulation, where we found that the total difference (error) percentage between numerical and experimental were 11.6% for 1.5l/minin and 8.7% for 3.5l/minin for the difference water temperature between the input and output. The total difference (error) percentage between numerical and experimental were 3.4% for 1.5l/minin and 3.1% for 3.5l/minin for the surface temperature of the collector as shown in figure (5.51).

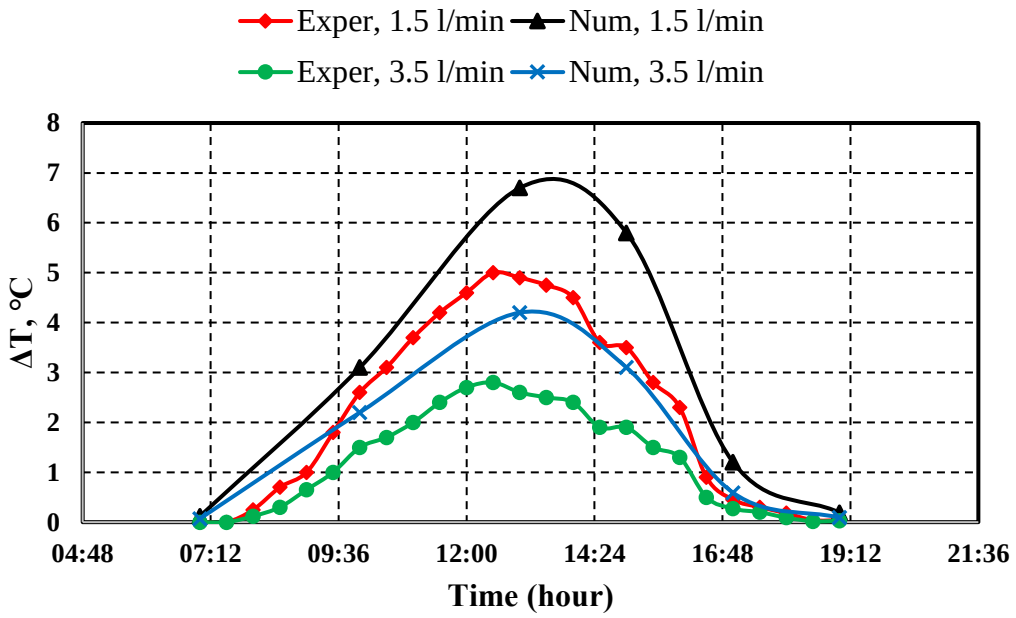

Figure 5.480. Compared results of difference water temperature between the inlet and output at 1.5 and 3.5l/minin flow rates for Model-SS.

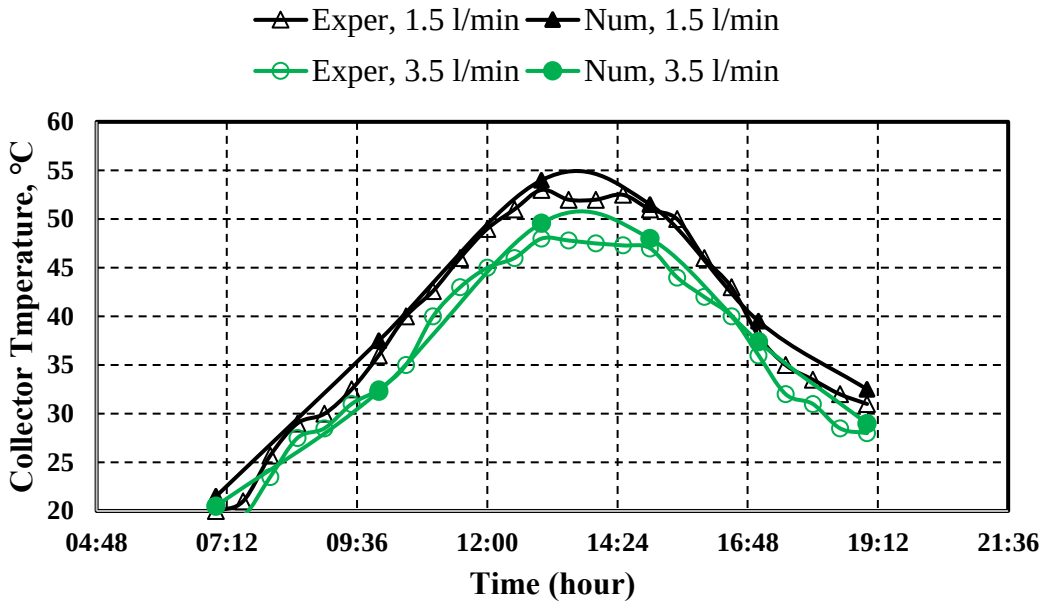

Figure 5.491. Compared results of average temperature of collector cover at 1.5 and 3.5 l/min flow rates for Model-SS.

5.3.2. Comparation Experimental Results with Published Works

By comparing the current work with some previous studies similar to this study.

The highest efficiency of 9.5% was reached by the researcher Al-Waeli [59] when using (Al_2O_3 / water) at a rate of 3% inside the laboratory and at one o'clock in the afternoon. The highest efficiency was obtained by Sangeetha [41] under the same conditions and using a plate-and-tube type collector equal to 11.5%.Compared to the current work, the highest electrical efficiency measured at one o'clock in the afternoon and under the same conditions was 14.7%.as shown in figure5.38. The researcher Bianco[58] did a numerical analysis of a model using (CFD) program to use Al_2O_3 /water as a coolant with a mixing ratio of 3%.The highest reduction in the surface collector temperature was obtained by 1.5 °C, which is equivalent to 5.7%, while the current study produced a reduction in temperature of 8.4% under the same conditions.

5.4. ECONOMIC ANALYSIS

One of the important things in every project is the financial cost of the project, which is one of the three basic elements of success. Table 5.1. Below shows the financial

costs of some parts of the system used in the current research for the purposes of the future economic feasibility study. Table 5.2 represents the total energy produced and utilized from the system during the life of the system, which is (20 years). Assuming the system works for (24 hours / day).The international price of (kilowatt-hour) was adopted at $0.161 to calculate the value of the total energy produced and recorded in Table 5.2. We note that the total produced energy increased by 900% when we used **PV/T CuO/water** compared to the total cost of the system, which increased by 700%

Table 5.1. The cost of the parts of the system and the benefits obtained from them.

No.	Part name	Cost	Electrical efficiency %	Thermal efficiency%	T cell, ℃
1	PV panel	80$	13.5	0	71
2	PV/T SS type	125$	14.5	66.6	58.5
3	PV/T SS type+ Al2O3	375$	14.8	88.7	55
4	PV/T SS type+CuO	650$	14.9	90.3	54

Table 5.2. The produced energy through design lifetime of the PV/T system

Part name	Elec. Power (Watt)	Thermal power (Watt)	Total produced energy (Watt)	Costs (us$)
pv	114.4	nill	114.4	3,183
PV/T water only	123	703	825	22,952
PV/T Al_2o_3/water	125	873	998	27,765
PV/T CuO/water	127	885	1012	28,132

PART 6

CONCLUSIONS AND RECOMMENDATIONS FOR FUTURE WORK

6.1. CONCLUSION

Through the practical and simulative results obtained in this study, we make the following observations:

1. We obtained a decrease in the cell surface temperature with increasing in flow rate and comparing it with a photovoltaic cell without cooling at (13:00) where the percentage of temperature decrease was (10%) at flow rate (1.5l/min) but it was (12.6%, 14.7%, 17.6%) at (2 ,2.5 and 3.5l/min) respectively.
2. Decrease in the collector temperature with an increase in the flow rates of the coolant. The highest temperature of the collector surface was at one o'clock in the afternoon (53) ℃ at a flow rate of 1.5 liters per minute, which decreased by 2.5% when using a flow rate of 2 liters per minute, and decreased to (5.6%, 9.4%) when using (2.5 and 3.5 liters per minute) respectively.
3. The ideal efficiency that was calculated for the cell = η ref = (17.1%) decreased to 13.5 % at one o'clock in the afternoon to increase by 3.7% when cooled with 1.5l/min ute of water and when the flow rate is increased to (2, 2.5 and 3.5l/min) the electrical efficiency increases by 5.6%, 6.4% and 7.5%, respectively, the highest electrical efficiency at a flow rate of (3.5l/min ute).
4. We notice an increase in the thermal energy absorbed with an increase in the flow rate. The absorbed thermal energy increased by (16%) when using a flow rate (2l/min) than that when using a flow rate (1.5l/min), and increased by (33%, 41%) when using a flow rate (2.5 and 3.5l/min), respectively.
5. The thermal efficiency increased at the flow rate (2l/min) by (7.7%) than the thermal efficiency when we used (1.5l/min) and increased by (16.5%, 27.4 %) when we used the flow rates (2.5, and 3.5l/min) respectively.

6. Using (cuo/water) at a mixing ratio 3% Vt reduces the cell temperature (24%), while it decreased by (22.5%,17.6%) when using (al2o3 / water) at a mixing rate of 3% and water alone, respectively.
7. Use of (cuo/water) at a mixing rate of 3% reduces the temperature of the collector (7%), while it decreased by (5%) when using (al2o3/water) by Mixing 3% for a flow rate of 3.5 liters per minute while for a flow rate of 1.5 liters per minute when use of (cuo/water) at a mixing rate of 3% reduces the temperature of the collector (6%), and decreased by (4.3%) when using (al2o3/water) by Mixing 3%.
8. There is an increase in the electrical efficiency when using(CuO /water) Nanofluid as a coolant with mixing ratios of (3%)Vt by (6.5%) while we get increasing by (5.6%) and (3.2%)when we use (al2o3/water) and (water) respectively at flow rate (1.5l/min) and we get an increasing in the efficiency when using(CuO /water) Nanofluid as a coolant with mixing ratios of (3%)Vt by (10%) while we get increasing by (9.1%) and (7%)when we use (al2o3/water) and (water) respectively at flow rate (3.5l/min).
9. There is an increase in (Δ T) when using (CuO /water) Nanofluid as a coolant with mixing ratios of (3%)Vt by (47 %) than when using only water while we get increasing by (40.8%) when we use (al2o3/water) at flow rate (1.5l/min) and there is an increase in (Δ T) when using (CuO /water) Nanofluid as a coolant with mixing ratios of (3%)Vt by (40.7 %) than when using only water while we get increasing by (37%) when we use (al2o3/water) at flow rate (3.5l/min).
10. There is an increasing in thermal efficiency when using (CuO /water) Nanofluid as a coolant with mixing ratios of (3%)Vt by (47 %) than when using only water while we get increasing by (40.8%) when we use (al2o3/water) at flow rate (1.5l/min) and when we use (CuO /water) Nanofluid as a coolant with mixing ratios of (3%)Vt by (40.7 %) than when using only water while we get increasing by (38%) when we use (al2o3/water) at flow rate (3.5l/min).
11. At one o'clock we note that using (cuo/water) at a mixing ratio 3% V% reduces the cell temperature (16%), while it decreased by (13%,11.8%) when using (2%) and (1%) mixing ratio respectively. While when using (cuo/water) at a

mixing ratio 3% VT reduces the cell temperature (9.6%), while it decreased by (5.8%, 2.2%) when using (2%) and (1%) mixing ratio respectively.

12. At one o'clock we note that using (cuo/water) at a mixing ratio 3% V% increases the electrical efficiency (16%), while it decreased by (13%, 11.8%) when using (2%) and (1%) mixing ratio respectively.
13. At one o'clock we note that using (cuo/water) at a mixing ratio 3% VT increase (Δ T) (16%), while it decreased by (13%, 11.8%) when using (2%) and (1%) mixing ratio respectively.
14. An increase in thermal efficiency when using (CuO /water) Nanofluid as a coolant with mixing ratios of (3%) VT% by (40.7 %) than when using only water while we get increasing by (38%) when we use (al2o3/water) at flow rate (3.5l/min).
15. The total difference (error) percentage between numerical and experimental were 11.6% for 1.5l/minin and 8.7% for 3.5l/minin for the difference water temperature between the input and output and the total difference (error) percentage between numerical and experimental were 3.4% for 1.5l/minin and 3.1% for 3.5l/minin for the surface temperature of the collector.

6.2. RECOMMENDATIONS FOR FUTURE WORK

1. Carrying out practical tests using porous filling as a cover for the collector and studying their effect on the performance of the (PV/T) system.
2. Carrying out practical tests using other concentrations of nano materials.

REFERENCES

1. Landrigan, P. J., "Air pollution and health", ***The Lancet Public Health,*** *2*(1): 4-5 (2017).

2. Alrikabi, N. K. M. A., "Renewable energy types", ***Journal of Clean Energy Technologies,*** *2*(1): 61-64 (2014).

3. Al-Waeli, A. H., Kazem, H. A., Chaichan, M. T., & Sopian, K., "Photovoltaic/thermal (PV/T) systems: principles, design, and applications", ***Springer,*** Germany, 34-56 (2019).

4. Mughal, S., Sood, Y. R., & Jarial, R. K., "A review on solar photovoltaic technology and future trends", ***International Journal of Scientific Research in Computer Science, Engineering and Information Technology,*** *4*(1): 227-235 (2018).

5. Internet: Donev et al., "Energy Education-Types of photovoltaic cells", **https://energyeducation.ca/encyclopedia/Types_of_photovoltaic_cells/**(2018).

6. Touati, F., Massoud, A., Hamad, J. A., & Saeed, S. A., "Effects of environmental and climatic conditions on PV efficiency in Qatar", ***In International Conference on Renewable Energies and Power Quality,*** Qatar, 12-22 (2013).

7. Kazem, H. A., Chaichan, M. T., & Yousif, J. H., "Evaluation of oscillatory flow Photovoltaic/Thermal system in Oman", ***International Journal of Computation and Applied Sciences,*** 10 (1): 429-436 (2019).

8. Bhatia, S. C., "Advanced renewable energy systems", ***CRC Press,*** USA, 23-34 (2014).

9. Ibrahim, A., Othman, M. Y., Ruslan, M. H., Mat, S., & Sopian, K., "Recent advances in flat plate photovoltaic/thermal (PV/T) solar collectors", ***Renewable and Sustainable Energy Reviews,*** 15(1): 352-365 (2011).

10. Timofeeva, E. V., Yu, W., France, D. M., Singh, D., & Routbort, J. L., "Nano fluids for heat transfer: an engineering approach", ***Nano scale Research Letters,*** *6*(1): 1-7 (2011).

11. Gaurav, K., & Verma, S. K. "Performance of Nano fluids Filled PV/T: A Review", ***Journal of Mechanical Engineering Research and Developments,*** 44(11): 50-62 (2021).

12. Gupta, S. K., & Pradhan, S., "A review of recent advances and the role of nanofluid in solar photovoltaic thermal (PV/T) system", ***Materials Today: Proceedings***, 4(4): 782-791 (2021).

13. Sachit, F. A., Rosli, M. A. M., Tamaldin, N., Misha, S., & Abdullah, A. L., "Nano fluids used in photovoltaic thermal (pv/t) systems", ***International Journal of Engineering & Technology,*** 7(20): 599-611 (2018).

14. Bashria, A., Yousef, A., Adam, N. M., Sopian, K., Zaharim, A., & Alghoul, M., "Analysis of single and double passes V-grooves solar collector with and without porous media", ***Int. J. Energy Environ,*** 2(1): 109-114 (2007).

15. Ozgen, F., Esen, M., & Esen, H., "Experimental investigation of thermal performance of a double-flow solar air heater having aluminium cans", ***Renewable Energy,*** 34(11): 2391-2398 (2009).

16. Bakari, R., Minja, R. J., & Njau, K. N., "Effect of glass thickness on performance of PV/Ts for fruits drying", ***Journal of Energy,*** 2(4):8 (2014).

17. Dubey, S., & Tay, A. A., "Testing of two different types of photovoltaic–thermal (PVT) modules with heat flow pattern under tropical climatic conditions", ***Energy for Sustainable Development,*** *17*(1): 1-12 (2013).

18. Jouhara, H., Szulgowska-Zgrzywa, M., Sayegh, M. A., Milko, J., Danielewicz, J., Nannou, T. K., & Lester, S. P., "The performance of a heat pipe based solar PV/T roof collector and its potential contribution in district heating applications", ***Energy,*** 13(6): 117-125 (2017).

19. Kazem, H. A., "Evaluation and analysis of water-based photovoltaic/thermal (PV/T) system", ***Case Studies in Thermal Engineering,*** 1(3): 100-401 (2019).

20. Podder, B., & Biswas, A., "Experimental analysis of the performance of a solar photovoltaic-thermal (pv/t) water collector with a modified absorber design for the climatic condition of Assam", NISCAIR-CSIR, India, 437-441 (2019).

21. Singh, K., Singh, S., Kandpal, D. C., & Kumar, R., "Experimental performance study of photovoltaic solar panel with and without water circulation", ***Materials Today: Proceedings***, 4(6): 6822-6827 (2021).

22. Sardarabadi, M., Passandideh-Fard, M., & Heris, S. Z., "Experimental investigation of the effects of silica/water nanofluid on PV/T (photovoltaic thermal units)", ***Energy,*** 6(6): 264-272 (2014).

23. Al-Shamani, A. N., Sopian, K., Mat, S., Hasan, H. A., Abed, A. M., & Ruslan, M. H., "Experimental studies of rectangular tube absorber photovoltaic thermal collector with various types of nano fluids under the tropical climate conditions", ***Energy Conversion and Management,*** 12(4): 528-542 (2016).

24. Gangadevi, R., Vinayagam, B. K., & Senthilraja, S., "Experimental investigations of hybrid PV/Spiral flow thermal collector system performance using Al2O3/water nano fluid", ***In IOP Conference Series: Materials Science and Engineering***, 19(1):12-41 (2017).

25. Al-Waeli, A. H., Sopian, K., Chaichan, M. T., Kazem, H. A., Hasan, H. A., & Al-Shamani, A. N., "An experimental investigation of SiC nanofluid as a base-fluid for a photovoltaic thermal PV/T system", ***Energy Conversion and Management,*** 14(2): 547-558 (2017).

26. Hasan, H. A., Sopian, K., Jaaz, A. H., & Al-Shamani, A. N., "Experimental investigation of jet array nano fluids impingement in photovoltaic/thermal collector", ***Solar Energy,*** 14(4): 321-334 (2017).

27. Sardarabadi, M., Passandideh-Fard, M., Maghrebi, M. J., & Ghazikhani, M., "Experimental study of using both ZnO/water nanofluid and phase change material (PCM) in photovoltaic thermal systems", ***Solar Energy Materials and Solar Cells,*** 16(1): 62-69 (2017).

28. Al-Waeli, A. H., Sopian, K., Kazem, H. A., & Chaichan, M. T., "Nanofluid based grid connected PV/T systems in Malaysia: A techno-economical assessment", ***Sustainable Energy Technologies and Assessments,*** 2(8): 81-95 (2018).

29. Aberoumand, S., Ghamari, S., & Shabani, B., "Energy and exergy analysis of a photovoltaic thermal (PV/T) system using nano fluids: An experimental study", ***Solar Energy,*** 16(5): 167-177 (2018).

30. Younis, A., Elsarrag, E., Alhorr, Y., & Onsa, M., "The influence of Al2O3-ZnO-H2O nanofluid on the thermodynamic performance of photovoltaic-thermal hybrid solar collector system", ***Innov Ener Res,*** *7*(18): 2576-1463 (2018).

31. Sharafeldin, M. A., & Gróf, G., "Experimental investigation of PV/T using CeO2-water nano fluid", ***Energy Conversion and Management,*** 15(5): 32-41 (2018).

32. Rukman, N. S. B., Fudholi, A., Razali, N. F. M., Ruslan, M. H., & Sopian, K., "Investigation of TiO2 and MWCNT nano fluids-based photovoltaic-thermal (PV/T) system", ***In IOP Conference Series: Earth and Environmental Science***, 26(8):12-76 (2019).

33. Rukman, N. S. B., Fudholi, A., Razali, N. F. M., Ruslan, M. H., & Sopian, K., "Energy and exergy analyses of photovoltaic-thermal (PV/T) system with TiO2/water nanofluid flow", ***In IOP Conference Series: Earth and Environmental Science,*** 26(8):12-75 (2019).

34. Al-Waeli, A. H., Chaichan, M. T., Sopian, K., Kazem, H. A., Mahood, H. B., & Khadom, A. A., "Modeling and experimental validation of a PVT system using nanofluid coolant and nano -PCM", ***Solar Energy,*** 17(7): 178-191 (2019).

35. Wole-Osho, I., Adun, H., Adedeji, M., Okonkwo, E. C., Kavaz, D., & Dagbasi, M., "Effect of hybrid nano fluids mixture ratio on the performance of a photovoltaic thermal collector", ***International Journal of Energy Research,*** 44(11): 9064-9081 (2020).

36. Jia, Y., Ran, F., Zhu, C., & Fang, G., "Numerical analysis of photovoltaic-thermal collector using nanofluid as a coolant", ***Solar Energy,*** 19(6): 625-636 (2020).

37. Samylingam, L., Aslfattahi, N., Saidur, R., Yahya, S. M., Afzal, A., Arifutzzaman, A., & Kadirgama, K., "Thermal and energy performance improvement of hybrid PV/T system by using olein palm oil with MXene as a new class of heat transfer fluid", ***Solar Energy Materials and Solar Cells***, 21(8): 110-754 (2020).

38. Fadli, A. F., Kristiawan, B., & Arifin, Z., "Analysis of TiO2/water-based photovoltaic thermal (PV/T) collector to improve solar cell performance", ***In IOP Conference Series: Materials Science and Engineering,*** 10(96): 12-53 (2021).

39. Praveen Bharathwaj, R., Pradeep, V., Raju, J. J., Satheesh, A., & Padmanathan, P., "Performance Study on Flat Plate Solar Water Heater with Copper Nano particles", ***In Proceedings of International Conference on Thermofluids***, Singapore, 39-553 (2021).

40. Adun, H., Adedeji, M., Dagbasi, M., Bamisile, O., Senol, M., & Kumar, R., "A numerical and exergy analysis of the effect of ternary nanofluid on performance of Photovoltaic thermal collector", ***Journal of Thermal Analysis and Calorimetry,*** *145*(3): 1413-1429 (2021).

41. Sangeetha, M., Manigandan, S., Ashok, B., Brindhadevi, K., & Pugazhendhi, A., "Experimental investigation of nanofluid based photovoltaic thermal (PV/T) system for superior electrical efficiency and hydrogen production", ***Fuel,*** 28(6): 119-422 (2021).

42. Abdul-Ganiyu, S., Quansah, D. A., Ramde, E. W., Seidu, R., & Adaramola, M. S., "Study effect of flow rate on flat-plate water-based photovoltaic-thermal (PVT) system performance by analytical technique", ***Journal of Cleaner Production,*** *3(21):* 128-985 (2021).

43. Coventry, J. S., "Performance of a concentrating photovoltaic/thermal solar collector", ***Solar Energy,*** 78(2): 211-222 (2005).

44. Brogren, M., & Karlsson, B., "Low-concentrating water-cooled PV-thermal hybrid systems for high latitudes", ***In Conference Record of the Twenty-Ninth IEEE Photovoltaic Specialists Conference***, New Orleans, USA, 1733-1736 (2002).

45. Bahaidarah, H., Subhan, A., Gandhidasan, P., & Rehman, S., "Performance evaluation of a PV (photovoltaic) module by back surface water cooling for hot climatic conditions", ***Energy,*** 5(9): 445-453 (2013).

46. Agbo, S. N., & Okoroigwe, E. G., “Analysis ofThermal Losses in the Flat-Plate Collector of a Thermosyphon Solar Water Heater”, ***Research Journal of Physics,*** 1(1): 35-41 (2007).

47. Klein, S. A., Duffie, J. A., & Beckman, W. A., “Transient considerations of flat-plate solar collectors”, ***Journal of Engineering for Power,*** 96(2): 109-113 (1974).

48. Zondag, H. A., De Vries, D. W., Van Helden, W. G. J., Van Zolingen, R. J. C., & Van Steenhoven, A. A., “The yield of different combined PV-thermal collector designs”, ***Solar Energy,*** *74*(3): 253-269 (2003).

49. Kroiß, A., Präbst, A., Hamberger, S., Spinnler, M., Tripanagnostopoulos, Y., & Sattelmayer, T., “Development of a seawater-proof hybrid photovoltaic/thermal (PV/T) solar collector”, ***Energy Procedia,*** 5(2): 93-103 (2014).

50. Kordzadeh, A., “The effects of nominal power of array and system head on the operation of photovoltaic water pumping set with array surface covered by a film of water”, ***Renewable Energy,*** 35(5): 1098-1102 (2010).

51. Jakhar, S., Soni, M. S., & Gakkhar, N., “Performance analysis of photovoltaic panels with earth water heat exchanger cooling”, ***In MATEC Web of Conferences,*** 5(5): 20-30 (2016).

52. Klein, S. A., Duffie, J. A., & Beckman, W. A., “Transient considerations of flat-plate solar collectors”, ***Journal of Engineering for Power,*** 96(2): 109-113 (1974).

53. Handbook, A. F., “American society of heating, refrigerating and air-conditioning engineers”, ***Inc.,*** Atlanta, USA, 45-77 (2009).

54. Hosseini, R., Hosseini, N., & Khorasanizadeh, H., “An experimental study of combining a photovoltaic system with a heating system”, ***In World Renewable Energy Congress-Sweden****;* Sweden, 2993-3000 (2011).

55. Zhang, T., Zheng, W., Wang, L., Yan, Z., & Hu, M., “Experimental study and numerical validation on the effect of inclination angle to the thermal performance of solar heat pipe photovoltaic/thermal system”, ***Energy,*** 22(3): 12-20 (2021).

56. Sidik, N. A. C., Mohammed, H. A., Alawi, O. A., & Samion, S., “A review on preparation methods and challenges of nano fluids”, ***International Communications in Heat and Mass Transfer,*** 5(4): 115-125 (2014).

57. Dubey, S., Sarvaiya, J. N., & Seshadri, B., “Temperature dependent photovoltaic (PV) efficiency and its effect on PV production in the world–a review”, ***Energy Procedia***, 3(3): 311-321 (2013).

58. Bianco, Vincenzo, Federico Scarpa, and Luca A. Tagliafico. "Numerical analysis of the Al2O3-water nanofluid forced laminar convection in an asymmetric heated channel for application in flat plate PV/T collector." Renewable Energy 116 (2018): 9-21.

59. Al-Waeli, Ali HA, et al. "Comparative study to use nano-(Al2O3, CuO, and SiC) with water to enhance photovoltaic thermal PV/T collectors." Energy Conversion and Management 148 (2017): 963-973.

APPENDIX A.

SPECIFICATIONS OF THE NANO MATERIAL'S USED

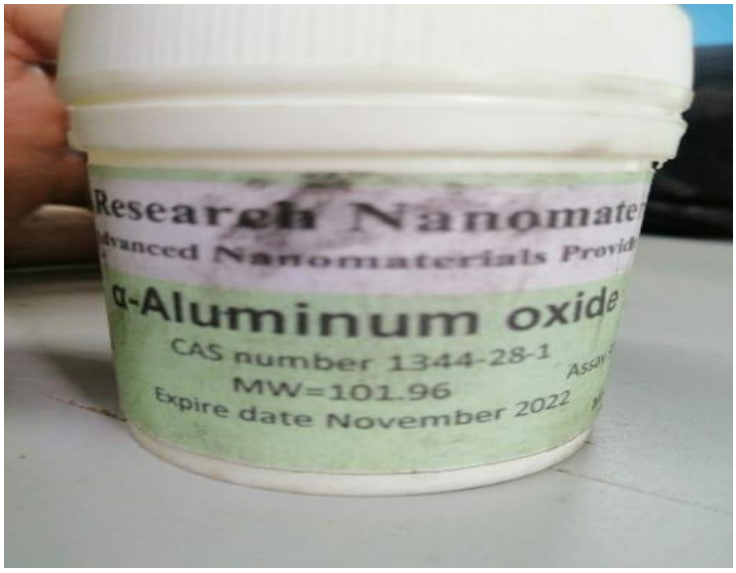

Figure Appendix A.1. Aluminuim oxide.

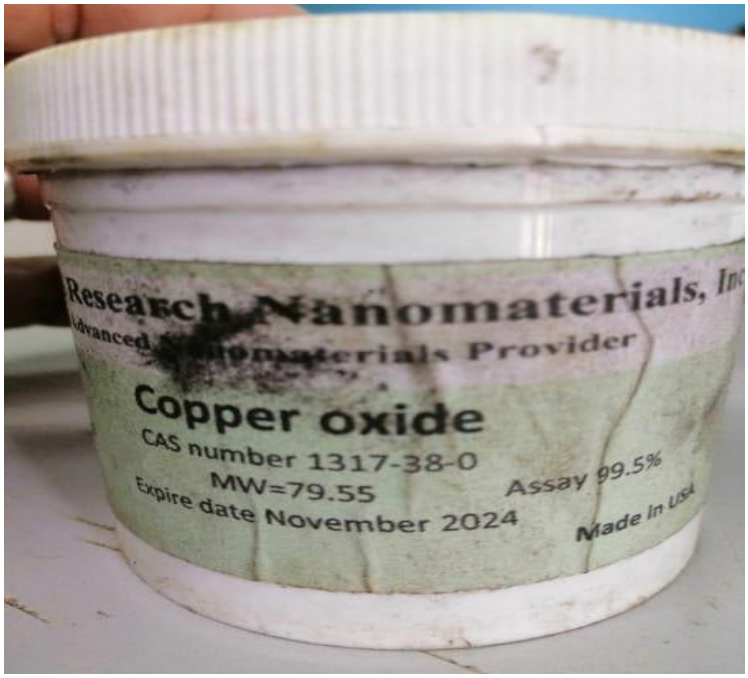

Figure Appendix A.2. Copper oxide.

Copper Oxide Nanoparticle (CuO, 99%, 40nm)

Stock #: US3070
Please click here for price information.

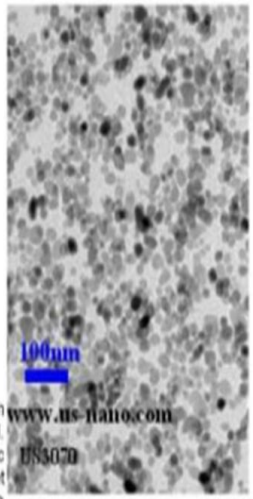

MSDS

Details:
Copper Oxide (CuO)
Purity: 99%
Color: black
APS: 40 nm
SSA: ~20 m2/g
Morphology: nearly spherical
Bulk density: 0.79 g/cm3
True density: 6.4 g/m3

Applications:
Insoluble in water. dissolve slowly in alcohol or ammonia solution. Soluble in dilute acids, NH4Cl, (NH4) 2CO3, potassium cyanide solution. Under high temperature, copper oxide meet with hydrogen or carbon monoxide, can restore copper metal. Nano-copper oxide is a widely used material. It has been applied to the catalyst, superconducting materials, thermoelectric materials, sensing materials, glass, ceramics and other fields. In addition, the nano-copper oxide can be used as rocket propellant combustion catalyst. It not only can significantly improve the homogeneous propellant burning rate, lower pressure index, but also can better perform as the catalyst for the AP composite propellant. More use such as: Ceramic resistors, Gas sensors, Magnetic storage media, Near-infrared filters, Photoconductive and photothermal applications, Semiconductors, Solar energy transformation, Catalysts, High-tech superconductors...

Certificate of Analysis-ppm											
Ba	Cd	Co	Zn	Sr.	Ca	K	P	Mg	Fe	Pb	Mn
0.75	2.5	6.4	195	2.3	400	300	300	75	87	90	3.5

US Research Nanomaterials, Inc.
3302 Twig Leaf Lane, Houston, TX 77084, USA
Phone: (Sales) 832-460-3661; (Shipping) 832-359-7887 **Fax**: 281-492-8628
E-mail: Service@us-nano.com; Tech@us-nano.com

Aluminum Oxide Nanoparticle (Al_2O_3, gamma, 99+%, 20 nm)

Stock #: US3023
Please click here for price information.

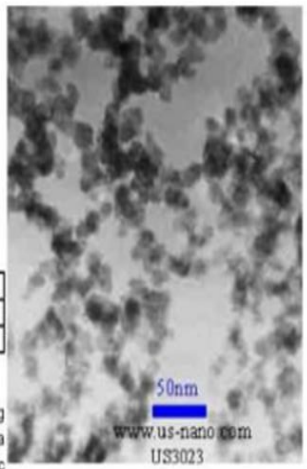

MSDS

Details:
Aluminum Oxide Nanopowder (gamma)
Purity: 99+%
APS: 20 nm
SSA: >138 m^2/g
Morphology: nearly spherical
Color: white

Certificate of Analysis						
Al_2O_3	Ca	Fe	Cr	Na	Mn	Co
≥99%	≤25ppm	≤80ppm	≤4ppm	≤70ppm	≤3ppm	≤2ppm

Product features:
US3023 g-phase nano-Al_2O_3 with small size, high activity and low melting temperature, it can be used for producing synthetic sapphire with the method of thermal melting techniques; the g-phase nano-Al_2O_3 with large surface area and high catalytic activity, it can be made into microporous spherical structure or honeycomb structure of catalytic materials. These kinds of structures can be excellent catalyst carriers. If used as industrial catalysts, they will be the main materials for petroleum refining, petrochemical and automotive exhaust purification. In addition, the g-phase nano-Al_2O_3 can be used as analytical reagent.

Applications:
1. transparent ceramics: high-pressure sodium lamps, EP-ROM window; 2. cosmetic filler; 3. single crystal, ruby, sapphire, sapphire, yttrium aluminum garnet; 4. high-strength aluminum oxide ceramic, C substrate, packaging materials, cutting tools, high purity crucible, winding axle, bombarding the target, furnace tubes; 5. polishing materials, glass products, metal products, semiconductor materials, plastic, tape, grinding belt; 6. paint, rubber, plastic wear-resistant reinforcement, advanced waterproof material; 7. vapor deposition materials, fluorescent materials, special glass, composite materials and resins; 8. catalyst, catalyst carrier, analytical reagent; 9. aerospace aircraft wing leading edge.

US Research Nanomaterials, Inc.
3302 Twig Leaf Lane, Houston, TX 77084, USA
Phone: (Sales) 832-460-3661; (Shipping) 832-359-7887 **Fax**: 281-492-8628
E-mail: Service@us-nano.com; Tech@us-nano.com

APPENDIX B.

INSTRUMENTATION CALIBRATION

B.1. CALIBRATION OF THERMOCOUPLE

Thermocouples type (K) has been used with data logger for temperature measuring at fixed positions of experimental model of the SVE. A thermocouple is a sensor consisting of two wire legs made from different metals, for type K are (positive leg is composed of 90% nickel, 10%chromium and a negative leg is composed of 95% nickel, 2% aluminum, 2% manganese and 1% silicon). The wires legs are welded together at one end, generating a junction. This junction is where the temperature is measured. When the junction experiences a change in temperature, a voltage is generated. The voltage can then be interpreted using a data logger to record the temperature. Thermocouples type K have a smaller temperature range and a shorter lifespan at higher temperatures. Thermocouples type K is well suited to oxidizing atmospheres as a bare consideration. Temperature range for thermocouples type K is -270˚C to 1260˚C.

Before commencing the measurements, a calibration of thermocouples type K was carried out with the digital thermometer. Thermocouples calibration curve, shown in figure A.1, has been analyzed and a linear expression was represented the calibration relationship as shown below:

$$y = 0.7939x + 6.1547 \quad \text{(A.1)}$$

Where *y* represents thermocouples reading and *x* represents the digital thermometer reading, all readings in centigrade scale. That's mean any corrected testing temperature used in analyzing the collected results can be calculated as below:

$$x = (y - 6.1547)/0.7939 \quad \text{(A.2)}$$

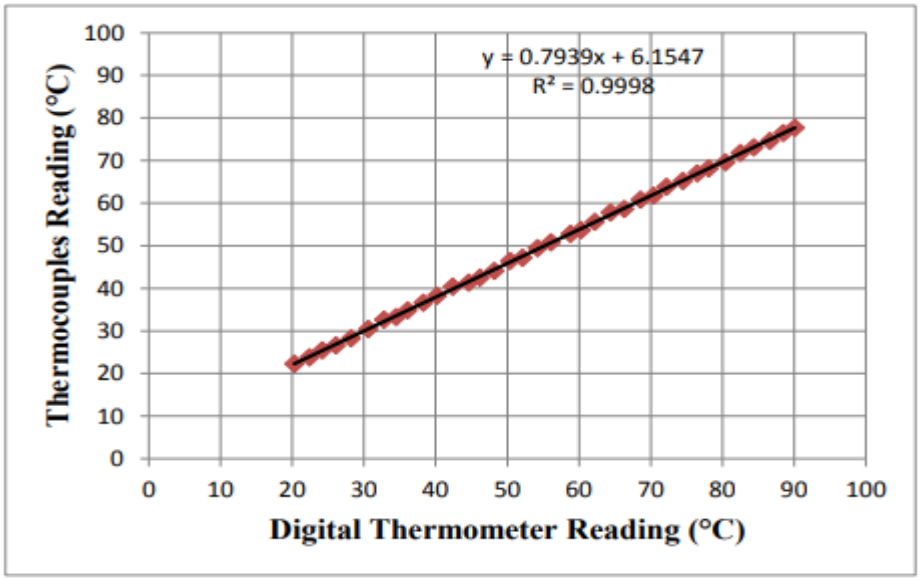

Figure Appendix B.1. Calibration curve of K-type thermocouples.

B.2. CALIBRATION OF FLOW METER

Before commencing the measurement, a calibration of Roto-meter was carried out by the volume of the calibrated tank was pre-calibrated by the volume and its height. The time taken to get 2 litter of water into the tank was recorded, calibration curve shown in Figure A.2.

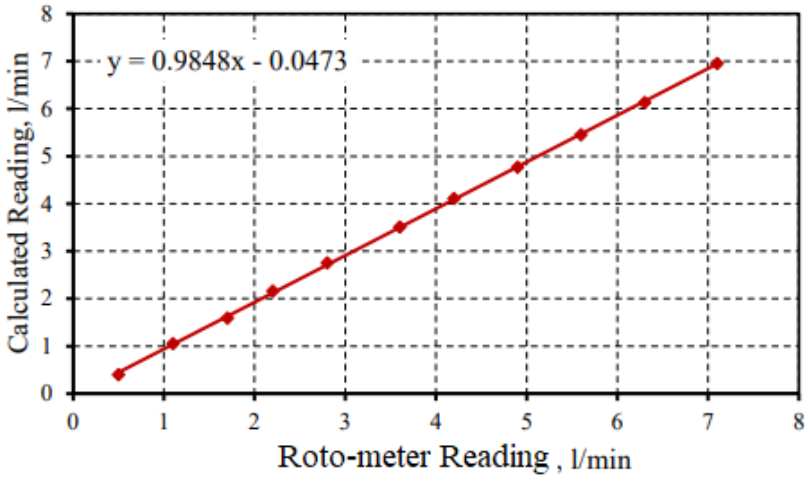

Figure Appendix B.2. Calibration curve of Roto-meter.

B.3. CALIBRATION OF VISCOMETER

The viscometer was calibrated using ethylene glycol and water (60:40 % by weight). The obtained readings were compared with data from the American society of heating, Refrigeration and air –conditioning engineers (ASHRAE) handbook, shown Figure A3. The ASHRAE data and the experimental values match nicely (maximum difference of ± 2%) with temperature range from 20ºC to 55ºC.

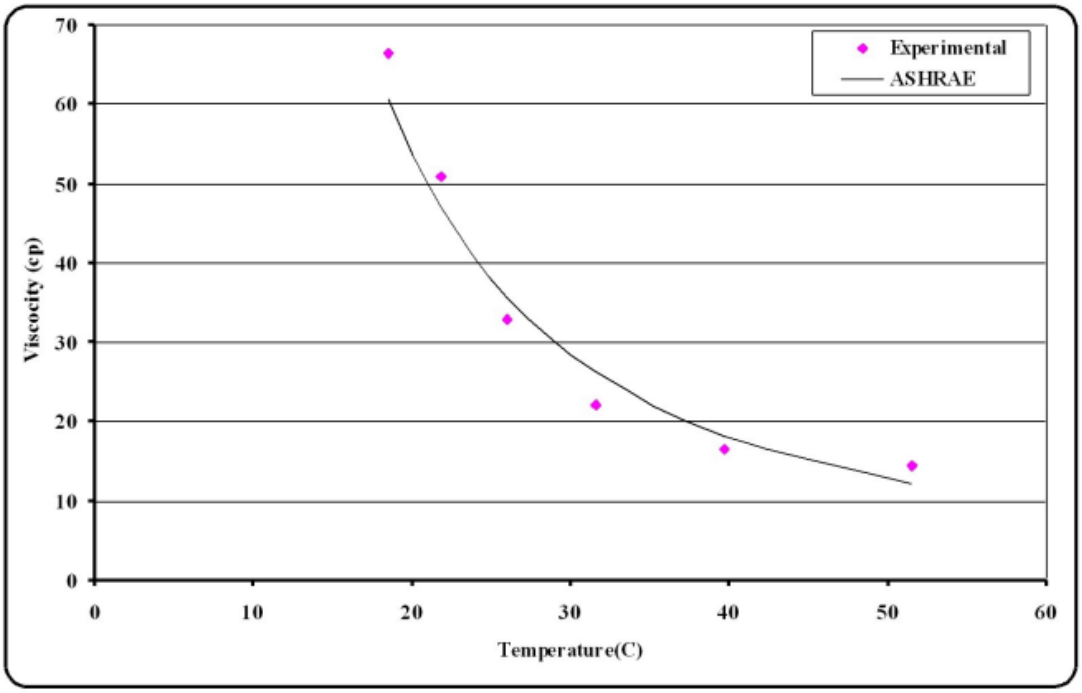

Figure Appendix B.3. Comparison of ASHRAE viscosity values of 60:40 ethylene glycol and water mixture (by weight) and experimental data.

APPENDIX C.

DATA

concentration= 3%Al2O3 ,flow rate = 3.5 l/m							
Time	**T Pv(C°)**	**Tpvt (C °)**	**To-Ti (C °)**	**T col (C °)**	**G w/m2**	**windS m/s**	**T amb (C°)**
07:00	21.7	20	0	19	2	1.1	22
08:00	28	23.3	0.23	24.1	271	1.2	22
09:00	35	28	1.15	27	575	1.6	24
10:00	45	34.5	2.5	32.4	811	1.8	26
11:00	57.3	41	3	39	949	1.9	35
12:00	65	51	3.7	45	1102	2	40
13:00	70.7	55	3.6	46.5	985	2.3	41
14:00	69	54	3.3	46.2	921	2.2	40
15:00	65	52	2.6	44.7	760	2	37
16:00	56	45	1.8	40.1	542	1.7	31
17:00	46	35.6	0.38	31.8	122	1.8	25
18:00	37.2	30	0.2	30	88	1.8	24
19:00	31	26.6	0.1	26	0	1.5	21

concentration= 3%CuO ,flow rate = 3.5 l/m							
Time	**T Pv(C°)**	**Tpvt (C °)**	**To-Ti (C °)**	**T col (C °)**	**G w/m2**	**windS m/s**	**T amb (C°)**
07:00	22	20	0	19	3	1	20
08:00	28.3	23	0.25	24	270	1.2	21
09:00	37.3	27.8	1.2	26.7	578	1	24
10:00	45.7	34	2.6	32	815	1.6	26
11:00	59.1	40.5	3.12	38.7	950	1.6	34
12:00	66	50.5	3.8	44.2	1109	2	40
13:00	70	54	3.65	44.7	993	2.3	41
14:00	68.6	53	3.4	44.5	935	2	39.5
15:00	66	51	2.7	44.3	774	2.2	34
16:00	57.3	44	1.9	39.7	558	1.7	30
17:00	43.6	35	0.4	31.2	133	1.9	26.5
18:00	37	29.75	0.23	29.6	102	2	25
19:00	30	26.2	0.12	25.7	0	1.4	20

concentration= 3%Al2O3 ,flow rate = 1.5 l/m							
Time	**T Pv(C°)**	**Tpvt (C °)**	**To-Ti (C °)**	**T col (C °)**	**G w/m2**	**windS m/s**	**T amb (C°)**
07:00	**21**	**20**	**0**	**19.5**	**3**	1	20
08:00	**26**	**25**	**0.5**	**21.8**	**278**	1.1	21
09:00	**35**	**32**	**2.5**	**26**	**580**	1.5	24
10:00	**42**	**38.8**	**4**	**30**	**800**	1.9	26.2
11:00	**53.9**	**48**	**5.2**	**38.6**	**946**	2	34
12:00	**66**	**56**	**6.7**	**44.6**	**1104**	2.1	40
13:00	**69.7**	**61**	**6.9**	**50.7**	**983**	2.3	41
14:00	**68**	**58.5**	**6.25**	**48**	**930**	2.2	40.1
15:00	**66**	**55.5**	**5**	**47.3**	**767**	2	36
16:00	**59**	**49.5**	**3.4**	**42.5**	**550**	1.9	35
17:00	**44**	**38.7**	**0.75**	**35.4**	**130**	1.8	29.5
18:00	**33.8**	**33.5**	**0.36**	**31.3**	**95**	1.5	27
19:00	**32**	**30.2**	**0.25**	**29.8**	**0**	1.1	21

concentration= 3% CuO ,flow rate = 1.5 l/m							
Time	**T Pv(C°)**	**Tpvt (C °)**	**To-Ti (C °)**	**T col (C °)**	**G w/m2**	**windS m/s**	**T amb (C°)**
07:00	**21.6**	**20**	**0**	**19**	**5**	1.2	20.2
08:00	**27.8**	**24.5**	**0.6**	**21.5**	**284**	1.4	22
09:00	**37**	**31.5**	**2.7**	**25.8**	**587**	2.4	25
10:00	**45**	**38**	**4.3**	**29.7**	**815**	2.2	27.3
11:00	**56**	**47**	**5.4**	**38**	**952**	2	35
12:00	**66.9**	**55.5**	**7**	**44.3**	**1110**	2.1	40.4
13:00	**70.7**	**59.5**	**7.2**	**49.8**	**990**	2.3	41
14:00	**66.8**	**57**	**6.4**	**47.3**	**935**	2.3	40.2
15:00	**65.3**	**55**	**5.25**	**47**	**770**	2.2	37
16:00	**59**	**49**	**3.5**	**42.1**	**554**	1.9	34
17:00	**45.2**	**38.5**	**0.8**	**35**	**135**	1.8	28
18:00	**36.1**	**33**	**0.4**	**30.1**	**98**	2	25
19:00	**33**	**30**	**0.3**	**29.6**	**0**	1.5	21

wate flow rate =1.5 l/m(water only)							
Time	**T Pv(C°)**	**Tpvt (C °)**	**To-Ti (C °)**	**T col (C °)**	**G w/m2**	**T amb (C°)**	**windS m/s**
07:00	21.2	21	0	20	9	20	1.1
07:30	23.5	23	0	21	24	20.3	1.1
08:00	27.3	27	0.25	25.7	204	20.8	1.1
08:30	32	31.9	0.7	29	406	22.7	2.1
09:00	35	34	1	30	572	23.6	2.2
09:30	40	38.5	1.8	32.5	617	24.8	1.7
10:00	42.8	41	2.6	36	793	25.7	1.7
10:30	51	48	3.1	40	862	26.3	1.7
11:00	55.7	51	3.7	42.6	921	34	1.7
11:30	60	55	4.2	46	944	36.7	1.7
12:00	65.4	60	4.6	49	972	39.5	1.7
12:30	68.5	61.5	5	51	1089	40	2.3
13:00	70	64	4.9	53	999	40.8	2.3
13:30	69	61.5	4.75	52	989	40	2.3
14:00	66.7	61	4.5	52	909	39.1	2.3
14:30	67.5	61	3.6	52.5	773	38	2.3
15:00	64.5	58.5	3.5	51	768	37	2.3
15:30	61	56	2.8	50	620	34.4	2.3
16:00	58	52	2.3	46	522	30	1.8
16:30	52.5	48	0.9	43	217	27	1.8
17:00	44	41	0.45	38	146	26.5	1.8
17:30	41	37	0.3	35	132	25	1.9
18:00	36	35	0.18	33.5	87	24	1.9
18:30	34	33.5	0.04	32	17	21	1.9
19:00	32	31.5	0.04	31	0	20	1.6

RESUME

Basam Asaad Shallal SHALLAL he graduated primary, elementary, and high school in this city, after that, he started studying the mechanical engineering at Al-Anbar University/College of Engineering, Department of mechanical Engineering in 1994. Then in 2020, he started at Karabuk University Mechanical Engineering to complete his M. Sc. education.